MASTER DISSERTATION

VEHICLE STABILITY CONTROLLER BASED ON MODEL PREDICTIVE CONTROL

Zoé Roberto Magalhães Júnior

Brasília, February de 2020

UNIVERSIDADE DE BRASÍLIA

FACULDADE DE TECNOLOGIA

UNIVERSIDADE DE BRASÍLIA
Faculdade de Tecnologia

MASTER DISSERTATION

VEHICLE STABILITY CONTROLLER BASED ON MODEL PREDICTIVE CONTROL

Zoé Roberto Magalhães Júnior

Master Dissertation submitted to the Department of Mechanical Engineering as a partial requirement for a Master of Science degree in Mecatronics Engineering

Examination Board

Prof. André Murilo de Almeida Pinto, Ph.D., FT/UnB _____
Advisor

Prof. Renato Vilela Lopes, Ph.D., FGA/UnB _____
Co-advisor

Prof. Evandro Leonardo Silva Teixeira, Ph.D., FGA/UnB _____
External Member

Profª. Suzana Moreira Ávila, Ph.D., FT/UnB _____
Internal Member

FICHA CATALOGRÁFICA

MAGALHÃES, ZOÉ ROBERTO
VEHICLE STABILITY CONTROLLER BASED ON MODEL PREDICTIVE CONTROL [Distrito Federal] 2020.
xvi, 92 p., 210 x 297 mm (ENM/FT/UnB, Master of science, Engenharia Mecânica, 2020).
Master Dissertation - Universidade de Brasília, Faculdade de Tecnologia.
Departamento de Engenharia Mecânica

1. Vehicle stability control	2. Model predictive control
3. Linear quadratic regulator	4. Real-time control system
I. ENM/FT/UnB	II. Título (série)

REFERÊNCIA BIBLIOGRÁFICA

MAGALHÃES, Z. R. (2020). *VEHICLE STABILITY CONTROLLER BASED ON MODEL PREDICTIVE CONTROL* . Master Dissertation, Departamento de Engenharia Mecânica, Universidade de Brasília, Brasília, DF, 92 p.

CESSÃO DE DIREITOS

AUTOR: Zoé Roberto Magalhães Júnior
TÍTULO: VEHICLE STABILITY CONTROLLER BASED ON MODEL PREDICTIVE CONTROL .
GRAU: Master of science in Mecatronics Engineering ANO: 2020

Zoé Roberto Magalhães Júnior
Depto. de Engenharia Mecânica (ENM) - FT
Universidade de Brasília (UnB)
Campus Darcy Ribeiro
CEP 70919-970 - Brasília - DF - Brasil

Agradecimentos

Agradeço aos meus orientadores, Prof. Renato e Prof. André, por acreditarem no meu potencial para realizar este trabalho, pelo conhecimento compartilhado, e pelas instruções que me guiaram até os resultados obtidos.
Agradeço à minha família por todo carinho, incentivo e suporte que tenho recebido durante toda a minha vida.
Agradeço à minha companheira, Denise, por estar sempre presente, me acalmando nos momentos de ansiedade e comemorando cada conquista.
Agradeço principalmente à minha avó Madalena por todo amor que tenho recebido na vida e por ser o meu maior exemplo e inspiração.

Zoé Roberto Magalhães Júnior

RESUMO

Os Sistemas Avançados de Assistência ao Motorista (ADAS) são dispositivos automotivos desenvolvidas para auxiliar o motorista na condução, com intuito de melhorar o desempenho dos veículos em diversos aspectos, incluindo segurança. Do ponto de vista da dinâmica veicular, segurança diz respeito a como o veículo responde aos comandos do motorista em manobras arriscadas. A melhoria de manobrabilidade em situações críticas pode ser obtida pela inclusão de controladores eletrônicos de estabilidade (ESCs). Os ESCs são ADAS desenvolvidos para evitar que o motorista perca o controle do veículo. Uma estratégia de atuação utilizada em ESCs é o controle dos torques transferidso para as rodas, de forma que seja aplicado no eixo de guinada um momento estabilizador resultante da diferença entre as forças geradas nos pneus. Essa estratégia é denominada controle direto do momento de guinada (DYC). O ESCs que utilizam DYC podem ser classificados em dois níveis: alto e baixo. O primeiro calcula o momento estabilizador, sem especificar como deve ser feita a distribuição de torque entre as rodas. E o segundo calcula o torque que deve ser transferido para cada roda, por isso é desenvolvido dedicado para o sistema de atuação disponível no veículo. Nessa pesquisa são propostos DYCs de alto e baixo nível baseados em controle preditivo (MPC). O MPC foi escolhido devido às suas capacidades de considerar os limites do sistema de atuação e prever a desestabilização. Porém, a aplicação do MPC em sistemas de controle em tempo real tem como desafio a obtenção de tempos de cálculo compatíveis com a velocidade da dinâmica do processo controlado. Por isso, foram aplicadas parametrizações da formulação do MPC que reduzem a sua complecidade computacional. E, para considerar a eficiência computacional na validação dos controladores, os algoritmos propostos foram implementados em ARM Cortex A8 e submetidos a um procedimento de sintonização, que define as configurações ótimas e caracteriza os tempos de cálculo. Simulações *model-in-the-loop* e *hardware-in-the-loop* foram realizadas para validação dos controladores. Os resultados dessas simulações mostram que os ESCs são eficazes em evitar a desestabilização da condução, e que os algoritmos possuem eficiência computacional para serem eficazes em tempo real, mesmo executando em um hardware de baixo custo. A comparação entre os resultados obtidos com MPC e regulador quadrático linear (LQR) mostrou que é mais vantajoso utilizar o MPC, mesmo seu tempo de cálculo sendo maior. A comparação entre os desempenhos obtidos com diferentes modelos de predição mostrou que, em manobras com maior risco de instabilidade, um melhor desempenho é obtido com o modelo que considera a rolagem, mesmo que insto impacte no aumento do tempo de cálculo. Além disso, dos resultados para veículos com parâmetros diferentes dos valores nominais assumidos na configuração dos controladores, observou-se que os ESCs são sensíveis ao descasamento entre planta e modelo, de forma que não são comprometidas suas eficácias em evitar que o motorista perca o controle do veículo.

ABSTRACT

Advanced Driver Assistance Systems (ADAS) are automotive devices developed to assist the driver, with the aim of improving vehicle performance in several aspects, including safety. From the point of view of vehicle dynamics, safety concerns how the vehicle responds to the driver's commands in risky maneuvers. The improvement of maneuverability in critical situations can be achieved by the inclusion of electronic stability controllers (ESCs). ESCs are ADAS designed to prevent the driver from losing control of the vehicle. An actuation strategy used in ESCs is to control the torques transferred to the wheels, so that a stabilizing moment resulting from the difference between the forces generated in the tires is applied to the yaw axis. This strategy is called direct yaw moment control (DYC). ESCs using DYC can be classified into two levels: high and low. The first calculates the stabilizing moment, without specifying how to distribute the torque between the wheels. And the second calculates the torque that must be transferred to each wheel, so it is developed dedicated to the actuation system available in the vehicle. In this research, high and low level DYCs based on Model Predctive Control (MPC) are proposed. The MPC was chosen because of its ability to consider the limits of the actuation system and to predict destabilization. However, the application of MPC in real-time control systems has the challenge of obtaining calculation times compatible with the speed of the dynamics of the controlled process. Therefore, parameterizations of the MPC formulation were applied to reduce the computational complexity. And, to consider the computational efficiency in the validation of the controllers, the proposed algorithms were implemented in ARM Cortex A8 and submitted to a tuning procedure, which defines the optimum configurations and characterizes the calculation times. Model-in-the-loop and hardware-in-the-loop simulations were performed to validate the controllers. The results of these simulations show that the ESCs are effective in avoiding the destabilization of driving, and that the algorithms have computational efficiency to be effective in real-time application, even running on low-cost hardware. The comparison between the results obtained with MPC and Linear Quadratic Regulator (LQR) showed that it is more advantageous to use MPC, even though its calculation time is longer. The comparison between the performances obtained with different prediction models showed that, in maneuvers with a higher risk of instability, a better performance is obtained with the model that considers the roll motion, even though it leads to the increase in calculation time. In addition, from the results for vehicles with different parameters from the nominal values assumed in the configuration of the controllers, it was observed that the ESCs are sensitive to the model-plant mismatch , however, their effectiveness in preventing the driver from losing control is maintained.

SUMÁRIO

List of Figures

List of Tables

Symbol list

$\mathbf{A}$	state matrix of state space model	
$\mathbf{a}$	acceleration of vehicle CG	[m/s²]
a	longitudinal distance from front track to vehicle CG	[m]
a_1,...a_{14}	Coefficients of Pacejka's Magic Formula	
$\mathbf{B}$	input matrix of state space model	
b	longitudinal distance from rear track to vehicle CG	[m]
$\mathbf{C}$	output matrix of state space model	
$c_{\phi r}$	roll dumping coefficient of front track	[N m s/rad]
$c_{\phi f}$	roll dumping coefficient of rear track	[N m s/rad]
C_α	cornering stiffness	[N/rad]
$C_{\alpha r}$	cornering stiffness coefficient of front track	[N/rad]
$C_{\alpha f}$	cornering stiffness coefficient of rear track	[N/rad]
$C_{\gamma fl}$	cambering stiffness coefficient of the left tire of front track	[N/rad]
$C_{\gamma rl}$	cambering stiffness coefficient of the right tire of front track	[N/rad]
$C_{\gamma fl}$	cambering stiffness coefficient of the left tire of rear track	[N/rad]
$C_{\gamma rl}$	cambering stiffness coefficient of the right tire of rear track	[N/rad]
$\mathbf{C}_r$	selection matrix of regulated states	
$\mathbf{D}$	feedward matrix of state space model	
$\mathbf{e}$	Euler angles	[m/s²]
$\mathbf{F}$	force on vehicle CG	[N]
F_x	longitudinal force on vehicle CG	[N]
F_y	lateral force on vehicle CG	[N]
F_{yfl}	lateral force on the left tire of front track	[N]
F_{yrl}	lateral force on the left tire of rear track	[N]
F_{yfr}	lateral force on the right tire of front track	[N]
F_{yrr}	lateral force on the right tire of rear track	[N]
F_{xfl}	longitudinal force on the left tire of front track	[N]
F_{xrl}	longitudinal force on the left tire of rear track	[N]
F_{xfr}	longitudinal force on the right tire of front track	[N]
F_{xrr}	longitudinal force on the right tire of rear track	[N]
F_{wxi}	longitudinal force on tire i-th tire	[N]
F_{wyi}	lateral force on tire i-th tire	[N]
F_y	lateral force on vehicle CG	[N]
g	gravitational acceleration	[m/s²]
h	height of vehicle CG	[m]
h_s	height from CG of sprung mass to roll center	[m]
$\mathbf{I}$	inertial tensor	[Kg m²]

I_s	steering coefficient	[rad/rad]
I_w	moment of inertial of wheel	[Kg m²]
I_{xx}	rolling moment of inertial	[Kg m²]
I_{zz}	yawing moment of inertial	[Kg m²]
I_{xz}	product of inertia of yaw and roll motions	[Kg m²]
J	cost function of optimal control theory	
$k_{\phi r}$	roll stiffness coefficient of front track	[N m/rad]
$k_{\phi f}$	roll stiffness coefficient of rear track	[N m/rad]
k	discrete time index	
K_γ	camber-by-roll gradient	[rad/rad]
$\mathbf{K}_{LQR}$	LQR gain matrix	
l	longitudinal distance between front and rear tracks	[m]
L_a	longitudinal distance from vehicle position to target point of driver model	[m]
m	vehicle mass	[Kg]
m_s	sprung mass	[Kg]
$\mathbf{M}$	Moment tensor on vehicle CG	[Kg m²/s]
M_z	yaw-momentum	[Kg m²/s]
M_x	roll-momentum	[Kg m²/s]
n_u	number of system inputs	
n_x	number of system states	
n_y	number of system outputs	
$n_e^{(j)}$	number of exponential terms in parameterization of j-th control siginal	
N	Prediction horizon	number of sample times
$\mathbf{p}$	Parameters of exponential parameterization of MPC formulation	
$p_n^{(j)}$	parameter of the n-th exponential term of the j-th control signal	
$\mathbf{Q}$	LQR weighting matrix of state errors	
$\mathbf{Q_u}$	MPC's weighting matrix of command energy	
$\mathbf{Q_y}$	MPC's weighting matrix of state error	
$\mathbf{R}$	LQR weighting matrix of command energy	
R_{eff}	effective radios of tire-wheel set	[m]
$\mathbf{s}$	vector of optimization variables of a cost function	
t_f	front track width	[m]
t_r	front track width	[m]
T	Torque transferred to wheel	[N/m]
T_k	Actuation delay coefficient of driver model	[s]
u	vehicle longitudinal speed	[m/s]

$\tilde{\mathbf{u}}$	control signals over prediction horizon	
$\mathbf{y}$	vector of system's control signals	
v	vehicle lateral speed	[m/s]
W	expertise coefficient of driver model	[m]
$\mathbf{x}$	vector of system's states	
$\tilde{\mathbf{x}}$	states over prediction horizon	
$\mathbf{y}$	vector of system's outputs	
$\mathbf{y}_r$	vector of regulated states	
y_{os}	current lateral displacement error	[m]
y_d	lateral position of target point of driver model	[m]
$\mathbf{y}_d$	vector of desired value for regulated states	
α_{fl}	side-slip angle of left tire of front track	[rad]
α_{fr}	side-slip angle of right tire of front track	[rad]
α_{rl}	side-slip angle of left tire of front track	[rad]
α_{rr}	side-slip angle of right tire of front track	[rad]
β	side-slip angle of vehicle body	[rad]
β_{th}^{on}	side-slip angle threshold of ESC activation criteria	[rad]
β_{th}^{off}	side-slip angle threshold of ESC deactivation criteria	[rad]
δ_D	angle of steering wheel	[rad]
δ_f	steering angle of front wheels	[rad]
$\delta_f l$	steering angle of left wheel of front track	[rad]
$\delta_f r$	steering angle of right wheel of front track	[rad]
δ_r	steering angle of rear wheels	[rad]
$\delta_r l$	steering angle of left wheel of rear track	[rad]
$\delta_r r$	steering angle of right wheel of rear track	[rad]
$\eta_j^{(n)}$	time coefficient of the n-th exponential term of parameterization of the j-th control signal	
γ	camber angle of wheels	[rad]
μ	tire-road friction coefficient	
ξ	tuning coefficient of exponential parameterization	
τ_{on}	activation time of ESC activation criteria	[s]
τ_{off}	deactivation time of ESC activation criteria	[s]
ψ	yaw angle of vehicle body	[rad]
$\dot{\psi}_{th}^{on}$	yaw-rate error threshold of ESC activation criteria	[rad/s]
$\dot{\psi}_{th}^{off}$	yaw-rate error threshold of ESC deactivation criteria	[rad/s]
ϕ	roll angle of sprung mass	[rad]
ω	angular speed of wheel	[rad/s]

Acronyms

4WAS	Four-wheel Active Steering
ABS	Anti-lock Braking System
ACC	Adaptive Cruise Control
ADAS	Advanced Driver Assistance System
AFS	Active Front Steering
ARS	Active Rear Steering
AS	Active Steering
CG	Center of Gravity
DOF	Degree of Freedom
DYC	Direct Yaw Control
ECU	Electronic Control Unit
E/E	Electrical/Electronic
ESC	Electronic Stability Control
ESP	Electronic Stability Program
HIL	Hardware-In-the-Loop
HL	High-level
LL	Low-level
LP	Linear Programming
TPMS	Typre Pressure Monitoring System
LQR	Linear Quadratic Regulator
MF	Magic Formula of Pacejka
MIL	Model-In-the-Loop
MPC	Model Predictive Control
PID	Proportional-Integral-Derivative
QP	Quadratic Programming
UDP	User Datagram Protocol
VDC	Vehicle Dynamic Control
VSC	Vehicle Stability Control
WHO	World Health Organization

1 INTRODUCTION

1.1 CONTEXTUALIZATION

The increase in computational power and the reduction in the cost of digital circuits have encouraged the use of embedded systems in the automotive industry. The vehicles which were mechanical machines became mechatronics systems, such that the relative costs of electrical/electronic (E/E) devices have grown from 1% of vehicle cost in 1980 to some 30% to 40% in 2012 [1]. Current top-of-the-range vehicles have E/E architectures comprising up to 100 Electronic Control Units (ECUs). Electronic Control Units are embedded systems composed of input and output interfaces, and processor cores. The input and output interfaces access the sensing and actuation systems, and the processor cores run the embedded software that performs the control algorithm. Most innovations in the modern vehicles are driven by ECUs because the development methods of embedded systems allow the rapid release of new technologies, and the same embedded software may implement multiple features that share the same hardware [2, 1].

Important systems implemented with ECU are the Advanced Driver Assistance Systems (ADAS), which are developed to help the driver in order to increase vehicle performance in several aspects. Some ADAS are active safety systems, which means that they help in driving to improve the safety performance. For vehicle dynamics, safety performance concerns the response of the movement to the driver's controls, i.e. how the vehicle behaves concerning the expected behavior when the driver brakes, speeds up, or turns the steering wheel. The vehicle response in critical condition may be the cause of traffic injuries. The handling becomes unstable when the vehicle responds to commands differently from how it does in conditions in conditions that the driver is able to drive [3]. In this sense, the active safety systems help in driving to keep the vehicle behavior close to driver's expectation, and thus contribute to avoid traffic accidents.

The development of these systems is a necessity because traffic accidents are the leading cause of death for people aged 5-29 years, and the eighth leading cause of death for all the age groups, according to the World Health Organization (WHO) [4]. In addition to deaths, the traffic accidents generate expenses for treating their victims and can lead to inactivity of workers. So, traffic safety is a public health problem, such that the legislation of some countries requires the inclusion of Electronic stability controllers (ESC) in passenger vehicles, which is an effective action to increase traffic safety, as has been shown by research based on traffic accident statistics carried out in different countries [5, 6, 7, 8, 9, 10, 11]. Due to this effectiveness, The Global Plan for the Decade of Action for Road Safety 2011-2020 implemented by WHO recommends the global development of ESCs to achieve the goals of advances in traffic safety [12].

Electronic stability controllers are active safety devices developed to improve driving dynamics and prevent accidents that result from loss of control. These systems enhance the maneuverability of vehicles enabling the handling stability in critical conditions such as emergency maneu-

ver, cornering at high speed, and low-friction conditions. They detect the movement expected by the driver and the vehicle's actual response and acts to approximate the vehicle movement to the driver's intention, by correcting undesired motion that may take the vehicle off the desired path or cause the loss of driving control [8, 5, 6].

The ESC was first introduced in 1995 with the Vehicle Dynamic Control (VDC) of Bosch, which determined the nominal vehicle behavior expected by the driver, from measurements of the steering wheel angle, the throttle position, and the brake pressure, and it predicted the actual vehicle response from measurements of the yaw rate, lateral acceleration, and wheel speed. A state-feedback controller was used to compute the nominal yaw moment, and PIDs were used to control the driveshaft and the braking systems to make the actual yaw moment to track the nominal value [3].

Since VDC, several ESC designs have been published in the literature. Regarding the architecture of the control systems, we may classify the ESC algorithms as upper or lower-level controllers. The lower-level algorithms are developed to control the actuation systems, hence their outputs are the inputs of the actuators. Whereas the upper-level algorithms calculate the moments or forces that must be imposed on the vehicle body to improve the lateral stability performance. The upper-level controllers have the potential to be applied to vehicles with different actuation systems, however, it has the drawback of needing a low-level controller to command the actuation system. The lower-levels algorithms may be self-sufficient, or they may be used in hierarchical architectures to command the actuators to generate the moments or forces requested by an upper-level algorithm. The Bosch's VDC is an example of hierarchical architecture, where the upper-level algorithm implements a state-feedback control, whose controlled states are the side-slip angle and the yaw rate, and the control output is the yaw moment required to lead the vehicle dynamics to the desired behavior, and the low-level algorithm controls the rotational speed of the driveshaft and the differential speed of the driven wheels by using a Proportional-Integral-Derivative (PID) controllers to command the torque transferred to the driveshaft and the brake pressured on the wheels, aiming to make the actual yaw moment track the nominal value computed by the upper-level controller [3].

In these designs presented in the literature, thanks to advances in computational power available for automotive systems, the researches have explored the benefits of modern control theories such as Sliding Mode Control (SMC) [13, 14, 15, 16], backstepping technique [17] and robust gain schedule [18, 19]. One of those theories is the optimal control theory, in which the control law is derived from the solution of an optimization problem. The Model Predictive Control (MPC) is one of the optimal techniques, in winch optimization problem is to found the sequence of commands that minimizes a cost function, which weights the control error and the actuation effort, over a finite time interval known as prediction horizon. The prevision of system evolution over the prediction horizon comes from defining the cost function based on a model of the controlled system. The MPC solves this minimization once at each sampling time and applies the first sample in the optimal sequence to the control signals [20, 21]. A strength of the MPC method is the capability to handle constraints on the solution to ensure values compatible with the limita-

tions of the actuation system, and to avoid commands that take the states of the controlled process out of desired ranges. However, the computational power required to solve an optimization at each sampling time is an implementation challenge.

In this sense, the computational efficiency is an important issue because it influences the calculation time and the hardware requirements to run the control algorithm in real-time applications, hence it affects the cost, which is an important aspect because of the production volume of the automotive industry.

Another important issue of ESC development is the quality assurance procedure. The growing complexity of ECUs increases the importance of testing their software components before the ECU release in a commercial vehicle [22]. Therefore, the development process includes several tests of the effectiveness of the control system along all stages. Useful methods are the Model-in-the-Loop (MIL) and the Hardware-in-the-loop (HIL). The Model-in-the-Loop (MIL) is a technique used to test the control algorithm on interaction with a model of the vehicle dynamics. The engineers may perform MIL testing since the early design stages to verify if the specifications met the requirements, even before the firmware and hardware implementation of the embedded control system. Hardware-in-the-Loop (HIL) is a technique used to test the embedded control systems on test benches that provide a real-time simulation of the automotive environment. The HIL method enables the test of the control system in a real-time application in a controlled environment, without damage risk in case of failure [22, 23, 24].

1.2 CONTRIBUTIONS

In this context, this research proposes the implementation of computational efficient MPC-based ESCs for lateral stability control. These implementations use the MPC formulation presented by Alamir [25] with the exponential parameterization for reducing the complexity of the optimization problem. To deal with the longitudinal steering angle, which is a command not controlled by the MPC and assumed constant during the prediction horizon, changes are proposed in this research for the MPC the exponential parameterization presented in [25]. An upper-level control is proposed to compute the additional moment applied on the yaw axis to improve handling stability. And a self-sufficient low-level DYC is developed to control the braking torque transferred to the wheels.

Concerning the state-of-the-art, the current literature includes several MPC-based ESCs [26, 27, 28, 29], but none of these designs address strategies for the reduction of the computational complexity of the ESC algorithm. A characteristic of MPC designs that affects the computational complexity is the mathematical model used for prediction, a simple model increases efficiency, however, the use of more representative models reduces the mismatch between the vehicle's response and that predicted by the model. The MPC-based ESCs proposed in the literature use different prediction models, but not all the papers present the effects of the chosen model on sta-

bility performances in comparison to other models. Also, the robustness of the proposed systems to model uncertainties are not evaluated in all these studies. When a linear model is used to predict the vehicle response there are differences between the vehicle response and the calculated by this model, since the vehicle motion is a nonlinear system.

In this research, strategies are used to reduce the calculation time of the MPC-based ESCs, so that ESC implementation may run with a command update rate high enough to be effective in real-time application. MIL and HIL simulations are performed to test the control algorithms, taking into account the computational power of the embedded control system. The test cases include a simulation performed to evaluate the effectiveness of the ESC in presence of model uncertainties, in which the nonlinear model used to simulate the vehicle response is configured with mass, position of the center of mass, tire-road friction coefficient, and speed different from the nominal parameters considered in ESC design.

This research investigates the effects of considering, in the prediction model, the influence of roll motion on the vehicle response. Also, the proposed MPC-based ESCs is implemented using linear models with and without roll-degree-of freedom, and comparing the performance got in each case.

This research also investigates the advantages of using MPC on stability control instead of using the LQR. The LQR was chosen for this comparison because it has a calculation time shorter than that presented by the MPC, but it does not have the same capabilities to deal with command restrictions and to predict instability before it occurs and act to avoid it. In this investigation, the proposed ESCs were implemented using the LQR instead of MPC, and the results got with both control techniques were compared with each other to verify if the benefits of using the MPC overcomes the negative effects of its long calculation time.

It was not found in the literature a work that brings together all these characteristics: use of strategies to increase the command update rate, comparative study between the use of prediction models with and without roll-degree-of-freedom, comparative study between addressing the MPC and the LQR to vehicle stability control, evaluation of the proposed system taking into account the computational efficiency of the embedded control system, and testing the robustness to the uncertainties of the prediction model.

1.3 OBJECTIVES

1.3.1 General Objective

The development and evaluation of computation efficient Vehicle Stability Controllers based on the Model-Based Predictive Control (MPC) concerning the real-time performance.

1.3.2 Specific Objectives

- Obtain ESCs that use the MPC to compute the yaw moment required to improve lateral stability and can handle with constraints of this corrective yaw moment.
- Obtain ESCs that use the MPC to compute the torques transferred to the wheels and can consider the limits of the actuation system;
- Evaluate the proposed ESCs in MIL and HIL simulations of double lane change (DLC) test of standard No. ISO 3888:1975, taking into account the computational power of the embedded control system.
- Evaluate the performance of the proposed ESCs in the presence of disturbances of vehicle response and that predicted by the linear model.
- Compare the performances obtained by addressing the MPC and the LQR to vehicle stability control;
- Compare the performances obtained by using in control design linear models with and without roll-degree-of-freedom.

1.4 OUTLINE OF THE DISSERTATION

The dissertation is organized in five chapters.

Chapter 2 presents a review of the main topics of this dissertation. First theoretical introductions to vehicle dynamics, MPC, and LQR are presented. Then, a literature review about the state-of-art of MPC-based and LQR-based ESCs are presented.

Chapter 3 presents the methodology of the development process of the implementations proposed in this research. This chapter shows the simulation scheme implemented for MIL and HIL validation of proposed systems; The proposed control architecture, the design of MPC and LQR controllers and the features of the control algorithm; And the procedures for tuning and evaluation of proposed implementations.

Chapter 4 shows the results from the tuning and evaluation procedures described in chapter 3. The discussion about these results includes the benefits of using the MPC method and the effects of including the roll control.

Finally, Chapter 5 presents a general conclusion of this dissertation and suggestions for future works.

2 THEORETICAL BACKGROUND

From the standpoint of vehicle dynamics, the vehicle performance concerns three major criteria: safety, comfort and energy economy. Electronic stability controllers are ADAS developed to improve the safety performance by ensuring good maneuverability in critical conditions. These systems detect from driver's commands the desired vehicle response and acts to make the actual response close to driver's intention. Hence, the knowledge of driver behavior on steering command and vehicle dynamics are necessary to analyze the control performance. Also, the knowledge of vehicle dynamics is necessary to implement ESCs based on model-based control techniques that derive the control law from a model of the controlled process. Which is the case of the optimal control theories used in the ESCs designs proposed in this work.

An example of model-based control theory is the optimal control theory, in which the control algorithm consist of solving an optimization problem defined based on the control objectives. The ESCs designs proposed in this research use optimal techniques to find the actuation that reduces the yaw-rate error, side-slip angle and roll angle.

In this sense, this chapter presents an overview of these major topics on this research: vehicle dynamics focusing on aspects that matter to stability performance; ESC systems and their key strategies; Optimal control theory with an emphasis on the model predictive control, which is THE optimal control technique used on the ESCs designs developed in this research, and the state-of-the-art for MPC-based ESC.

2.1 VEHICLE DYNAMICS

The vehicle movement can understand by mathematical models that express how the driver interacts with the vehicle, how the automotive systems respond to the driver's commands, and which are the effects of this response on the vehicle movement. These dynamics can understand by the behavior of each of its subsystems and the interaction between them [30, 31]:

- The vehicle-body movement in response to the forces generated on tires.
- The steering of each wheel commanded by the steering wheel angle.
- The vertical load transference between tires because of vehicle motion;
- The lateral and longitudinal slipping of the tires in response to the steering and rotation of the wheels and the vehicle motion;
- The rotational motion of the wheels in response to the torque transferred to the wheels;

- The forces generated on each tire by the deformation of its rubber in reaction to the tire movement relative to the wheel (i.e the tire slip);

Hence the mathematical modeling may be simplified by using a model to each subsystem and mapping the interfaces between them. The following sections present this modeling.

2.1.1 Vehicle-body movement

The vehicle-body is a system with six-degrees-of-freedom (6DOF), 3DOF of translation and 3DOF of rotation. The translation motion includes the longitudinal, lateral and vertical motions. And the rotation motion includes the roll, pitch and yaw motions, which are the rotations around the x-axis, y-axis, and z-axis of the vehicle-body coordinated system, respectively. Figure 2.1 presents the free body diagram of the vehicle model considered in this research.

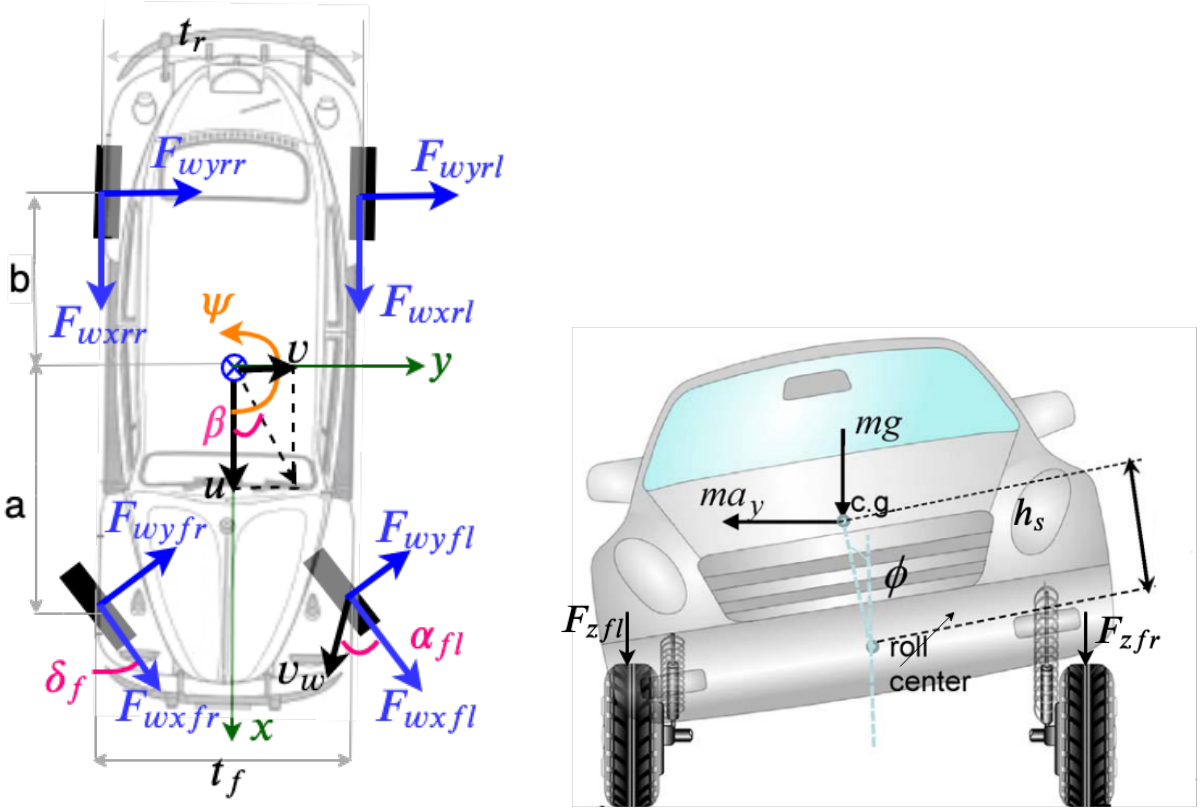

(a) Top view with indexes for tire dynamics and longitudinal and lateral translation of vehicle body.

(b) Front view with index for roll motion, adapted from [16].

Figure 2.1: Free body diagram of vehicle model.

In the model presented in Fig. 2.1, it is considered that the vehicle exhibits lateral and longitudinal speeds (v and u), yaw rotation of vehicle body (ψ), and roll rotation of the sprung mass (ϕ). The vertical translation and the pitch rotation are neglected since lateral stability controllers are systems developed to control the vehicle at the ground, i.e. movements in which the vehicle's wheels leaves the ground are not within the scope of this research. In the translational motion and

yaw rotation, the vehicle behaves roughly as a single solid body in which the yaw moment and the force at the vehicle's CG are generated only by the forces acting on the tires, which are decomposed in lateral components (F_{wyfl}, F_{wyfr}, F_{wyrl}, F_{wyrr}) and longitudinal components (F_{wxfl}, F_{wxfr}, F_{wxrl}, F_{wxrr}). Whereas in the roll motion, the vehicle splits into sprung and unsprung parts, as illustrated in Figure 2.1, in which the sprung part has roll-degree-of-freedom, while the unsprung part is physically constrained to roll, such that the sprung part rotates towards a roll axis that is not in the vehicle's CG.

An important variable of this model to analyze the lateral stability performance is the side-slip angle of the vehicle body β, defined as the angle between the direction of motion and longitudinal axis of the vehicle, it is a measure of how much the vehicle is slipping sideways, which is calculated as follows:

$$\beta = \arctan v/u \tag{2.1}$$

Regarding the mathematical modeling, the equations of the translation motions are derived from Newton's law:

$$m\mathbf{a} = \mathbf{F} \tag{2.2}$$

in which m is the vehicle total mass, and $\mathbf{a}$ denotes the acceleration vector and $\mathbf{F}$ the total force vector. And the equations of the rotation motions are derived from the Euler's law:

$$\mathbf{I}\ddot{\mathbf{e}} + \ddot{\mathbf{e}} \times (\mathbf{I}\ddot{\mathbf{e}}) = \mathbf{M} \tag{2.3}$$

in which $\mathbf{I}$ is the inertia tensor of the vehicle body concerning its center of mass, M is the vector torque, and $\mathbf{e}$ is the angular velocity vector.

Since this model includes the lateral and longitudinal translation and the yaw and roll rotations, the acceleration and the angular velocity vectors are defined as follows:

$$\mathbf{a} = \begin{pmatrix} \dot{u} & \dot{v} \end{pmatrix}^T \qquad \dot{\mathbf{e}} = \begin{pmatrix} \dot{\psi} & \dot{\phi} \end{pmatrix}^T \tag{2.4}$$

in which u denotes the longitudinal speed, v denotes the lateral speed, $\dot{\psi}$ denotes the yaw rate of the vehicle-body, and $\dot{\phi}$ denotes the roll rate of the sprung mass towards the roll center.

From equations 2.2 and 2.4, the equations of translational motions are derived as follows [28, 32, 33, 34]:

Longitudinal motion

$$m\left(\dot{u}-\dot{\psi}v\right)+m_s h_s\dot{\psi}\dot{\phi}=\sum F_x \tag{2.5}$$

Lateral motion

$$m\left(\dot{v}+\dot{\psi}u\right)-m_s h_s\ddot{\phi}=\sum F_y \tag{2.6}$$

where m_s denotes the is sprung mass, h_s the height from the longitudinal axis of the vehicle to the rolling axis. and $\sum F_y$,$\sum F_x$ are the sums of the lateral forces generated by tires on vehicle-body's CG.

And from equations 2.3 and 2.4, the equations of rotational motions are derived as follows [28, 32, 33, 34]:

Yawing motion

$$I_{zz}\ddot{\psi}-I_{xz}\ddot{\phi}=\sum M_z \tag{2.7}$$

Rolling motion of sprung mass

$$I_{xx}\ddot{\phi}-I_{xz}\ddot{\psi}=m_s h_s\left(\dot{v}+\dot{\psi}u\right)+m_s h_s g\sin(\phi)-\left(k_{\phi f}+k_{\phi r}\right)\phi-\left(c_{\phi f}+c_{\phi r}\right)\dot{\phi} \tag{2.8}$$

where m_s denotes the sprung mass, h_s the height from the longitudinal axis of the vehicle to the rolling axis, $k_{\phi f}$ and $k_{\phi r}$ the front and rear roll stiffness coefficient, respectively, $c_{\phi f}$ and $c_{\phi r}$ the front and rear roll dumping coefficient, respectively, I_{xx} and I_{zz} the rolling and yawing inertial moments, respectively, I_{xz} the product of inertia related to yawing and rolling, M_z the total moment on vehicle's yaw axis, and g the gravitational acceleration.

The relationship of the force and the yaw moment on the vehicle-body's CG with the forces generated in each tire is given by:

$$\begin{aligned}
\sum F_y &= F_{yfl}+F_{yfr}+F_{yrl}+F_{yrr}\\
\sum F_x &= F_{xfl}+F_{xfr}+F_{xrl}+F_{xrr}\\
\sum M_z &= a\left(F_{yfl}+F_{yfr}\right)-b\left(F_{yrl}+F_{yrr}\right)\\
&\quad+\frac{t_f}{2}\left(F_{xfr}-F_{xfl}\right)-\frac{t_r}{2}\left(F_{xrr}-F_{xrl}\right)
\end{aligned} \tag{2.9}$$

where a denotes the distance from the front axis to CG, b the distance from the rear axis to CG, t_f and t_r the front and rear track width, respectively, and F_{xi} and F_{yi} are the resultant longitudinal and lateral forces on vehicle's CG generated by the forces acting on the i-th tire, respectively,

which are obtained as follows:

$$\begin{pmatrix} F_{xi} \\ F_{yi} \end{pmatrix} = \begin{pmatrix} cos(\delta_i) & sin(\delta_i) \\ -sin(\delta_i) & cos(\delta_i) \end{pmatrix} \begin{pmatrix} F_{wxi} \\ F_{wyi} \end{pmatrix} \tag{2.10}$$

where $i \in fl, fr, rl, rr$, in which fl, fr, rl, rr index the front-left, front-right, rear-left and rear-right tires, respectively, and δ_i is the steering angle of i-th tire.

2.1.2 Tire dynamics

The forces are generated on the tire by the deformation of the rubber, in contact with the road, which occurs when there is a relative speed between the tire and the road [31]. This relative speed may be decomposed in longitudinal and lateral components. The longitudinal component is observed by the tire slip ratio, which is the relative difference between the rolling speed of the tire and the longitudinal speed of the vehicle. And the lateral component is observed by the tire-slip angle, which is the angle between the tire longitudinal axis and its direction of motion, i.e. the angle between the tire's direction of motion and longitudinal axis. Figure 2.2 illustrate the tire slip angle. The tire slip ratio λ_i and slip angle α_i of each tire is given by [34]:

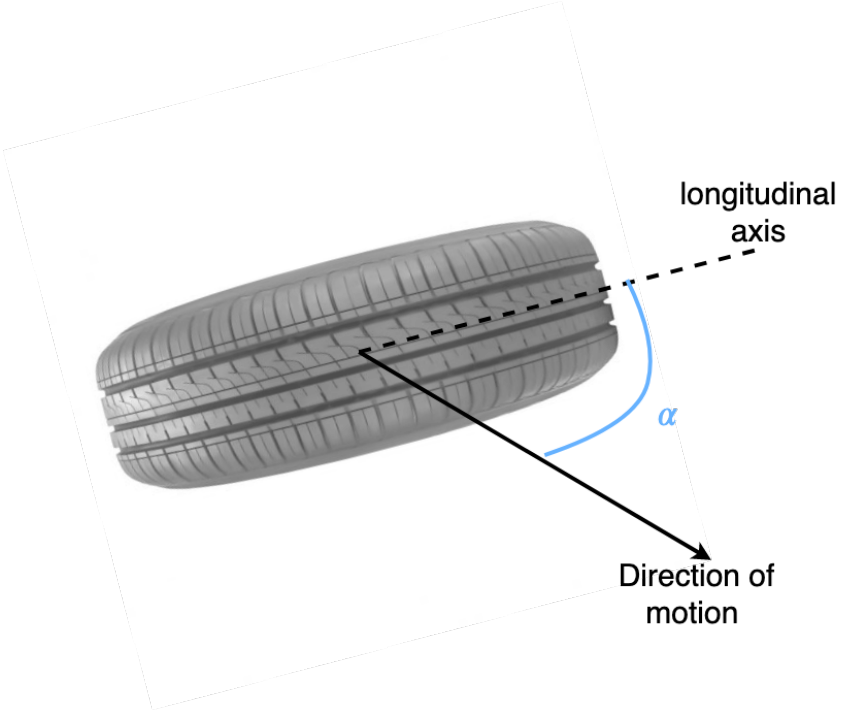

Figure 2.2: Illustration of the tire slip angle, which is the angle between the tire longitudinal axis and its direction of motion

$$\lambda_i = \begin{cases} \dfrac{\omega_i R_{eff} - v}{\omega_i R_{eff}}, & \text{if } \omega_i R_{eff} > v \\ \dfrac{v - \omega_i R_{eff}}{v}, & \text{otherwise} \end{cases} \tag{2.11}$$

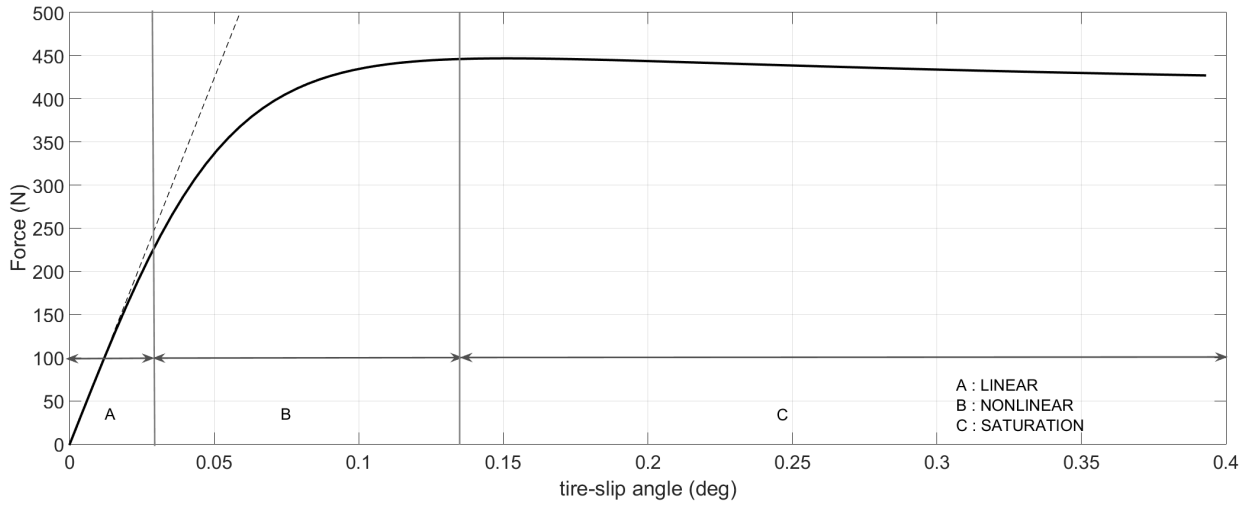

Figure 2.3: Operating regions of lateral force generation on tyre: Linear, non-linear and saturation.

$$\begin{aligned} \alpha_{fl} &= \delta_f - \arctan\left(\frac{v + a\dot{\psi}}{u - \frac{t_f}{2}\dot{\psi}}\right) \qquad \alpha_{fr} = \delta_f - \arctan\left(\frac{v + a\dot{\psi}}{u + \frac{t_f}{2}\dot{\psi}}\right) \\ \alpha_{rl} &= -\arctan\left(\frac{v - b\dot{\psi}}{u - \frac{t_r}{2}\dot{\psi}}\right) \qquad \alpha_{rr} = -\arctan\left(\frac{v - b\dot{\psi}}{u + \frac{t_r}{2}\dot{\psi}}\right) \end{aligned} \tag{2.12}$$

where ω_i is the angular speed of the i-th tire and R is the effective radius.

According to these slip values, the force generation on tires may be split into three regions with distinct behavior: linear, nonlinear and saturation. Figure 2.3 presents these three regions in the generation of lateral forces in response to the slip angle. The behavior for longitudinal force generation in response to the slip ratio is analogous. For low tire slip, the tire dynamics is in the linear region where the relations between the longitudinal force and the slip ratio and between the lateral force and tire-slip angle are approximately linear.

As the slip increases, the tire dynamics enter the nonlinear region, in which the amount of rubber element available to deform reduces, so the force becomes less responsive to the slip changing, and the non-linearities of tire dynamics are more noticeable, such that the relation between the forces generated and the slips are no longer approximately linear. In this condition, the vehicle motion becomes less responsive to the acceleration, braking and steering commands. When the force reaches the maximum, the treads start to saturate and the tire dynamics enter the saturation region, in which then the force decreases until all elements become saturated.

The forces generated on tires are governed by complex rules that depend on many parameters, e.g. tire-road friction, tire shape, inner pressure, vertical load, the side-slip angle. The Magic Formula (MF) of Pacejka is an empirical formulation derived from experimental tests that can be used to compute forces acting on tires, as shown in [31]. In the general formulation of MF, the forces acting on a tire is obtained as follows:

$$F(\kappa) = D\sin(Sv_i C\arctan(B(1-E)(\kappa + Sh_i) + E\arctan(B(\kappa + Sh_i)))) \tag{2.13}$$

in which, for computation of the lateral force F_{yi} of i-th, the argument κ is the tire side-slip angle α_i and B, C, D, E, Sh_i, Sv_i are defined by MF coefficients a_n as follows:

$$\begin{aligned} C &= a_0 \\ D &= F_{zi}(a_1 F_{zi} + a_2) \\ B &= \frac{a_3 \sin(2 \arctan \frac{F_{zi}}{a_4})}{CD}(1 - a_5 |\gamma_i|) \\ E &= a_6 F_{zi} + a_7 \\ Sh_i &= a_8 \gamma_i + a_9 F_{zi} + a_{10} \\ Sv_i &= \left(a_{11} F_{zi}^2 + a_{12} F_{zi}\right) \gamma_i + a_{13} F_{zi} + a_{14} \\ i &= fl, fr, rl, rr \end{aligned} \tag{2.14}$$

in which γ_i denotes the camber angle, which is the angle between the plane of rotation of the tire and the normal axis of the track as shown in Figure 2.4.

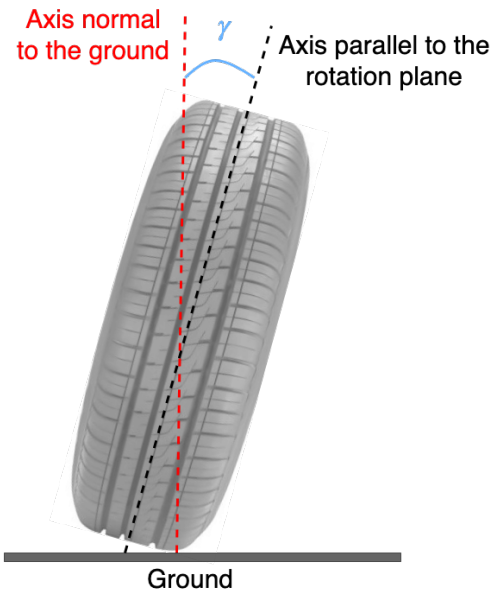

Figure 2.4: Illustration of the tire camber angle, which is the angle between the plane of ration of the tire and axis normal to the ground.

In addition to its influence on load transference, the roll motion also affects the camber angle of the wheels, the camber response to the roll motion depends on the sprung system. However, the study of the effect of specific sprung designs on stability performance is not included in this research. Taking into account the effects of roll motion on tire dynamics, the camber angle of four wheels are considered ideally the same, simplified as follows:

$$\gamma = K_\gamma \phi \tag{2.15}$$

where ϕ is the roll angle, K_γ denotes the camber-by-roll gradient, which represents variation of camber due to rolling given by $K_\gamma = \frac{\partial \gamma}{\partial \phi}$ [35].

An important parameter of the vehicle dynamics is the cornering stiffness coefficient, which is the variation of lateral force in relation to slip angles for small angles, i.e. the slope of the linear approximation for small angles, obtained as follows [36, 31]:

$$C_\alpha = \left.\frac{\partial F_{wy}}{\partial \alpha}\right|_{\alpha,\gamma=0} = BCD. \tag{2.16}$$

For computation of longitudinal force F_{xi} of i-th wheel, the argument x of Equation 2.13 is the tire slip ratio λ_i and B, C, D,E, Sh_i, Sv_i are defined by MF coefficients $b_n, \quad n = 0, 1 \ldots 14$ as follows:

$$\begin{aligned} C &= a_0 \\ D &= F_{zi}(b_1 F_{zi} + b_2) \\ B &= \frac{b_3 \sin(2 \arctan \frac{F_{zi}}{b_4}) \exp(b_5 F_{zi})}{CD} \\ E &= b_6 F_{zi}^2 + b_7 F_{zi} + b_8 \\ Sh_i &= b_9 F_{zi} + b_{10} \\ Sv_i &= 0 \\ i &= fl, fr, rl, rr \end{aligned} \tag{2.17}$$

Considering the wheel-tire set to be a solid body, the longitudinal force generated in the tire is related to angular velocity of the wheel by the following equation or rotational motion:

$$I_w \dot{\omega} = T - R_{eff} F_x \tag{2.18}$$

in which I_w is the moment inertia of the wheel about the axis of rotation, R_{eff} is the effective rolling radios, T is the torque transferred to the wheel and F_x is the longitudinal force in the tire.

The vertical load on each wheel is given by the vehicle weight transferred to it. When the vehicle is moving, the vertical force in each wheel is given by [28, 34]:

$$\begin{aligned} F_{zfl} &= \frac{mgb}{2l} - \frac{m\dot{u}h}{2l} - \frac{m\dot{v}ah}{lt_f} - \frac{k_{\phi f}\phi}{t_f} - \frac{c_{\phi f}\dot{\phi}}{t_f} \\ F_{zfr} &= \frac{mgb}{2l} - \frac{m\dot{u}h}{2l} + \frac{m\dot{v}ah}{lt_f} + \frac{k_{\phi f}\phi}{t_f} + \frac{c_{\phi f}\dot{\phi}}{t_f} \\ F_{zrl} &= \frac{mga}{2l} + \frac{m\dot{u}h}{2l} - \frac{m\dot{v}ah}{lt_r} - \frac{k_{\phi r}\phi}{t_r} - \frac{c_{\phi r}\dot{\phi}}{t_r} \\ F_{zrr} &= \frac{mga}{2l} + \frac{m\dot{u}h}{2l} + \frac{m\dot{v}ah}{lt_r} + \frac{k_{\phi r}\phi}{t_r} + \frac{c_{\phi r}\dot{\phi}}{t_r} \end{aligned} \tag{2.19}$$

in the above equations, h denotes the height of the center of gravity, a the distance from longitudinal track to vehicle's CG, b the distance from lateral track to vehicle's CG, $\dot{u}$ the longitudinal acceleration of vehicle-body, $\dot{v}$ the lateral acceleration of vehicle-body, m the vehicle total mass, t_f the front track width, t_r the rear track width, g the gravitational acceleration, and l the wheelbase.

From Equation 2.19, one can see that the load transference between tires is affected by the vehicle's acceleration and roll motion.

The roll motion also affects the steering angle of wheels, which may be obtained by the sum of a portion generated by the roll motion and a portion generated by the driver's command. For a passenger car, where only front wheels are controlled by the steering wheel, the front and rear steer angles can be obtained as follows:

$$\begin{pmatrix} \delta_{fl} \\ \delta_{fr} \\ \delta_{rl} \\ \delta_{rr} \end{pmatrix} = \mathbf{G}_\delta \delta_D + \begin{pmatrix} \frac{\partial \delta_f}{\partial \phi} \\ \frac{\partial \delta_f}{\partial \phi} \\ \frac{\partial \delta_r}{\partial \phi} \\ \frac{\partial \delta_r}{\partial \phi} \end{pmatrix} \phi \tag{2.20}$$

$$\mathbf{G}_\delta = \begin{pmatrix} 1/I_s & 1/I_s & 0 & 0 \end{pmatrix}^T$$

where δ_D is the steering wheel angle, I_s is the steering coefficient, and $\partial\delta_r/\partial\phi$ and $\partial\delta_f/\partial\phi$ are rear and front steer-by-roll coefficient, respectively.

2.1.3 Intelligent Driver Model

The lateral stability of the vehicle in a maneuver depends on how the driver behaves in the steering control. The steering instability is not determined only by the vehicle dynamics, but it occurs when the driver that is driving the vehicle loses the control, no matters if an ideal skillful driver would be able to drive the same vehicle in the same condition. Therefore, the driver behavior in the steering command should be considered in the lateral stability analysis.

By analyzing the model of vehicle dynamics presented, one can see that the driver input δ_D has a strong influence on vehicle dynamics because it controls the steering angle of the wheels (Eq. 2.20), which affects the tire slip angle (Eq. 2.12, which changes the lateral force generated on the tire (Eq. 2.14), which influences the lateral and yaw motion of vehicle body (Eq. 2.6 and 2.7), which affects the roll motion of vehicle body and the load distribution between the wheels (Eq. 2.8 and 2.19).

In [37], a model is proposed to simulate an intelligent human driver controlling the steering wheel. This model considers that the driver controls the yaw rate to achieve a speed direction for moving towards a target point A at a distance of L_a from the current position. The feedback signals observed by this simulated driver are the current lateral position y_{os}, the desired position lateral $\mathbf{y}_d$ and the yaw angle ψ. Figure 2.5b shows the block diagram of the control law used to

simulate the driver behavior to obtain a steering wheel angle of δ_D. The parameters of this model are the distance L_a from the vehicle position to target point, actuation delay T_k and steering gain W that represents driver expertise. The Fig. 2.5a illustrates this model.

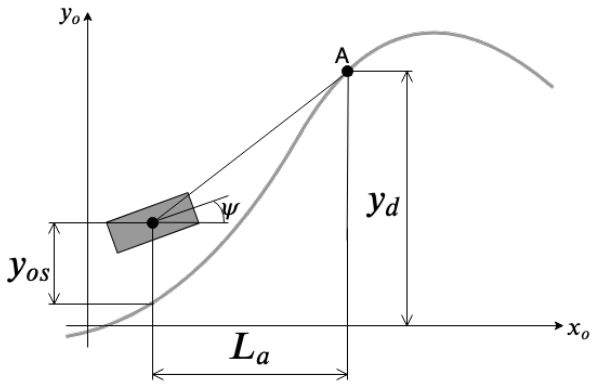

(a) Illustration of driver modeling.

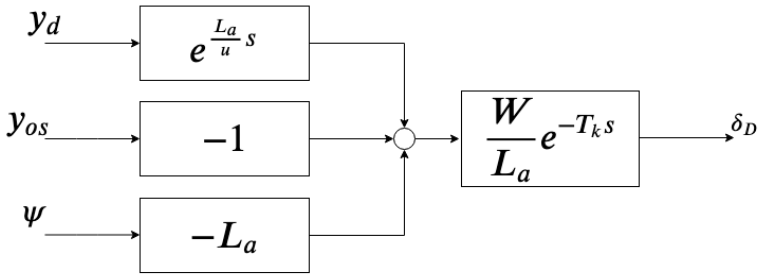

(b) Block diagram of the driver model.

Figure 2.5: Intelligent driver model. Adapted from [37]

2.2 ELECTRONIC STABILITY CONTROL

Traffic fatalities are a concern of nations' governments because of its consequences for mortality rates, health, mobility, and economy. As the number of vehicles on the roads growths, the need for actions to improve traffic safety increases as well. The development of safer vehicles is an efficient action to enhance traffic safety. The automotive design can reduce risk factors by including in commercial car features that reduce the probability of accident occurrence and limit their effects when an accident happens. Automotive safety systems can be grouped into two classes: passive safety and active safety:

Passive safety aims at reducing the damages of accidents. It includes mainly structural designs and materials used to prevent or reduce injuries to passengers, during an accident, e.g. mounting parts that are deformed by a collision in a controlled manner to prevent impact transfer to passengers and limit deceleration. ECUs are primarily used in these systems for detecting events such as collision and rollover to trigger actions like airbag activation.

Active safety aims at reducing the possibilities for an accident occurs. The safety performance

may be increased by improving the driver and the vehicle behaviors. Active safety systems can help the driver to exhibit a better response by providing useful information for accident avoidance, (e.g vehicle or pedestrian alerts), and they can enhance the vehicle by directly controlling the steering systems to increase the maneuverability or to reduce the accident risk (e.g electronic stability controllers and anti-lock braking systems (ABS)). Due to the sensing, processing and actuation requirements, active safety features are usually included in vehicles using electronic systems.

Active safety systems have been proposed since the early 1980s [38]. Some of these are Anti-lock braking system (ABS), which reduces the braking distance and prevent the wheels from locking during the braking, [39, 40], Lane departure warning [41], which warns the driver about the lane exiting risk, Adaptive Cruise Control (ACC), which controls vehicle speed to keep a safe distance from a vehicle ahead [42], and Tyre Pressure Monitoring System (TPMS), which warns the driver when the tire pressure is out of the safe range [43].

One of the main systems developed for vehicle directional control is the electronic stability control (ESC), also known as the vehicle stability control (VSC) and lateral stability control, and commercially labeled Electronic Stability Program (ESP). These systems assist in driving by controlling the lateral motion to track the path commanded by the driver, based on their understanding about the driver's intention, the vehicle behavior and its current state. The knowledge of vehicle dynamics is added to ESC by using model-based control techniques. However, there is always a discrepancy between the actual vehicle behavior and the response predicted by mathematical models. Hence, an issue to be considered in ESC design is the model used in control design and the robustness of the control law to model uncertainties such as different road surface conditions, varying vehicle parameters, and crosswind disturbance.

The ESC aims to help in driving to keep the directional motion stable by improving the vehicle's response to the driver's command. From the driver's point of view, the movement remains stable while the vehicle behaves roughly as a linear system. Unfortunately, vehicle dynamics have nonlinearities that can make the direction of movement differ from the driver's intention. For this reason, the ESC's approach to action is to prevent vehicle dynamics from entering states where these nonlinearities are most notable.

These nonlinearities come mainly from the limit for the generation of forces on tires in response to the lateral sliding of the tires. Drivers are used to driving under normal conditions in which the vehicle exhibits an approximately linear response. Steering becomes unstable as the forces generated by the tires approach saturation limits. In this condition the vehicle movement is less responsive to the driver's commands, so the vehicle's response to the driver's commands is very different from that expected by the driver, causing the driver to lose control of the steering and the vehicle to get off track. Therefore, the correction of the lateral motion of the vehicle plays a significant role in keeping the handling stability [44].

2.2.1 Control objectives

The lateral stability performance is improved by control of vehicle yaw rate and vehicle body side-slip angle denoted by ψ and β in Figure 2.1, respectively [45]. Since the yaw rate control helps to maintain the rate and direction of yaw motion required to keep the vehicle properly oriented on the road to follow the desired path. The desired yaw rate ψ_d tracked by the controller is given by the following reference model [46]:

$$\begin{aligned} \dot{\psi}_d =& min\left(\left|\frac{u\delta_f}{l + lK_u u^2}\right|, \left|\frac{\mu g}{u}\right|\right) sign(\delta_f) \\ K_u =& \frac{m}{l^2}\left(\frac{b}{C_{\alpha r}} - \frac{a}{C_{\alpha f}}\right) \end{aligned} \tag{2.21}$$

in which $C_{\alpha f}$ and $C_{\alpha r}$ denote the cornering stiffness coefficient of the front and rear track, respectively.

However, maintaining the required orientation is not enough, the vehicle must maintain the desired positioning on the road, which is achieved by the side-slip correction that helps to prevent the vehicle from slip sideways from the desired path. For the steady-state condition, the desired side-slip angle is always zero, that is, $\beta_d = 0$ [46].

The side-slip control also helps prevent handling instability. As can be seen in Figure 4.11, at a high side-slip angle, the forces generated on tires as a reaction to the lateral movement starts to decrease with the increasing of the side-slip angle. In a dry asphalt, the handling becomes unstable when the side-slip reaches ± 12 degrees, and in a wet asphalt, this stability margin is reduced to ± 2 degrees [47, 38, 30, 3].

2.2.2 Actuation strategy

The ESC assists in driving by directly controlling the actuation system of vehicle chassis. Regarding the actuation, there are two actuation strategies widely used in lateral stability control: the Direct Yaw-moment Control (DYC) and Active Steering (AS) [46, 38].

Direct yaw control is an efficient method for lateral stability control [48, 47]. The DYC strategy consists of acting on torque transferred to each wheel to change the forces generated on tires, such that the corrective moment is generated on the yaw axis as a result of the differences between the forces acting on the tires.

Active steering (AS) is another efficient method for lateral stability control [49, 50]. In AS, extra steering input is added to the steering commanded by the driver, such that the resultant steer angle drives the vehicle through the desired path. Active steering can be classified according to the set of wheels in which it operates, that is active front steering (AFS) control, active rear steering (ARS) control, and four-wheel active steering (4WAS) control.

A disadvantage of the AS is the saturation of the forces acting on tires that become less responsive to the steering angle, at high tire slipping, which means the reduction of AS control capability. Whereas, at high tire slipping, the forces acting on tires remain sensitive to the torque transferred to the wheels. In this condition, the nonlinearities of the vehicle dynamics are more influence on vehicle response, which makes the driving quite difficult for a not skillful driver. The DYC remains effective in the nonlinear region of tire lateral force, the actuation by interference on wheel rotation has undesired effects on the longitudinal vehicle motion. A few works have proposed to integrate the DYC and AS strategy, this strategy can be referred to as integrated vehicle dynamics control (IVDC).

2.3 CONTROL THEORIES

The vehicle model presented in the previous section is a highly coupled system with multiple inputs and multiple outputs (MIMO), where there is a strong influence of the states on each other. The control strategies for such systems are usually designed based on models that represent the relationship between inputs and outputs by a set of equations.

The use of simpler models can simplify the computational complexity of control algorithms. For controllers with digital circuits that provide a periodic update of commands, discrete-time modeling is used to simplify the mathematical representation of the control law and the controlled process response to the periodic update of the commands. Another strategy is to simplify the process in linear time-invariant (LTI) systems. A classical representation in control theory to represent LTI systems is the state-space representation. Where each dynamics is represented by a variable called state, and the model is composed of equations of the time variation of each state as a function of the set of states. The generic discrete-time state-space representation of LTI systems is:

$$\begin{aligned} \mathbf{x}(k+1) &= \mathbf{A}\mathbf{x}(k) + \mathbf{B}\mathbf{u}(k) \\ \mathbf{y}(k) &= \mathbf{C}\mathbf{x}(k) + \mathbf{D}\mathbf{u}(k) \end{aligned} \tag{2.22}$$

where:

- k is the current discrete-time instant;
- $\mathbf{x} \in \mathbb{R}^{n_x}$ is the vector of system's states, and n_x is the number of states;
- $\mathbf{u} \in \mathbb{R}^{n_u}$ is the vector of control signals and n_u is the number of inputs;
- $\mathbf{y} \in \mathbb{R}^{n_y}$ is the vector of system's output and n_y is the number of outputs;
- $\mathbf{A} \in \mathbb{R}^{n_x \times n_x}$ is the state matrix;

- $\mathbf{B} \in \mathbb{R}^{n_x \times n_u}$ is the input matrix;
- $\mathbf{C} \in \mathbb{R}^{n_y \times n_x}$ is the output matrix;
- $\mathbf{D} \in \mathbb{R}^{n_y \times n_u}$ is the feedward matrix.

This definition is a basic concept for the control theories applied in this research, where the commands are calculated from the feedback of the output vector $\mathbf{y}$, and the matrices A, B, C, and D are inputs of the design of the control algorithms.

2.3.1 Optimal Control

The optimal control theory is a successful class of control techniques that have been applied to several fields such as biology, economics, ecology, engineering, finance, management, and medicine. In these techniques, the control signals are defined by solving an optimization problem [51].

The optimization problem is a mathematical abstraction of the problem of search for the best choice of values within a set of candidates, which has the form [52].

$$\begin{aligned} \text{minimize or maximize} \quad & J(\mathbf{s}) \\ \text{subject to} \quad & f_i(\mathbf{s}) \leq b_i \quad i = 1, \ldots, m \end{aligned} \tag{2.23}$$

In Eq. 2.23, the vector $\mathbf{s} \in \mathbb{R}^{n_s}$ is the optimization variable (model's inputs) and n_s is the number of variables of the optimization, the function $J : \mathbb{R}^{n_s} \to \mathbb{R}$ is the objective function, also known as cost function, and the inequations $f_i : \mathbb{R}^{n_s} \to \mathbb{R} \leq b_i$ define the constraints imposed to the solution.

In optimal control, $\mathbf{s}$ is the vector of controlled inputs, the cost function is a function of states and inputs of controlled process, and the inequality equations $f_i(\mathbf{s}) \leq b_i$ express the constraints imposed on search space for the optimal solution to address limitations or to meet some control requirements.

Optimization solving depends on the characteristics of the cost function and constraint set. Only a few problems have a known analytical solution. Fortunately, some problems without an analytical solution can be grouped into known classes that have an efficient numerical method to solve them, and good software implementations available. Therefore, a useful strategy for optimal control is the formulation of the problem in the form of a known class. Two important and well-known examples are linear programming (LP) and quadratic programming (QP) [52].

The QP is characterized by a quadratic cost function and linear constraint function as follows

$$
\begin{aligned}
J(\mathbf{s}) =& (1/2)\mathbf{s}^T\mathbf{P}\mathbf{s} + \mathbf{q}^T\mathbf{s} + r \\
f_i(\mathbf{s}) =& \mathbf{a}_i^T\mathbf{s}
\end{aligned}
\tag{2.24}
$$

where the vectors $\mathbf{q}, \mathbf{a}_1, \ldots, \mathbf{a}_m \in \mathbb{R}^{n_s}$, the matrix $\mathbf{P} \in \mathbb{R}^{n_s \times n_s}$ and the constant r are the parameters of the quadratic programming.

The LP is the special case of the QP when the elements of vector q and the matrix Q are equal to zero, such that the cost function and constraint function are linear as follows:

$$
\begin{aligned}
J(\mathbf{s}) &= \mathbf{c}^T\mathbf{s} \\
f_i(\mathbf{s}) &= \mathbf{a}_i^T\mathbf{s}
\end{aligned}
\tag{2.25}
$$

where the vectors $\mathbf{c}, \mathbf{a}_1 \ldots, \mathbf{a}_m \in \mathbb{R}^{n_s}$ are the parameters of the linear programming.

There is no simple analytical solution for QP. Fortunately, there are some effective methods for solving them. One of those methods is the active set method. It solves QP by estimating the set of equality linear-constraints satisfied only at the optimal point so that these constraints form a linear system of equations whose solution is equivalent to the QP solution. Its interactions consist of solving a linear system composed of the estimated constraints equations and then updating the estimate based on the value of the cost function for the linear system. This class of algorithms is computationally efficient for small-to-medium scale QPs. An example of solver using this method is the quadprog function provided by Matlab software. Another example is the qpOASES, which is a C++ implementation presented in [53], popularly used in the implementation of embedded applications for on-line solving optimizations.

2.3.2 Model Predictive Control

Model Predictive Control (MPC) is an optimal method, in which the control signals are obtained from solution of an optimization problem, whose cost function is based on the open-loop response of the controlled system over a finite horizon. The optimization is performed at each sampling time to obtain the optimal sequence of periodic updates of the control sequence, whose first value is applied to the control signals [20, 25, 54]. Figure 2.6 illustrate the MPC method.

The optimization problem is formulated by defining a cost function in terms of the control performance over the prediction horizon, such that the solution is the sequence of periodic updates of the control signals that minimize this function. The prediction of the control performance over the prediction horizon comes from the definition of the cost function based on the open-loop model of the controlled system. Constraints can be imposed on the optimization problem so that only feasible commands that do not take controlled systems to the unstable zones are given as a solution [25, 54, 20].

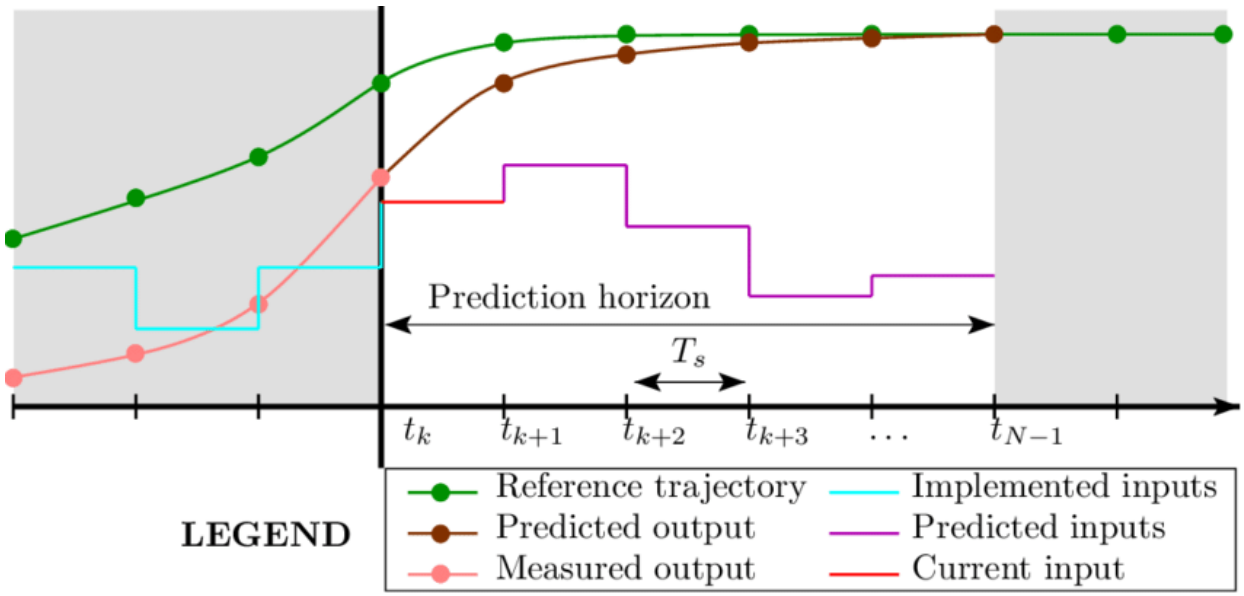

Figure 2.6: Characteristic behavior of Model Predictive Control. Figure obtained from [55]

The control algorithm of the MPC method consists of performing the following steps at each sampling instant:

1. Measure the states of the controlled system;
2. Update the constraints of the optimization problem;
3. Solve the constrained optimization problem to obtain the optimal sequence;
4. Update the control signals with the first element of the optimal sequence.

A benefit that justifies using MPC is its ability to handle constraints. The MPC is capable of providing commands that respect the physical constraints of the actuation system and imposing state constraints so that the command does not take states out of the restricted range. Another reason for using MPC is its ability to adapt to process conditions. The QP and its constraints can be updated at each sampling time so that control objectives are adapted to the current system condition.

These benefits are the result of developments and research conducted in the field of control theory and digital electronics. The following topic presents an introduction to the history of MPC and then presents the theoretical aspects of the formulation used in this research.

2.3.2.1 MPC for linear time-invariant systems

In [25], an MPC formulation is presented for the control of systems represented by Linear Time-invariant (LTI) models. In this formulation, the optimization problem is defined in the QP form, whose cost function penalizes the mean square error of regulated outputs and the power of control sequence over the prediction horizon. The search space is limited within a convex region

by linear constraints imposed to avoid solutions that cannot be performed by the actuator system or that drive states out of acceptable range.

This QP is defined based on the state-space model of the open-loop system to include the prediction of states in response to the control sequence. The control sequence of N samplings of control signal starting at the instant k is denoted by:

$$\tilde{\mathbf{u}}(k) = \begin{pmatrix} \mathbf{u}_c(k) \\ \mathbf{u}_c(k+1) \\ \vdots \\ \mathbf{u}_c(k+N-1) \end{pmatrix} \in \mathbb{R}^{Nn_u} \tag{2.26}$$

where $\mathbf{u}_c(k+i) \in \mathbb{R}^{n_u}$ is the command vector in the i-th instant after the instant k, and n_u is the number of system's inputs controlled by the MPC. And the resultant sequence of states obtained in response to the control sequence $\tilde{\mathbf{u}}(k)$ is denoted by:

$$\tilde{\mathbf{x}}(k) = \begin{pmatrix} \mathbf{x}(k+1) \\ \mathbf{x}(k+2) \\ \vdots \\ \mathbf{x}(k+N) \end{pmatrix} \in \mathbb{R}^{Nn_x} \tag{2.27}$$

where $\mathbf{x}(k+i) \in \mathbb{R}^{n_x}$ is the state vector in the i-th instant after the instant k, and n_x is the number of system's states.

The states at any sampling instant are predicted from the current states and the future control sequence by the following equation derived from the state-space model:

$$\mathbf{x}(k+i) = \Theta_i \mathbf{x}(k) + \Xi_i \tilde{\mathbf{u}}(k)$$

$$\Theta_i = \mathbf{A}^i \in \mathbb{R}^{n_x \times n_x} \qquad \Xi_i = \begin{pmatrix} \mathbf{A}^{i-1}\mathbf{B} \\ \vdots \\ \mathbf{AB} \\ \mathbf{B} \end{pmatrix} \begin{pmatrix} \Upsilon_1^{(n_\mathrm{u},N)} \\ \Upsilon_2^{(n_\mathrm{u},N)} \\ \vdots \\ \Upsilon_i^{(n_\mathrm{u},N)} \end{pmatrix} \in \mathbb{R}^{n_x \times N n_\mathrm{u}} \tag{2.28}$$

In Eq. 2.28, Θ_i and Ξ_i are the state and input prediction matrices, respectively, $\mathbf{A}$ and $\mathbf{B}$ are the matrix of the discrete-time state-space model (Eq 2.22), and $\Upsilon_i^{(n,N)}$ is the selection matrix defined as:

$$\Upsilon_i^{(n,N)} = \begin{pmatrix} \mathbb{O}_{n \times n(i-1)} & \mathbb{I}_n & \mathbb{O}_{n \times n(N-i)} \end{pmatrix} \in \mathbb{R}^{n \times Nn} \tag{2.29}$$

where $\mathbb{O}_{n_1,n_2} \in \mathbb{R}^{n_1 \times n_2}$ is a zero matrix, and $\mathbb{I}_n \in \mathbb{R}^{n \times n}$ is a identity matrix. The matrix $\Upsilon_i^{(n,N)}$ is called selection matrix because it selects the i-th n-dimension vector from the vector composed by the concatenation of N n-dimension vectors, such that $\Upsilon_i^{(n_u,N)}\tilde{\mathbf{u}}(k) = \mathbf{u}_c(k+i-1)$ and $\Upsilon_i^{(n_x,N)}\tilde{\mathbf{x}}(k) = \mathbf{x}(k+i)$.

This MPC formulation enables the control of outputs defined as a linear combination of the states, so the regulated vector composed of the regulated outputs is defined as:

$$\mathbf{y_r}(k) = \mathbf{C}_r\mathbf{x}(k) \tag{2.30}$$

where $\mathbf{y_r} \in \mathbb{R}^{n_r}$ is the regulated vector composed of n_r regulated outputs, and $\mathbf{C}_r \in \mathbb{R}^{n_r \times n_x}$ is the regulation matrix that relates the regulated outputs to the states.

The cost function of MPC formulation is updated dynamically at each sampling instant k depending on current states $\mathbf{x}(k)$, desired regulated-output $\mathbf{y}_d(k) \in \mathbb{R}^{n_c}$ and desired input $\mathbf{u}_d \in \mathbb{R}^{n_u}$, as follows:

$$J(k) = \sum_{i+1}^{N} |\mathbf{y}(k+i) - \mathbf{y}_d(k+i)|^2_{\mathbf{Q_y}} + \sum_{i+1}^{N} \left| \Upsilon_i^{(n_u,N)}\tilde{\mathbf{u}}(k) - \tilde{\mathbf{u}}_d \right|^2_{\mathbf{Q_u}} \tag{2.31}$$

in which, $\mathbf{Q_u} \in \mathbb{R}^{n_u \times n_u}$ is a symmetric positive weighting matrix that penalizes command's difference from its desired value, and $\mathbf{Q_y} \in \mathbb{R}^{n_c \times n_c}$ is a symmetric weighting matrix that defines the penalty of the tracking error of each controlled output. The Equation 2.31 can be expanded in the QP representation whose decision variable is $\tilde{\mathbf{u}}(k)$:

$$\begin{aligned}
J(k) =& \frac{1}{2}\tilde{\mathbf{u}}^T(k)\mathbf{H}\tilde{\mathbf{u}}(k) + \mathbf{F}^T(k)\tilde{\mathbf{u}}(k) \\
H =& 2\sum_{i=1}^{N}\left[\Theta_i^T\mathbf{C}_r^T\mathbf{Q_y}\mathbf{C}_r\Xi_i + (\Upsilon_i^{(n_u,N)})^T\mathbf{Q_u}(\Upsilon_i^{(n_u,N)})\right] \\
F(k) =& \left(2\sum_{i=1}^{N}\Theta_i^T\mathbf{C}_r^T\mathbf{Q_y}\mathbf{C}_r\Theta_i\right)\mathbf{x}(k) \\
&- \left(2\sum_{i=1}^{N}\Theta_i^T\mathbf{C}_r^T\mathbf{Q_y}\mathbf{C}_r\Upsilon_i^{(2,N)}\right)\mathbf{y}_d \\
&+ \left(2\sum_{i=1}^{N}(\Upsilon_i^{(n_u,N)})^T\mathbf{Q_u}\right)\mathbf{u}_d
\end{aligned} \tag{2.32}$$

2.3.2.2 Constrains of MPC solution

Without constraints and with an infinite-prediction horizon, the quadratic problems have an analytical solution determined by the Riccati equation. Using this solution to obtain the control signals is what defines the LQR technique [56, 57]. In the MPC method, the commands are obtained by solving an optimization problem for a finite-prediction horizon and constraints, which can be updated dynamically depending on the current states of the controlled process [20, 54]. In the MPC formulation presented in [25], the optimal command sequence $\tilde{u}$ is obtained by minimizing the cost function (2.32) taking into account the constraints on the states and control signals, or any linear combination of them, which are linear constraints represented by the following inequality:

$$\mathbf{A}_{\text{ineq}}\tilde{\mathbf{u}} \leq \mathbf{B}_{\text{ineq}} \tag{2.33}$$

where $\mathbf{A}_{\text{ineq}} \in \mathbb{R}^{n_{\text{const}} \times (n_{\mathbf{u}} N)}$ is a constant matrix, and $\mathbf{B}_{\text{ineq}} \in \mathbb{R}^{n_{\text{const}}}$ is updated, at each sampling instant, in function of the current states and control signals.

The output restriction, command restriction, and command variation restriction are applied to the system in the formulation presented in [25]. Each of these constraints has a maximum and a minimum limit, as follows:

$$\begin{aligned} &\mathbf{y}_c^{\min} \leq \mathbf{y}_c(k) \leq \mathbf{y}_c^{\max} \\ &\boldsymbol{\delta}^{\min} \leq \mathbf{u}(k+i) - \mathbf{u}(k+i-1) \leq \boldsymbol{\delta}^{\max} \\ &\mathbf{u}^{\min} \leq \mathbf{u}(k) \leq \mathbf{u}^{\max} \end{aligned} \tag{2.34}$$

where

- $\mathbf{y}_c \in \mathbb{R}^{n_r}$ is the constrained output;
- $\mathbf{y}_c^{\min}, \mathbf{y}_c^{\max} \in \mathbb{R}^{n_r}$ are the minimum and maximum limits of the constrained output;
- $\boldsymbol{\delta}^{\min}, \boldsymbol{\delta}^{\max} \in \mathbb{R}^{n_u N}$ are the minimum and maximum limits of the commands between two consecutive sampling instants;
- $\tilde{\mathbf{u}}^{\min}, \tilde{\mathbf{u}}^{\max} \in \mathbb{R}^{n_u N}$ are the minimum and maximum limits of the control sequence.

The constrained output vector at the i-th instant of the prediction horizon starting at the sampling k is given by a linear combination of the states in the same instant and previous command vector:

$$\mathbf{y}_c(k+i) = \mathbf{C}_c\mathbf{x}(k+i) + \mathbf{D}_c\mathbf{u}_c(k+i-1) = \mathbf{C}_c\Upsilon_i^{(n_x,N)}\tilde{\mathbf{x}}(k) + \mathbf{D}_c\Upsilon_i^{(n_u,N)}\tilde{\mathbf{u}}(k) \tag{2.35}$$

where $\mathbf{C}_c \in \mathbb{R}^{n_r \times n_x}$ is the restricted-output matrix, and $\mathbf{D}_c \in \mathbb{R}^{n_r \times n_u}$ is the feedward restricted-output matrix.

From equations (2.28) and (2.35), the constrained output $\mathbf{y}_c(k+i)$ in the i-th instant of the prediction horizon starting in the instant k is given by:

$$\mathbf{y}_c(k+i) = \mathbf{C}_c \Upsilon_i^{(n_x,N)} \Theta_i \mathbf{x}(k) + \left(\mathbf{C}_c \Upsilon_i^{(n_x,N)} \Xi_i + \mathbf{D}_c \Upsilon_i^{(n_u,N)} \right) \tilde{\mathbf{u}}(k) \tag{2.36}$$

So the set of output restriction for each instant in the prediction horizon is represented by:

$$\begin{pmatrix} \mathbf{y}_c^{\min} \\ \vdots \\ \mathbf{y}_c^{\min} \end{pmatrix} \leq \begin{pmatrix} \mathbf{C}_c \Upsilon_1^{(n_x,N)} \Theta_1 \\ \vdots \\ \mathbf{C}_c \Upsilon_N^{(n_x,N)} \Theta_N \end{pmatrix} \tilde{\mathbf{x}}(k) + \begin{pmatrix} \mathbf{C}_c \Upsilon_1^{(n_x,N)} \Xi_1 + \mathbf{D}_c \Upsilon_1^{(n_u,N)} \\ \vdots \\ \mathbf{C}_c \Upsilon_N^{(n_x,N)} \Xi_N + \mathbf{D}_c \Upsilon_N^{(n_u,N)} \end{pmatrix} \tilde{\mathbf{u}}(k) \leq \begin{pmatrix} \mathbf{y}_c^{\max} \\ \vdots \\ \mathbf{y}_c^{\max} \end{pmatrix} \tag{2.37}$$

which can be rewritten in the form:

$$\underbrace{\begin{pmatrix} +(\mathbf{C}_c \Upsilon_1^{(n_x,N)} \Xi_1 + \mathbf{D}_c \Upsilon_1^{(n_u,N)}) \\ \vdots \\ +(\mathbf{C}_c \Upsilon_N^{(n_x,N)} \Xi_N + \mathbf{D}_c \Upsilon_N^{(n_u,N)}) \\ -(\mathbf{C}_c \Upsilon_1^{(n_x,N)} \Xi_1 + \mathbf{D}_c \Upsilon_1^{(n_u,N)}) \\ \vdots \\ -(\mathbf{C}_c \Upsilon_N^{(n_x,N)} \Xi_N + \mathbf{D}_c \Upsilon_N^{(n_u,N)}) \end{pmatrix}}_{\mathbf{A}_{\text{ineq}}^{(1)}} \tilde{\mathbf{u}}(k) \leq \underbrace{\begin{pmatrix} -\mathbf{C}_c \Theta_1 \\ \vdots \\ -\mathbf{C}_c \Theta_N \\ +\mathbf{C}_c \Theta_1 \\ \vdots \\ +\mathbf{C}_c \Theta_N \end{pmatrix}}_{\mathbf{G}_1^{(1)}} \mathbf{x}(k) + \underbrace{\begin{pmatrix} +\mathbf{y}_c^{\max} \\ \vdots \\ +\mathbf{y}_c^{\max} \\ -\mathbf{y}_c^{\min} \\ \vdots \\ -\mathbf{y}_c^{\min} \end{pmatrix}}_{\mathbf{G}_3^{(1)}} \tag{2.38}$$

The set of constraints obtained from the command variation constraint for all sampling instant within the prediction horizon can be written as follows:

$$\begin{pmatrix} \boldsymbol{\delta}^{\min} \\ \boldsymbol{\delta}^{\min} \\ \vdots \\ \boldsymbol{\delta}^{\min} \end{pmatrix} \leq \begin{pmatrix} \mathbb{I}_{n_u} & \mathbb{O}_{n_u} & \mathbb{O}_{n_u} & \dots & \mathbb{O}_{n_u} & \mathbb{O}_{n_u} \\ -\mathbb{I}_{n_u} & \mathbb{I}_{n_u} & \mathbb{O}_{n_u} & \dots & \mathbb{O}_{n_u} & \mathbb{O}_{n_u} \\ \vdots & \vdots & \vdots & \vdots & \vdots & \vdots \\ \mathbb{O}_{n_u} & \mathbb{O}_{n_u} & \mathbb{O}_{n_u} & \dots & -\mathbb{I}_{n_u} & \mathbb{I}_{n_u} \end{pmatrix} \tilde{\mathbf{u}}(k) + \begin{pmatrix} -\mathbb{I}_{n_u} \\ \mathbb{O}_{n_u} \\ \vdots \\ \mathbb{O}_{n_u} \end{pmatrix} \mathbf{u}(k-1) \leq \begin{pmatrix} \boldsymbol{\delta}^{\max} \\ \boldsymbol{\delta}^{\max} \\ \vdots \\ \boldsymbol{\delta}^{\max} \end{pmatrix} \tag{2.39}$$

where $\mathbb{I}_{n_u}$ and $\mathbb{I}_{n_u}$ are the identity and zero matrices of the $\mathbb{R}^{n_u \times n_u}$ space.

The Eq. 2.39 can be rewritten in the form:

$$\underbrace{\begin{pmatrix} \mathbb{I}_{n_u} & \mathbb{O}_{n_u} & \mathbb{O}_{n_u} & \dots & \mathbb{O}_{n_u} & \mathbb{O}_{n_u} \\ -\mathbb{I}_{n_u} & \mathbb{I}_{n_u} & \mathbb{O}_{n_u} & \dots & \mathbb{O}_{n_u} & \mathbb{O}_{n_u} \\ \vdots & \vdots & \vdots & \vdots & \vdots & \vdots \\ \mathbb{O}_{n_u} & \mathbb{O}_{n_u} & \mathbb{O}_{n_u} & \dots & -\mathbb{I}_{n_u} & +\mathbb{I}_{n_u} \\ -\mathbb{I}_{n_u} & \mathbb{O}_{n_u} & \mathbb{O}_{n_u} & \dots & \mathbb{O}_{n_u} & \mathbb{O}_{n_u} \\ \mathbb{I}_{n_u} & -\mathbb{I}_{n_u} & \mathbb{O}_{n_u} & \dots & \mathbb{O}_{n_u} & \mathbb{O}_{n_u} \\ \vdots & \vdots & \vdots & \vdots & \vdots & \vdots \\ \mathbb{O}_{n_u} & \mathbb{O}_{n_u} & \mathbb{O}_{n_u} & \dots & \mathbb{I}_{n_u} & -\mathbb{I}_{n_u} \end{pmatrix}}_{\mathbf{A}_{\text{ineq}}^{(2)}} \tilde{\mathbf{u}}(k) \leq \underbrace{\begin{pmatrix} \mathbb{I}_{n_u} \\ \mathbb{O}_{n_u} \\ \vdots \\ \mathbb{O}_{n_u} \\ -\mathbb{I}_{n_u} \\ \mathbb{O}_{n_u} \\ \vdots \\ \mathbb{O}_{n_u} \end{pmatrix}}_{\mathbf{G}_2^{(2)}} \mathbf{u}(k-1) + \underbrace{\begin{pmatrix} \boldsymbol{\delta}^{\max} \\ \boldsymbol{\delta}^{\max} \\ \vdots \\ \boldsymbol{\delta}^{\max} \\ -\boldsymbol{\delta}^{\min} \\ -\boldsymbol{\delta}^{\min} \\ \vdots \\ -\boldsymbol{\delta}^{\min} \end{pmatrix}}_{\mathbf{G}_3^{(2)}} \tag{2.40}$$

The set of constraints obtained from the command constraint for all sampling instant within the prediction horizon starting at the discrete instant k can be represented as follows:

$$\underbrace{\begin{pmatrix} \mathbf{u}^{\min} \\ \vdots \\ \mathbf{u}^{\min} \end{pmatrix}}_{\tilde{\mathbf{u}}^{\min}} \leq \tilde{\mathbf{u}}(k) \leq \underbrace{\begin{pmatrix} \mathbf{u}^{\max} \\ \vdots \\ \mathbf{u}^{\max} \end{pmatrix}}_{\tilde{\mathbf{u}}^{\max}} \tag{2.41}$$

which can be rewritten as:

$$\begin{pmatrix} \mathbb{I}_{Nn_u} \\ -\mathbb{I}_{Nn_u} \end{pmatrix} \tilde{\mathbf{u}}(k) \leq \begin{pmatrix} \tilde{\mathbf{u}}^{\max} \\ -\tilde{\mathbf{u}}^{\min} \end{pmatrix} \tag{2.42}$$

where $\mathbb{I}_{Nn_u}$ is the identity matrix of the $\mathbb{R}^{Nn_u \times Nn_u}$ space.

Combining the equations (2.38), (2.40) and (2.42), the constraints on the decision variable $\tilde{\mathbf{u}}(k)$ can be express in the form of equation Eq. 2.33 with the matrix $\mathbf{A}_{\text{ineq}}$ and $\mathbf{B}_{\text{ineq}}$ defined by:

$$\mathbf{A}_{\text{ineq}} = \begin{pmatrix} \mathbf{A}_{\text{ineq}}^{(1)} \\ \mathbf{A}_{\text{ineq}}^{(2)} \\ \mathbb{I}_{Nn_u} \\ -\mathbb{I}_{Nn_u} \end{pmatrix} \qquad \mathbf{B}_{\text{ineq}} = \Big(\mathbf{G}_1 \mathbf{x}(k) + \mathbf{G}_2 \mathbf{u}_c(k-1) + \mathbf{G}_3 \Big) \tag{2.43}$$

$$\mathbf{G}_1 = \begin{pmatrix} \mathbf{G}_1^{(1)} \\ \mathbb{O}_{4Nn_u \times n_x} \end{pmatrix} \qquad \mathbf{G}_2 = \begin{pmatrix} \mathbb{O}_{2Nn_u \times n_u} \\ \mathbf{G}_2^{(2)} \\ \mathbb{O}_{2Nn_u \times n_u} \end{pmatrix} \qquad \mathbf{G}_3 = \begin{pmatrix} \mathbf{G}_3^{(1)} \\ \mathbf{G}_3^{(2)} \\ \tilde{\mathbf{u}}^{\max} \\ -\tilde{\mathbf{u}}^{\min} \end{pmatrix} \tag{2.44}$$

2.3.2.3 MPC parameterization

Alamir also presents in [25] an exponential parameterization of the MPC formulation to reduce the calculation time of the QP solving, by reducing the number of decision variables. In this parameterization, each of the control signals is decomposed over the prediction horizon into a linear combination of exponential signals as follows:

$$u_j(k+i) = \sum_{n=1}^{n_e^{(j)}} e^{-\eta_j^{(n)} i\tau} p_n^{(j)} \tag{2.45}$$

where k is the sample instant in which the prediction horizon starts, i is the sample index within the prediction-horizon, i.e. the number of sample periods since the prediction horizon start, τ is the sampling period, u_j is the jth control signal, i.e. the jth element of the control vector $\mathbf{u}_c$, $n_e^{(j)}$ is the number of exponential terms used in the parameterization of u_j, p_n^j is the nth parameter of the parameterization of u_j, $\eta_j^{(n)}$ is the time coefficient of the nth exponential term in the parameterization of u_j defined as fallows:

$$\eta_j^{(n)} = \frac{\eta_j}{(n-1)\xi + 1} \tag{2.46}$$

in which η_j and ξ are the tuning coefficients of the exponential parameterizations, which must be defined to make the exponential terms met the slew rate of the actuators response. Since the equation 2.45 is a linear combination, it can be write in the following compact form:

$$\mathbf{u}_c(k+i) = \begin{pmatrix} u_1(k+1) \\ u_2(k+1) \\ \vdots \\ u_{n_u}(k+1) \end{pmatrix} = \Upsilon_e^{(i)} \mathbf{p}(k) \tag{2.47}$$

where $\Upsilon_e^{(i)}$ is the parameterization matrix that according the Equation 2.45 relates the command vector $u_c(k+i)$ with the parameter vector $\mathbf{p}$, which is defined as:

$$\mathbf{p} = \begin{pmatrix} \mathbf{p}^{(1)} \in \mathbb{R}^{n_e^{(1)}} \\ \vdots \\ \mathbf{p}^{(n_\mathrm{u})} \in \mathbb{R}^{n_e^{(n_\mathrm{u})}} \end{pmatrix} \qquad \mathbf{p}^{(j)} = \begin{pmatrix} p_1^{(j)} & \dots & p_{n_e^{(j)}}^{(j)} \end{pmatrix} \tag{2.48}$$

In this way, from Equations 2.26 and 2.47, the parameterized command sequence $\tilde{\mathbf{u}}$ is give by:

$$\tilde{\mathbf{u}}(k) = \Upsilon_e \mathbf{p}(k) \qquad \Upsilon_e = \begin{pmatrix} \Upsilon_e^{(0)} \\ \Upsilon_e^{(1)} \\ \vdots \\ \Upsilon_e^{(N-1)} \end{pmatrix} \tag{2.49}$$

For fixed parameters η_j and ξ, the control sequence is profiled by the vector $\mathbf{p}$. Therefore, the objective of the optimization problem changes from founding the control sequence $\tilde{\mathbf{u}}$ to founding the parameter vector $\mathbf{p}$. As a result of this parameterization, the cost function presented in Equation 2.31 comes down to a QP in terms of p, i.e:

$$J(k) = \frac{1}{2}\mathbf{p}^T(k)\mathbf{H}_p\mathbf{p}(k) + \mathbf{F}_p^T(k)\mathbf{p}(k)$$

$$\mathbf{H}_p = \Upsilon_e^T \mathbf{H} \Upsilon_e \qquad \mathbf{F}_p(k) = \Upsilon_e^T \mathbf{F}(k) \tag{2.50}$$

and constraint inequality becomes:

$$\mathbf{A}_{p\,\text{ineq}}\mathbf{p} \leq \mathbf{B}_{\text{ineq}} \qquad \mathbf{A}_{p\,\text{ineq}} = \mathbf{A}_{\text{ineq}}\Upsilon_e \tag{2.51}$$

The benefit of this technique is that instead of finding all the control signals for all the sampling instants of the prediction horizon, the MPC needs to find only an optimal $\mathbf{p}(k)$.

2.3.3 Linear quadratic regulator (LQR)

The Linear Quadratic Regulator (LQR) is an optimal control with closed-loop stability, guaranteed levels of robustness to disturbances, and simple control law given by [58, 57]:

$$\mathbf{u}_c(k) = \mathbf{u}_d - \mathbf{K}_{\text{LQR}}(\mathbf{x}(k) - \mathbf{x}_d(k)) \tag{2.52}$$

and $u_d(k) \in \mathbb{R}^{n_\text{u}}$ and $x_d(k) \in \mathbb{R}^{n_\text{x}}$ are the desired values in the sampling instant k of the command and the state vectors, respectively, in which $\mathbf{K}_{\text{LQR}} \in \mathbb{R}^{n_\text{x} \times n_\text{x}}$ is the state-feedback matrix defined by minimizing the fallowing cost function without constraints:

$$J = \sum_0^{\inf} (\mathbf{x}^T(k)\mathbf{Q}\mathbf{x}(k) + \mathbf{u}_c^T(k)\mathbf{R}\mathbf{u}_c(k)) \tag{2.53}$$

in which the matrix $\mathbf{Q} \in \mathbb{R}^{n_\text{x} \times n_\text{x}}$ and $\mathbf{R} \in \mathbb{R}^{n_\text{u} \times n_\text{u}}$ weights the state error and the control energy, respectively, in a infinite horizon, without imposing restrictions on states or command errors. Q and R are weighting parameters for the tuning between the control effort and performance on

control of each output.

Since $\mathbf{Q}$ is a symmetric positive semi-definite matrix, and $\mathbf{R}$ is a symmetric positive definite matrix, the $\mathbf{K}_{\text{LQR}}$ matrix that solves the minimization of the cost function (2.53) is given by the solution of the Ricatti equation:

$$\begin{aligned} \mathbf{K}_{\text{LQR}} &= (\mathbf{R} + \mathbf{B}_d^T \mathbf{S}(k+1)\mathbf{B}_d)^{-}1\mathbf{B}_d^T \mathbf{S}(k+1)\mathbf{A}_d \\ \mathbf{S}(k) &= \mathbf{A}_d^T[\mathbf{S}(k+1) - \mathbf{S}(K+1)\mathbf{B}_d\mathbf{R}^{-1}\mathbf{S}(k+1)]\mathbf{F}_d + \mathbf{Q} \end{aligned} \tag{2.54}$$

which has an analytical solution for the $\mathbf{S}(k)$ matrix such as the closed-loop system is stable [59].

The LQR is a specific case of MPC when the prediction horizon tends to infinity and the problem does not consider restrictions. In this case, the solution is analytical using the Ricatti equation [57].

2.4 STATE OF THE ART

2.4.1 MPC-based ESCs

The capability to adjust the optimization problem based on the states feedback, to deal with the limitations of the actuators, and to avoid commands that take the states out of the stability margins, make the MPC an useful technique for ESC. From research in the Web of Science website[60], which provides information from multiple databases of scientific publications, one can see that the number of papers about MPC-based ESCs has been growing in the last years, as shown in Fig. 2.7, but none of these papers propose designs concerning the computational efficiency on low-cost hardware.

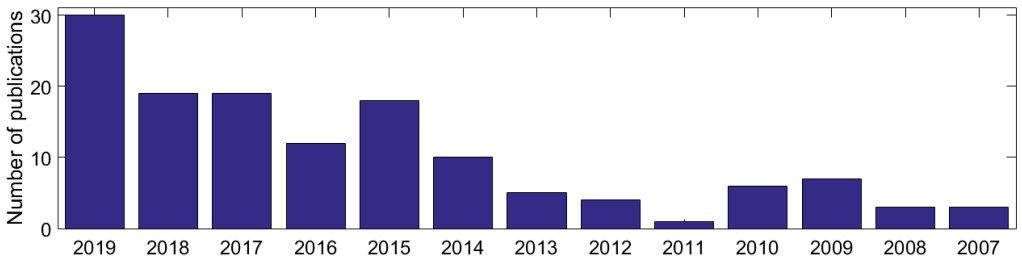

Figure 2.7: Rate of publications per year proposing MPC-based ESCs. Numbers obtained from Web of Science website [60].

The computational complexity is an issue for implementation of MPC based systems because an optimization must be solved at each sampling period, so the sampling period is constrained to the solver's calculation time. Since the cost function is defined based on a prediction model, this model has a strong influence on the calculation time. The use of a linear model for prediction helps to fit the optimization into the quadratic programming (QP) form [25]. However, the complexity of the QP problem is still a challenge for real-time MPC applications with low-cost hardware.

This section presents the results from the literature review on MPC-based ESCs proposed in the recent years (i.e. 2014-2019) that address practical implementation aspects. A summary table of these articles is shown in Table 2.1.

Table 2.1: Summary table of the literature on MPC-based ESCs that address practical issues

Reference	Description	Strengths	Weakness
Choi,2014[61]	ESC based on Explicit MPC formulation	Closed solution form to avoid the QP solving.	Unconstrained optimization problem that does not handle the actuation limits.
Ataei,2018[62] Ataei,2019[63]	ESC reconfigurable for different actuation systems	Configuration for different actuation systems.	The effects of the configuration on calculation time is not presented.
Cheng,2019[26]	ESC integrated with the longitudinal collision avoidance	The matrices of the QP is configured according to the driver conditions.	The effects of the configuration on the calculation time is not included.

In [62],[63], reconfigurable MPC-based ESCs are proposed to vehicles with different actuation systems. The MPC is designed based on a linear model that considers the roll motion and can predict the response to different combinations of control inputs. The set-up is performed by setting a selector matrix that makes the prediction model unresponsive to unavailable control inputs, without taking off those inputs from the linear model, which does not affect the length of the Hessian matrix of the QP problem. Simulations are performed with CarSim and Simulink to demonstrate the effectiveness of proposed ESCs with different configurations. However, the implementation of the embedded control system to execute the proposed algorithm is not presented, as well as no simplification of the optimization problem is applied to the QP to improve the computation time required to solve it.

In [26], an MPC is designed to integrate the objectives of the longitudinal collision avoidance and lateral stability. The proposed algorithm dynamically alters the weight matrices of the QP problem according to driving conditions. An 2DOF model is used as prediction model that includes only the yaw rate and the side-slip of the vehicle body. HIL simulations are performed in a platform where the vehicle motion and the control algorithm are simulated by computers that access from a CAN bus a brake system, a yaw rate sensor and a wheel-speed simulator. The embedded control system is also not presented in [26], and no method is presented to reduce the computation time of MPC.

An MPC for yaw stability with practical concerns is presented in [61], where the cost function of MPC is defined without inequality constraints such that a closed-form solution can be defined as the optimization problem. Therefore, the computational efficiency of ESC is improved by avoiding the QP solving. However, the proposed approach removes the MPC capability to handle the constraints of the actuation system.

2.4.2 LQR-based ESCs

The LQR is an optimal controller that in addition to its low computational cost, it has good robustness properties when feedback of all states is available, due to its stability margins [57].

In [34], an LQR-based upper-level ESC is presented. The model used for control design includes side-slip and yaw motion, without consideration of rolling effects on lateral stability. Other LQR-based ESC design is presented in [64], where the LQR gain matrix is defined based on a linear model that includes vehicle side-slipping, yawing and rolling of the vehicle body and steering angle of front wheels. In [65], an LQR-based ESC design is presented, which uses a linear model with roll degree-of-freedom for the definition of the gain matrix.

This chapter presented an introduction to the major topics of this research, which served as a theoretical basis for the methodology presented in the following chapter. The nonlinear model of vehicle dynamics is useful for implementation of the computational simulations, and to obtain the linear models used in control design. Control theories are fundamental for the implementation of the controllers. And the presentation on stability controllers and the state-of-the-art are important for understanding the goals of this research, which is the development of computationally efficient ESC to run on a low-cost processor, capable of handling the limits performance system.

3 METHODOLOGY

This chapter presents the development process of the ESCs proposed in this research, which consist of the following stages:

- Definition of the mathematical models used in the implementation of vehicle dynamics simulations and the development of control algorithms.
- Implementation of the mathematical models in Matlab and Simulink real-time to perform MIL and HIL simulations for the evaluation of the control algorithms.
- Implementation the control algorithms.
- Implementation the control algorithms in Matlab.
- Evaluation of the control algorithms in MIL testing on control of the vehicle represented by its simulation model running in Matlab.
- Implementation of the embedded control system
- Evaluation of the embedded control system in HIL testing on control of the vehicle represented by its simulation model running in Simulink real-time.

This chapter presents the methodology followed in this research. First, it presents the requirements and the architecture of the proposed ESCs. Following, it describes the simulation methods used to test the these controllers, and the parameters of the models used in theses simulations. Finally, it shows the application of vehicle dynamics and control theories in the development of these systems.

3.1 CONTROL STRATEGY

The control strategy of the systems developed in this research is based on the following requirements:

- The over-actuation is avoided to preserve passengers' comfort and actuators' integrity.
- The commands that greatly increase rollover risk as good solutions are not considered as good solutions.
- For MPC-based ESCs that can handle constraints on actuation, the limits of actuation is taking into account.

The control architecture proposed to met this requirement is presented in Fig. 3.1. As the objectives of stability control can be summed up as improving the response of vehicle movements to driver commands, the core of this architecture is a model-based control, to insert the existing knowledge about vehicle dynamics into the control algorithm. This research is focused on the implementation of these control algorithms and their computational efficiencies, the acquisition strategies of the feedback signals are not included in the scope, therefore, we assume that measures of yaw rate, roll rate, and roll angle are available, whereas side-slip angle is calculated from measures of lateral and front speed.

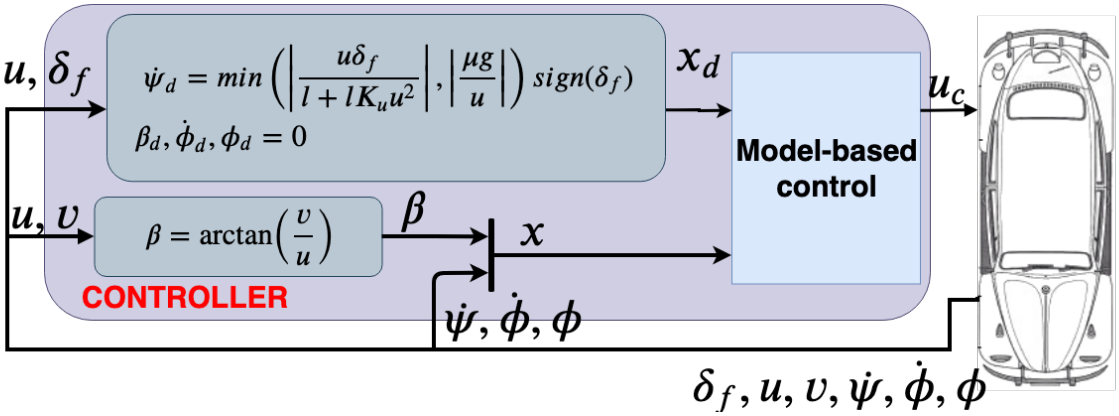

Figure 3.1: Block Diagram of the control systems proposed in this work.

The side-slipping and rolling angle are unwanted motions, not directly controlled by the driver and that divert the vehicle from the driver's intention. Therefore the desired value for the side-slip angle β, roll rate $\dot{\phi}$ and roll angle ϕ states are as small as possible. To spare the computational processing for dynamically calculating the minimum possible value, the desired value of these states is assumed to equal to zero, as they are often assumed in ESC design [46].

The desired yaw rate depends on the steering wheel angle commanded by the driver in response to vehicle movement. For a given vehicle, characterized by its geometric parameters and cornering stiffness coefficients, the desired yaw rate can be computed using the Equation 2.21.

3.2 PROPOSED SYSTEMS

This research presents within its results the implementations of high-level and low-level MPC-based DYCs. To compare the benefits of the MPC with another method that does not have the same capabilities, but requires much less computational processing, high and low-level LQR-based DYCs are also presented. In addition to the performance comparisons between MPC and LQR, comparisons between MPCs with two prediction models are also presented. The first model has 4DOF which includes lateral speed, yaw rate, roll rate and roll angle. The second model has 2DOF, including only lateral speed and yaw rate. The advantage of the first model is a prediction closer to the vehicle's response because it considers the effects of rollover. Whereas the second model is simpler and therefore reduces the complexity of the MPC's optimization problem, which

lead to a shorter calculation time, i.e. it enables a higher sampling rate. Table 3.1 summarizes all the systems developed in this research. The following sections of this chapter describe this systems.

Table 3.1: Summary table of the ESCs developed in this research

Label	Control	Model	Command	Description
HL_LQR_4DOF	LQR	4DOF	Extra yaw moment	High-level LQR-based ESC derived from a linear model that includes the roll motion.
HL_MPC_2DOF	MPC	2DOF	Extra yaw moment	High-level MPC-based ESC derived from a linear model that does not include the roll motion.
HL_MPC_4DOF	MPC	4DOF	Extra yaw moment	High-level MPC-based ESC derived from a linear model that includes the roll motion.
LL_LQR_4DOF	LQR	4DOF	Braking torque transferred to each wheel	Low-level LQR-based ESC derived from a linear model that includes the roll motion.
LL_MPC_2DOF	MPC	2DOF	Braking torque transferred to each wheel	Low-level MPC-based ESC derived from a linear model that does not include the roll motion.
LL_MPC_4DOF	MPC	4DOF	Braking torque transferred to each wheel	Low-level MPC-based ESC derived from a linear model that includes the roll motion.

3.2.1 High-level LQR-based ESC

The research begins with the literature review about the vehicle dynamics models used for lateral stability control and analysis. To start prof-of-concept, no assumption about the actuation system available on the vehicle was considered. The result of this review was the implementation of the a simulation model for MIL and HIL testing, which is a 4DOF model including within the states the lateral speed, yaw rate, roll rate and roll angle, that assumes a constant longitudinal speed, and whose control input is the corrective yaw moment. This is a useful model for evaluating high-level DYC algorithms that calculate corrective yaw momentum without explicitly controlling the torque transferred to each wheel.

The next step was to define a reference control method for comparison with MPC to study the advantages and weakness of using this control technique. The discrete-time LQR was chosen as a reference method because it is also an computational and optimal control method, which does not have the MPCs capabilities to deal with restrictions, but requires much less computational effort, which allows to LQR a higher command update rate. Hence, the first ESC implemented was a high-level DYC based on LQR. Figure 3.2 shows the block diagram of this system. The controller computes the side-slip angle and desired states, then it compares the error between current states and desired states, and the corrective is computed as a linear combination of states error, whose coefficients are defined by the discrete-time LQR method.

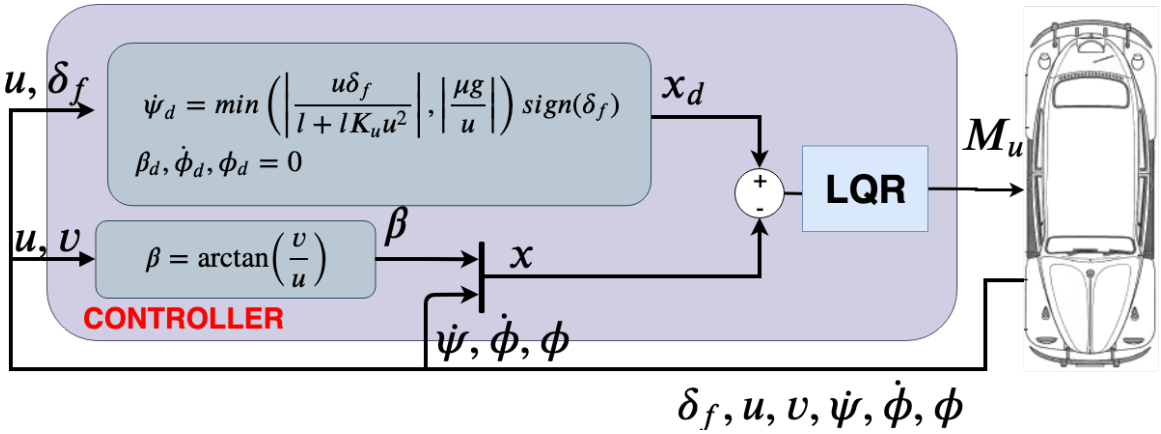

Figure 3.2: Block Diagram of the LQR-based high-level DYC.

In this development, the MIL and HIL simulation environments were implemented, and the overall architecture of the control system was defined.

3.2.1.1 High-level MPC-based ESC

The second study and development was on the MPC-based high-level DYC. Since the interface of this controller is the same as the LQR-based high-level DYC, the same MIL and HIL simulation environments used to validate the LQR-based were used to validate the LQR-based. Therefore, the development process followed consists only of the following steps:

- Implement the control algorithm based on the MPC.
- Evaluate the MPC-based algorithm in the same MIL environment implemented in case study 1.
- Change the LQR-based algorithm in the embedded control system implemented in case study 1 with the MPC-based algorithm.
- Evaluate the embedded control system in the same HIL environment implemented in case study 1.

Figure 3.3 shows the block diagram of the MPC-based high-level DYC. In this system, the controller reads vehicle states, computes the side-slip angle and desired states, then the MPC computes the corrective yaw moment from desired and current states.

Since the increase in the complexity of the QP reduces the MPC real-time performance, the exponential parameterization of the MPC formulation proposed in [25] was used to reduce the MPC computation time by reducing the QP complexity.

Another effort to reduce the MPC's calculation time was the simplification of the vehicle model used in control design by removing the roll-degree-of-freedom, to reduce the QP complexity at the cost of disabling the ability to consider the roll motion influences on stability perfor-

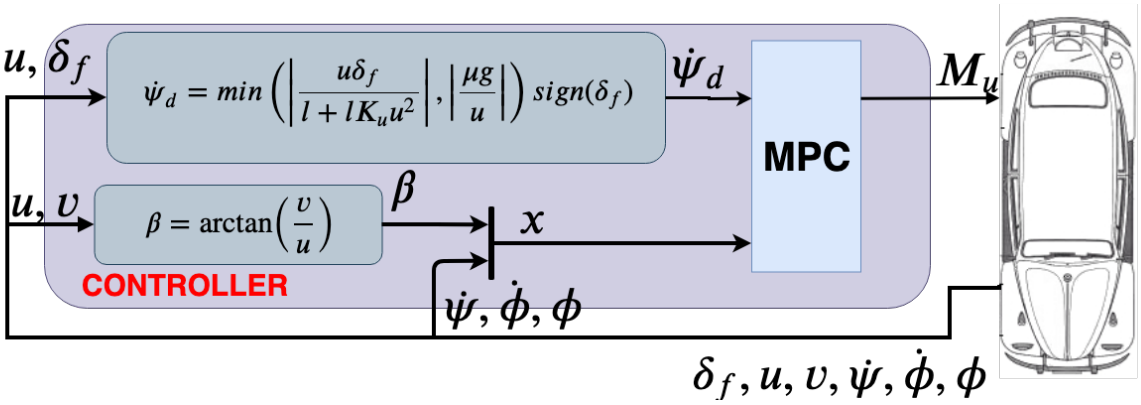

Figure 3.3: Block Diagram of the MPC-based high-level DYC.

mance. The MPC-based ESC with roll control off is designed using a linear prediction model that does not include the roll angle and the roll rate withing the states.

3.2.1.2 Low-level LQR-based ESC

The research on low-level ESCs begins with the literature review of vehicle dynamics models used to design and test these control systems. The result of this review was the definition of a 4DOF simulation model including lateral, longitudinal, yaw and roll motion, whose control signals are the corrective torques transferred to each wheel.

The Fig. 3.4 shows the block diagram of the LQR-based low-level DYC, in which the controller reads the vehicle states, computes the side-slip angle and desired states, the error between desired and current states, and calculates the torque transferred to each of the four wheels as linear combinations of the states error, whose coefficients are defined by the discrete LQR method.

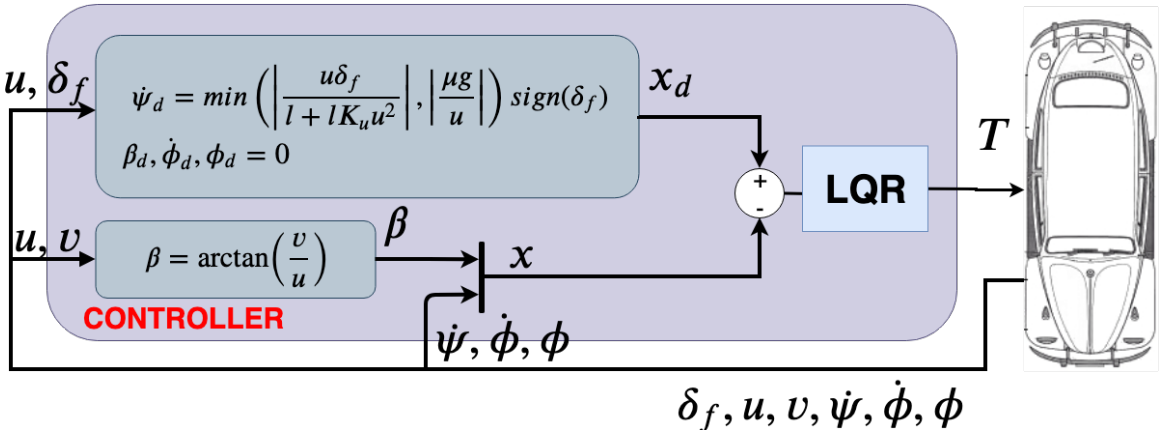

Figure 3.4: Block Diagram of the LQR-based low-level DYC.

The LQR-based low-level DYC was developed to test the simulation environment of low-level ESC and to get a reference design to compare with the MPC-based low-level DYC. Since the LQR is not able to handle constraints on command value, the LQR control law is manipulated to ensure negative torque transferred to the fours wheels, such that it can be tested on control of a vehicle

model that assumes that the differential braking system is available for actuation.

3.2.2 Low-level MPC-based ESC

And the last development performed in this research was the MPC-based low-level DYC. Since the interface (input and output signals) of this controller is the same as the LQR-based high-level DYC, the MIL and HIL simulation environments used to validate the LQR-based were used to validate this MPC-based. Therefore, the development process consists of the following steps:

- Implement the control algorithm based on the MPC.
- Evaluate the MPC-based algorithm in the same MIL environment implemented in case study 1.
- Change the LQR-based algorithm in the embedded control system implemented in case study 1 with the MPC-based algorithm.
- Evaluate the embedded control system in the same HIL environment implemented in case study 1.

The Fig. 3.5 shows the block diagram of the MPC-based low-level DYC, in which the controller reads the vehicle states, computes the side-slip angle and desired states, the error between desired and current states, then the torque transferred to each wheel is computed as linear combination of states error, whose coefficients are defined by the discrete LQR method.

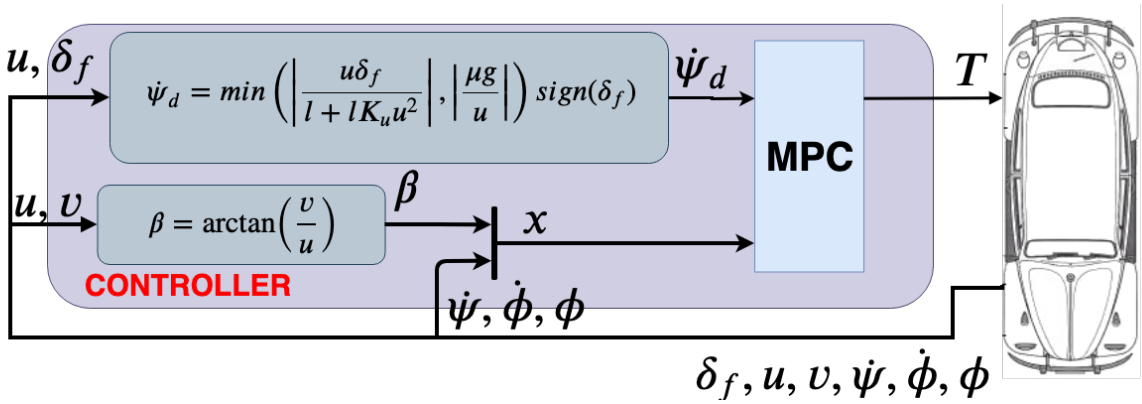

Figure 3.5: Block Diagram of the MPC-based low-level DYC.

The same approaches used in the MPC-based high-level DYC to improve the computational efficiency were also applied in the MPC-based low-level DYC:

- The formulation was changed to add the ability to handle the steering angle that is an uncontrolled input.

- The exponential parameterization was used to reduce the number of decision variables of the QP problem.
- MPC formulations with roll control on and off were tested to compare if the inclusion of control at the cost of reducing the update rate of the control commands is something worthwhile.

3.3 QUALITY ASSURANCE METHODOLOGY

Tests with embedded controllers into real vehicles need a safe environment and a skill pilot, which adds an extra cost for each test execution. To reduce the number of execution tests and the damage risk of experiments, model-in-the-loop (MIL) and hardware-in-the-loop (HIL) simulations are useful methodologies for control strategy validation.

In MIL simulations, the control algorithm and the vehicle dynamics are simulated in a computational environment. This method allows testing without hardware design costs or material damage risks. In case of failure, the algorithm model can be changed and tests can be repeated at low cost, if compared to costs of hardware/software redesigning and experimental testing. In addition to that, the simulations may be performed for maneuvers that can not be safely performed by a human driver driving a real car, and it is possible to observe the behavior of variables that are difficult to be physically measured [23, 24].

The approval requirements of MIL tests are:

- The controller does not increase the maneuvering error that the driver is able to perform without assistance.
- The controller is able to prevent destabilization in maneuvers as the driver loses control without assistance.

Computational simulation can predict the performance of the control strategy before its implementation, but it is not expected that these simulations can predict all the problems faced by the embedded control system in a real-time application. Therefore, after the algorithm approval on MIL tests, the embedded control system is implemented, and this implementation is evaluated on HIL simulations, in which the controller is tested on interaction with a platform that runs a real-time simulation of vehicle motion response to ESC command, supplying real-time updated signals that are measured by the controller [22, 23, 24].

Therefore, once the controller's effectiveness is validated by MIL simulations, the firmware that implements the control algorithm is developed, and the hardware running this firmware is subjected to HIL tests. The approval requirements in this stage is that the results from HIL test are similar to the results from MIL simulation. Because large differences between the results can indicate failures in the implementation of simulations or firmwares.

When an implementation is not approved on HIL tests, an investigation is performed to indicate if the fault is due to algorithm issues or implementation issues. If an implementation issue is detected, the implementation is fixed and HIL tests are performed again. But, if algorithm issues are detected, the algorithm is fixed, the MIL simulation is updated, and the development stages since MIL tests are repeated. The whole procedure is repeated until the controller be approved on HIL tests. The Figure 3.6 shows a flow char that describes the development process.

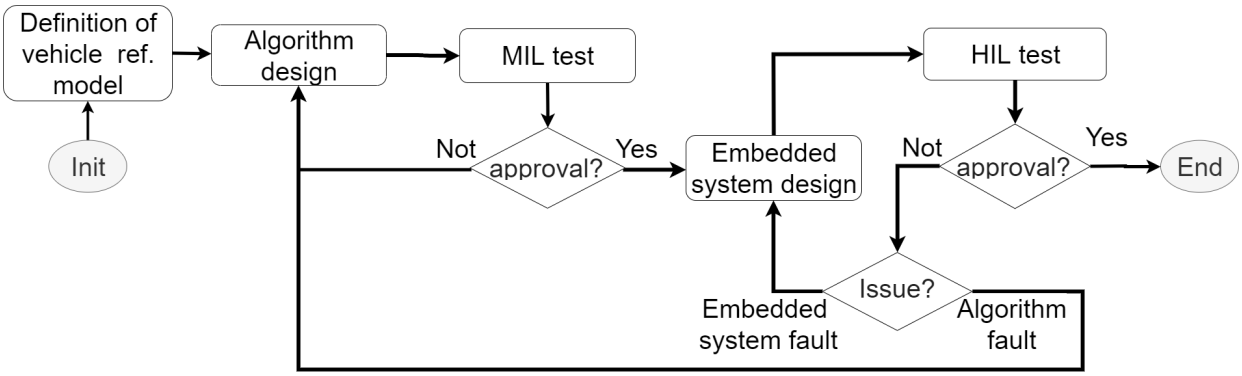

Figure 3.6: Flow chart of control development process adopted.

In this research, the vehicle simulation used in MIL and HIL testing was implemented as Matlab/Simulink models. Later, these models were used for obtaining the discrete-time state-space model required in the design of the model-based controllers developed in this work.

In the first simulation, the implementation of the vehicle model was tested in simulations of open-loop (without stability control) scenarios presented in the literature. The validation consisted of verifying if the simulated vehicle response was consistent with that presented in the literature. After validating the open-loop model, the maneuvers tested in the open-loop simulation were tested in closed-loop (with stability control) simulation for different speeds.

Fig. 3.7 shows the block diagram of the simulation implemented for MIL and HIL tests, whose blocks are:

- Path generation: this block generates the longitudinal x_d and lateral y_d coordinates of the desired path based on the vehicle's dimension;
- Driver model: this block generate the steering angle from the feedback of vehicle states and desired path by simulating the response of an intelligent driver;
- Vertical load: this block computes the vertical load on each tire;
- Tire slip-angle: this block computes the slip angle of each tire;
- Camber angle: this block computes the camber angle of each tire;
- Slip-ratio: this block computes the longitudinal slip-ratio of each tire;
- Pacejka's MF: this block computes the forces acting on each tire;

- Vehicle model: this block computes the states of the vehicle model;
- Rotation motion: this block computes the angular speed of each wheel;
- Control algorithm: this block performs the control algorithm to generate the control signals.

The symbols in Fig. 3.7 denote the variables of model presented in Section 2.1.

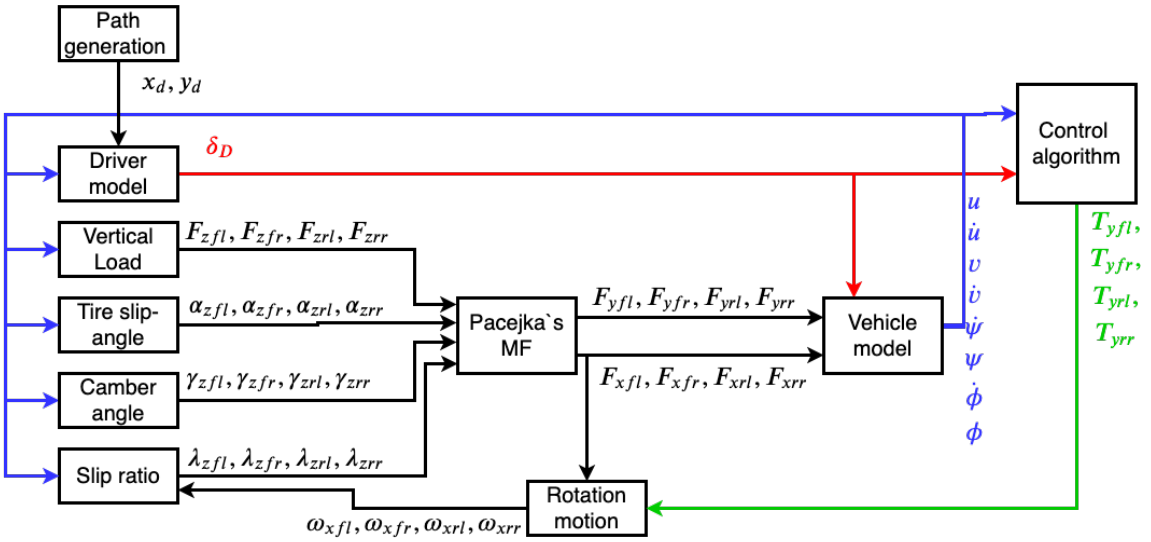

Figure 3.7: Block diagram of the nonlinear model implemented for MIL and HIL simulations, including a model of vehicle dynamics and a model for intelligent driver behavior on the steering wheel command

In addition to detect implementation faults, the HIL simulation is used for fine-tuning of the control coefficients taking into account the effects on real-time performance.

The HIL platform used in this research is based on the framework proposed by [66]. Fig. 3.8 illustrates this platform, which consists of a host computer, a digital-analog converter PCI-DAC6703DA2 and Ethernet connection. The host runs under Simulink Real-Time environment a real-time simulation of vehicle response to control yaw-moment command, providing real-time updated signals read by the controller, which are longitudinal speed, lateral speed, yaw rate, roll rate, roll angle, and front wheels steering angle. The PCI-DAC6703DA2 is used to send these signals to the analog inputs of the controller, which in this work is the Beagle Bone Black. And Ethernet connection is used to send over UDP the yaw-moment given as control input to host.

3.3.1 Test scenarios

The test cases are based on the double lane change (DLC) test of standard No. ISO 3888:1975 as presented in [37]. In the DLC test, the maneuver is approved if the vehicle does not cross boundaries defined based on its track width. However, even if the maneuver is not successfully performed, the test may confirm that the proposed ESC is effective to improve the lateral stability, if the errors obtained with the proposed system are smaller than the obtained without ESC assistance. The test cases performed for each of proposed ESC (Section 3.2) aims at:

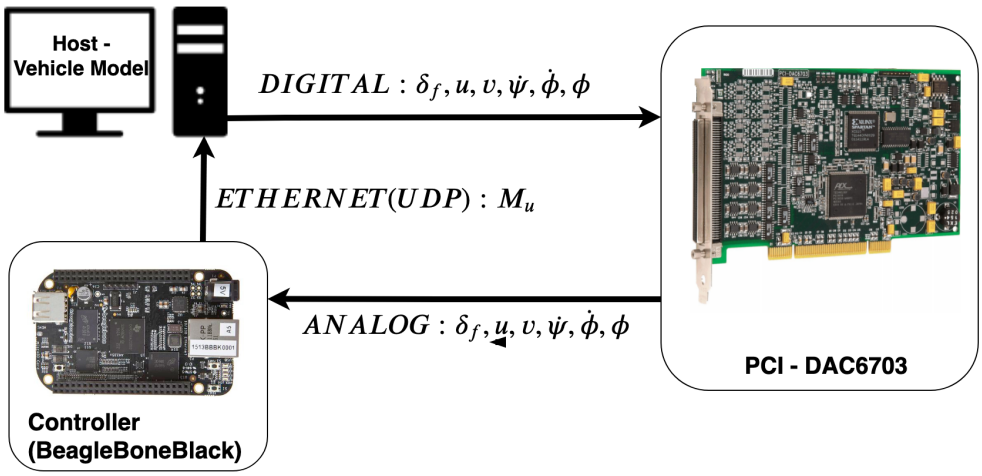

Figure 3.8: Hardware-in-the-loop setup Illustration.

- Test if the ESC shows unnecessary actuation when the driver can perform the maneuver without assistance.
- Test if the ESC is effective to improve the maneuverability when there's no instability risk.
- Evaluate the ESC on control of a vehicle whose response is close to the predicted by the linear model used in control design.
- Evaluate The ESC on a vehicle with an initial speed greater than the constant assumed in the linear model.
- Evaluate the ESC in the presence of model uncertainties, when the vehicle's mass, position of the center of mass, tire-road friction coefficient and velocity are different from the nominal values assumed in the configuration of the linear model used in control design.

All the proposed systems were tuned and evaluated in MIL and HIL simulations DLC test, which allows to observe the vehicle's response when entering a curve, switching between curves and when recovering the movement in a straight line. The nonlinear model of vehicle movements presented in Section 2.1 is used to simulate the vehicle response. This scenario was performed for each ESC with the vehicle at different initial speeds, and in presence of model uncertainties due to differences between the parameters of the vehicle models used to simulation and to control design. Table 3.2 provides a summary of the test cases described below.

Table 3.2: Summary table of the ESCs developed in this research

Label	Method	Stability without ESC	Description
1	MIL	Stable	MIL simulation of high-level ESC on control of a vehicle at constant speed of 80km/h.

Table 3.2: Summary table of the ESCs developed in this research. Continued from last page.

#	Method	Stability without ESC	Description
2	MIL	Unstable	MIL simulation of high-level ESC on control of a vehicle at constant speed of 100km/h.
3	MIL	Unstable	MIL simulation of high-level ESC on control of a vehicle at constant speed of 120km/h.
4	HIL	Unstable	HIL simulation of high-level ESC on control of a vehicle at constant speed of 100km/h
5	MIL	Unstable	MIL simulation of high-level ESC on control of a vehicle at constant speed of 100km/h, and in presence of model uncertainties.

3.4 CONTROL DESIGN

This sections presents the application of the vehicle-dynamics and control theories in ESC designs. The systems proposed in this research employ the LQR and MPC techniques, in which the control equations are derived from a linear model of the controlled process. For this reason, the application of this control methods starts the definition of the linear model used in control design.

3.4.1 Linearization of vehicle model

The linear model of vehicle response is obtained from linearization of the non-linear dynamics presented in the previous chapter (Section 2.1) for small angles, such that $\sin(\phi) \approx \phi$, $\sin(\delta_i) \approx 0$, $\cos(\delta_i) \approx 1$, and $\beta \approx v/u$. The obtained model is presented in Fig. and represented by the following equation:

$$\begin{aligned} \mathbf{K}_{\mathrm{x}}\dot{\mathbf{x}} &= \mathbf{G}_{\mathrm{x}}\mathbf{x} + \mathbf{G}_F F_Y + \mathbf{G}_u \mathbf{u_c} \\ F_Y &= \begin{bmatrix} F_{yfl} & F_{yfr} & F_{yrl} & F_{yrr} \end{bmatrix}^T \end{aligned} \tag{3.1}$$

in which $\mathbf{x}$ and $\mathbf{u}_c$ denote the states and control inputs of the vehicle model. The vectors $\mathbf{x}$ and u, and the matrices $\mathbf{G}_{\mathrm{x}}$, $\mathbf{G}_F$ and $\mathbf{G}_{\mathrm{u}}$ are:

- For high-level ESC with roll control on

$$
\begin{aligned}
\mathbf{x} &= \begin{bmatrix} \beta & \dot{\psi} & \dot{\phi} & \phi \end{bmatrix}^T \\
\mathbf{u}_c &= M_u \\
F_Y &= \begin{bmatrix} F_{yfl} & F_{yfr} & F_{yrl} & F_{yrr} \end{bmatrix}^T \\
\mathbf{K}_{\mathrm{x}} &= \begin{bmatrix} mu & 0 & -m_s h_s & 0 \\ 0 & I_{zz} & -Ixz & (c_{\phi f} + c_{\phi r}) \\ -m_s h_s u & I_{xz} & I_{xx} & 0 \\ 0 & 0 & 0 & 1 \end{bmatrix} \\
\mathbf{G}_{\mathrm{x}} &= \begin{bmatrix} 0 & -mu & 0 & 0 \\ 0 & 0 & 0 & 0 \\ 0 & m_s h_s u & 0 & (m_s h_s g - k_{\phi f} - k_{\phi r}) \\ 0 & 0 & 1 & 0 \end{bmatrix} \\
\mathbf{G}_F &= \begin{bmatrix} 1 & 1 & 1 & 1 \\ a & a & -b & -b \\ 0 & 0 & 0 & 0 \\ 0 & 0 & 0 & 0 \end{bmatrix} \\
\mathbf{G}_{\mathrm{u}} &= \begin{bmatrix} 0 & 1 & 0 & 0 \end{bmatrix}^T
\end{aligned}
\tag{3.2}
$$

- For low-level ESC with roll control on

$$
\begin{aligned}
\mathbf{x} &= \begin{bmatrix} \beta & \dot{\psi} & \dot{\phi} & \phi \end{bmatrix}^T \\
\mathbf{u}_c &= \begin{bmatrix} T_{fl} & T_{fr} & T_{rl} & T_{rr} \end{bmatrix}^T \\
F_Y &= \begin{bmatrix} F_{yfl} & F_{yfr} & F_{yrl} & F_{yrr} \end{bmatrix}^T \\
\mathbf{K}_{\mathrm{x}} &= \begin{bmatrix} mu & 0 & -m_s h_s & 0 \\ 0 & I_{zz} & -Ixz & (c_{\phi f} + c_{\phi r}) \\ -m_s h_s u & I_{xz} & I_{xx} & 0 \\ 0 & 0 & 0 & 1 \end{bmatrix} \\
\mathbf{G}_{\mathrm{x}} &= \begin{bmatrix} 0 & -mu & 0 & 0 \\ 0 & 0 & 0 & 0 \\ 0 & m_s h_s u & 0 & (m_s h_s g - k_{\phi f} - k_{\phi r}) \\ 0 & 0 & 1 & 0 \end{bmatrix} \\
\mathbf{G}_F &= \begin{bmatrix} 1 & 1 & 1 & 1 \\ a & a & -b & -b \\ 0 & 0 & 0 & 0 \\ 0 & 0 & 0 & 0 \end{bmatrix} \\
\mathbf{G}_{\mathrm{u}} &= \begin{bmatrix} 0 & 0 & 0 & 0 \\ \frac{-t_f}{2} & \frac{t_f}{2} & \frac{-t_r}{2} & \frac{t_f}{2} \\ 0 & 0 & 0 & 0 \\ 0 & 0 & 0 & 0 \end{bmatrix}
\end{aligned}
\tag{3.3}
$$

- For high-level ESC with roll control off

$$
\begin{aligned}
\mathbf{x} &= \begin{bmatrix} \beta & \dot{\psi} \end{bmatrix}^T \\
\mathbf{u}_c &= M_u \\
F_Y &= \begin{bmatrix} F_{yfl} & F_{yfr} & F_{yrl} & F_{yrr} \end{bmatrix}^T \\
\mathbf{K}_{\mathrm{x}} &= \begin{bmatrix} mu & 0 \\ 0 & I_{zz} \end{bmatrix} \\
\mathbf{G}_{\mathrm{x}} &= \begin{bmatrix} 0 & -mu \\ 0 & 0 \end{bmatrix} \\
\mathbf{G}_F &= \begin{bmatrix} 1 & 1 & 1 & 1 \\ a & a & -b & -b \end{bmatrix} \\
\mathbf{G}_{\mathrm{u}} &= \begin{bmatrix} 0 & 1 \end{bmatrix}^T
\end{aligned}
\tag{3.4}
$$

- For low-level ESC with roll control off

$$
\begin{aligned}
\mathbf{x} &= \begin{bmatrix} \beta & \dot{\psi} \end{bmatrix}^T \\
\mathbf{u}_c &= \begin{bmatrix} T_{fl} & T_{fr} & T_{rl} & T_{rr} \end{bmatrix}^T \\
F_Y &= \begin{bmatrix} F_{yfl} & F_{yfr} & F_{yrl} & F_{yrr} \end{bmatrix}^T \\
\mathbf{K}_{\mathrm{x}} &= \begin{bmatrix} mu & 0 \\ 0 & I_{zz} \end{bmatrix} \\
\mathbf{G}_{\mathrm{x}} &= \begin{bmatrix} 0 & -mu \\ 0 & 0 \end{bmatrix} \\
\mathbf{G}_F &= \begin{bmatrix} 1 & 1 & 1 & 1 \\ a & a & -b & -b \end{bmatrix} \\
\mathbf{G}_{\mathrm{u}} &= \begin{bmatrix} 0 & 0 & 0 & 0 \\ \frac{-t_f}{2} & \frac{t_f}{2} & \frac{-t_r}{2} & \frac{t_f}{2} \end{bmatrix}
\end{aligned}
\tag{3.5}
$$

For smalls tire slip and camber angles, the lateral force generated by tires is approximated by [33]:

$$
\begin{aligned}
F_Y &= \mathbf{G}_\alpha \boldsymbol{\alpha} + \mathbf{G}_\gamma \mathbf{x} \\
\boldsymbol{\alpha} &= \begin{bmatrix} \alpha_{fl} & \alpha_{fr} & \alpha_{rl} & \alpha_{rr} \end{bmatrix}^T \\
\mathbf{G}_\alpha &= \text{diag}\left(C_{\alpha fl}, C_{\alpha fr}, C_{\alpha rl}, C_{\alpha rr}\right) \\
\mathbf{G}_\gamma &= \text{diag}\left(C_{\gamma fl}, C_{\gamma fr}, C_{\gamma rl}, C_{\gamma rr}\right) \Pi_\phi
\end{aligned}
\tag{3.6}
$$

where $C_{\alpha i}$ and $C_{\gamma i}$ are the cornering and cambering stiffness coefficients, and Π_ϕ is a selector matrix that selects the roll angle within the states.

In models that do not include the roll motion, the camber angle should not be included as well, because the camber angle is being considered as proportional to roll angle, given by Eq. 2.15. Therefore, the matrix Π_ϕ differs for models that include and do not include the roll angle in the state vector $\mathbf{x}$:

$$
\Pi_\phi = \begin{cases} \begin{bmatrix} 0_{4\times 3} & 1_{4\times 1} \end{bmatrix}, & \text{if } \mathbf{x} = \begin{bmatrix} \beta & \dot{\psi} & \dot{\phi} & \phi \end{bmatrix}^T \\ 0_{4\times 2}, & \text{if } \mathbf{x} = \begin{bmatrix} \beta & \dot{\psi} \end{bmatrix}^T \end{cases}
\tag{3.7}
$$

The cornering stiffness and the cambering stiffness coefficients are the angular coefficients of the linear approximation of the Pacejka's Magic Formula (Eq. 2.14) [31], given by:

$$
C_{\alpha i} = \left.\frac{\partial F_{yi}}{\partial \alpha_i}\right|_{a_x, a_y, \gamma, \alpha, \phi, \dot{\phi}=0} \qquad C_{\gamma i} = \left.\frac{\partial F_{yi}}{\partial \gamma_i}\right|_{a_x, a_y, \gamma, \alpha, \phi, \dot{\phi}=0}
\tag{3.8}
$$

Fig. 3.9 shows the forces obtained from Pacejka's Magic Formula and its linear approximation, where one can see that for small angles the Equation 3.6 is a good approximation.

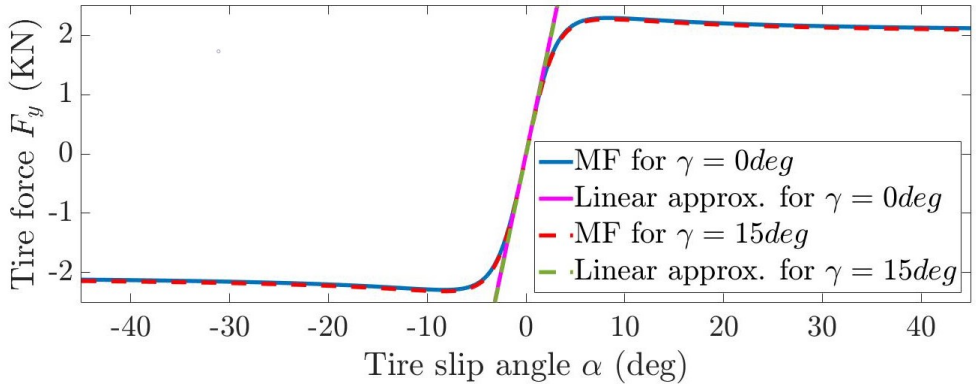

Figure 3.9: Lateral tire forces computed by the Magic formula of Pacejka and its linear approximation.

The front and rear wheels slip angle are approximated by linear functions of vehicle slip angle, yaw

rate and wheels steer angle [27, 34]:

$$\boldsymbol{\alpha} = \begin{bmatrix} -1 & -a/u \\ -1 & -a/u \\ -1 & b/u \\ -1 & b/u \end{bmatrix} \Pi_{(\beta,\dot{\psi})}\mathbf{x} + \begin{bmatrix} \delta_{fl} \\ \delta_{fr} \\ \delta_{rl} \\ \delta_{rr} \end{bmatrix} \tag{3.9}$$

in which the matrix $\Pi_{(\beta,\dot{\psi})}$ extracts the vector $\begin{bmatrix} \beta & \dot{\psi} \end{bmatrix}$ from the vector state $\mathbf{x}$. Therefore, the matrix$\Pi_{(\beta,\dot{\psi})}$ differs for models that include and do not include the roll angle in the state vector $\mathbf{x}$:

$$\Pi_{(\beta,\dot{\psi})} = \begin{cases} \begin{bmatrix} \mathbb{I}_{2\times 2} & 0_{2\times 2} \end{bmatrix}, & \text{if } \mathbf{x} = \begin{bmatrix} \beta & \dot{\psi} & \dot{\phi} & \phi \end{bmatrix}^T \\ \mathbb{I}_{2\times 2}, & \text{if } \mathbf{x} = \begin{bmatrix} \beta & \dot{\psi} \end{bmatrix}^T \end{cases} \tag{3.10}$$

From Equation 3.9 and assuming that the steering control acts only on the front wheels ($\delta_{rr} = \delta_{rl} = 0$) and that the left and right angles are the same ($\delta_{fr} = \delta_{fl} = \delta_f$), the following equations are obtained:

$$\begin{aligned} \boldsymbol{\alpha} &= \mathbf{G}_{\mathrm{A}}\mathbf{x} + \begin{bmatrix} 1 & 1 & 0 & 0 \end{bmatrix}^T \delta_f \\ \mathbf{G}_{\mathrm{A}} &= \begin{bmatrix} -1 & -a/u \\ -1 & -a/u \\ -1 & b/u \\ -1 & b/u \end{bmatrix} \Pi_{(\beta,\dot{\psi})} + \mathrm{diag}\left(\frac{\partial \delta_f}{\partial \phi}, \frac{\partial \delta_f}{\partial \phi}, \frac{\partial \delta_r}{\partial \phi}, \frac{\partial \delta_r}{\partial \phi} \right) \Pi_{\phi} \end{aligned} \tag{3.11}$$

The linear model of vehicle dynamics in the state space form can be obtained by combining the Equations from 3.1 to 3.11:

$$\begin{aligned} \dot{\mathbf{x}} &= \mathbf{A}\mathbf{x} + \mathbf{B}\mathbf{u}_c + \mathbf{E}\delta_f \\ \mathbf{A} &= \mathbf{K}_{\mathrm{x}}^{-1} \left[\mathbf{G}_{\mathrm{x}} + \mathbf{G}_F \left(\mathbf{G}_{\alpha}\mathbf{G}_{\mathrm{A}} + \mathbf{G}_{\gamma} \right) \right] \\ \mathbf{B} &= \mathbf{K}_{\mathrm{x}}^{-1}\mathbf{G}_{\mathrm{u}} \\ \mathbf{E} &= \mathbf{K}_{\mathrm{x}}^{-1}\mathbf{G}_F\mathbf{G}_{\alpha}\mathbf{G}_{\gamma} \end{aligned} \tag{3.12}$$

3.4.2 LQR-based ESC

The discrete-time LQR is used in the ESCs designs proposed in this research, such that it can be implemented as software component of an ECU. The Matlab's function *lqrd* is used to obtain the gain matrix from the matrices of the continuous state-space model. In this model, the steering angle is considered as a state whose desired value is equal to its current sampling, such that the error of this virtual state is always equal to zero and thus does not interfere with the calculated command. The continuous state-space model used in LQR design is obtained from the matrices of the Equation 3.12 as follows:

$$
\begin{aligned}
\mathbf{x}_e &= \begin{bmatrix} \mathbf{x} & \delta_f \end{bmatrix} \\
\dot{\mathbf{x}}_e &= A'\mathbf{x}_e + B\mathbf{u}_c \\
A' &= \begin{bmatrix} A & E \end{bmatrix}
\end{aligned}
\tag{3.13}
$$

The LQR computes a control signal as a weighted sum of the error of the state without imposing any constraint to handle the actuation limits. In the LQR-based ESCs proposed in this work, the control algorithm outputs a control signal which is a constrained LQR result. For LQR-based high-level ESCs, the corrective yaw moment M_u at the sampling instant n is computed as follows:

$$
\begin{aligned}
M_{LQR} &= K(\mathbf{x}_d(n) - \mathbf{x}_e(n)) \\
M_u &= \begin{cases} -M_{th}, & \text{if } M_{LQR} \leq -M_{th} \\ M_{th}, & \text{if } M_{th} \leq M_{LQR} \\ M_{LQR} & \text{otherwise} \end{cases}
\end{aligned}
\tag{3.14}
$$

in which $\mathbf{x}_d$ denotes the desired value of the states $\mathbf{x}_e$, K is the discrete-time LQR gain matrix and M_{th} is the maximum allowable value of the corrective yaw moment.

For LQR-based low-level ESCs, the braking torques (i.e. negative torque) transferred to the wheels $\mathbf{T}_u$ at the sampling instant n are obtained by manipulating the LQR output to ensure negative torques greater than a threshold. This manipulation aims at preserving the moment generated in the yaw axis, considering that the moment generated by accelerating a wheel is equivalent to the moment generated when braking the wheel of the same axis on the opposite side. The braking torque transferred to the wheels are computed as follows:

$$
\mathbf{T}_{LQR} = \begin{bmatrix} T_{LQR,fl} \\ T_{LQR,fr} \\ T_{LQR,rl} \\ T_{LQR,rr} \end{bmatrix} = K(\mathbf{x}_d(n) - \mathbf{x}(n))
\tag{3.15}
$$

$$
\begin{aligned}
T'_{fl} &= \begin{cases} T_{LQR,fl} - T_{LQR,fr} & \text{if} T_{LQR,fl} \leq 0, T_{LQR,fr} > 0 \\ T_{LQR,fl} & \text{if} T_{LQR,fl}, T_{LQR,fr} \leq 0 \\ -T_{LQR,fr} & \text{if} T_{LQR,fl}, T_{LQR,fr} > 0 \\ 0 & \text{if} T_{LQR,fl} > 0, T_{LQR,fr} \leq 0 \end{cases} \\
T'_{fr} &= \begin{cases} T_{LQR,fr} - T_{LQR,fl} & \text{if} T_{LQR,fr} \leq 0, T_{LQR,fl} > 0 \\ T_{LQR,fr} & \text{if} T_{LQR,fr}, T_{LQR,fl} \leq 0 \\ -T_{LQR,fl} & \text{if} T_{LQR,fr}, T_{LQR,fl} > 0 \\ 0 & \text{if} T_{LQR,fr} > 0, T_{LQR,fl} \leq 0 \end{cases} \\
T'_{rl} &= \begin{cases} T_{LQR,rl} - T_{LQR,rr} & \text{if} T_{LQR,rl} \leq 0, T_{LQR,rr} > 0 \\ T_{LQR,rl} & \text{if} T_{LQR,rl}, T_{LQR,rr} \leq 0 \\ -T_{LQR,rr} & \text{if} T_{LQR,rl}, T_{LQR,rr} > 0 \\ 0 & \text{if} T_{LQR,rl} > 0, T_{LQR,rr} \leq 0 \end{cases} \\
T'_{rr} &= \begin{cases} T_{LQR,rr} - T_{LQR,rl} & \text{if} T_{LQR,rr} \leq 0, T_{LQR,rl} > 0 \\ T_{LQR,rr} & \text{if} T_{LQR,rr}, T_{LQR,rl} \leq 0 \\ -T_{LQR,rl} & \text{if} T_{LQR,rr}, T_{LQR,rl} > 0 \\ 0 & \text{if} T_{LQR,rr} > 0, T_{LQR,rl} \leq 0 \end{cases} \\
T_i &= \begin{cases} -T_{th}, & \text{if } T'_i \leq -T_{th} \\ 0, & \text{if } T'_i \leq 0 \\ T'_i & \text{otherwise} \end{cases} \\
i &\in fl, fr, rl, rr \\
\mathbf{T}_u &= \begin{bmatrix} T_{fl} \\ T_{fr} \\ T_{rl} \\ T_{rr} \end{bmatrix}
\end{aligned}
\tag{3.16}
$$

in which T_{th} is the absolute value of the maximum braking torque that can be transferred to the wheels.

3.4.3 MPC-based ESC

The MPC formulation used in this work and presented in [25] does not consider the existence of commands that are not controlled by the MPC, as it is the case with the steering angle. Then the development stage following the definition of the prediction model was the definition of a strategy to deal with this uncontrolled command. The first attempt was to change the state space model to include the steering angle as a constant state. In this way, the prediction model is able to consider the effects of the steering angle on vehicle's response, assuming it remains constant over the prediction horizon. However, the increase in the number of states makes the update of the vector B_{ineq} more complex, such that this approach is not efficient to be addressed to lateral stability control in real-time application. Therefore, another strategy is adopted

to handle the steering angle, in which the state-space model is changed to include the steering angle within the controlled states and, to prevent the MPC from searching for optimal solutions for this uncontrolled command, the QP is constrained such that the only solution for the steering angle in the optimal control sequence is constant equal to its measured value. In this way, the prediction model can consider the effects of the steering angle on vehicle response, assuming it remains constant over the prediction horizon. This approach is used in the MPC-based ESCs developed in this work because it is computational efficient to be addressed to lateral stability control. The linear model used in MPC design is the discretization of the state-space model presented in equation 3.12, with the steering angle included in the control vector $\mathbf{u}_c$. So the control vector $\mathbf{u}_c$ is :

- For high-level ESC:

$$\mathbf{u}_c = \begin{bmatrix} M_u & \delta_f \end{bmatrix}^T \tag{3.17}$$

- For low-level ESC:

$$\begin{aligned} \mathbf{u}_c &= \begin{bmatrix} \mathbf{T}^T & \delta_f \end{bmatrix}^T \\ \mathbf{T} &= \begin{bmatrix} T_{fl} & T_{fr} & T_{rl} & T_{rr} \end{bmatrix}^T \end{aligned} \tag{3.18}$$

In addition to the equality constraint of the steering angle, the proposed MPC design considers the constraints on amplitude and slew rate of the controlled commands. Therefore, the constraint set is presented by the following inequalities:

$$\begin{bmatrix} \mathbb{I}_{n_\mathrm{u}} \\ -\mathbb{I}_{n_\mathrm{u}} \\ \mathbb{I}_{n_\mathrm{u}} \\ -\mathbb{I}_{n_\mathrm{u}} \end{bmatrix} \mathbf{u}_c(k) \leq \begin{bmatrix} \mathbf{u}_c^{max}(k) \\ -\mathbf{u}_c^{min}(k) \\ \Delta_{\mathbf{u}}^{max} - \mathbf{u}_c(k-1) \\ -\Delta_{\mathbf{u}}^{min} + \mathbf{u}_c(k-1) \end{bmatrix} \tag{3.19}$$

where $\mathbf{u}_c^{max}(k)$ and $\mathbf{u}_c^{min}(k)$ define the maximum and minimum values of the control signals, and $\Delta_{\mathbf{u}}^{max}$ and $\Delta_{\mathbf{u}}^{min}$ define the maximum and minimum variation of the control signals between consecutive sampling instants. S

For the high-level control, the constraining vectors are given by:

$$\begin{aligned} \mathbf{u}_c^{max}(k) &= \begin{bmatrix} M_u^{max} & \delta_f(k) \end{bmatrix}^T & \Delta_{\mathbf{u}}^{max} &= \begin{bmatrix} \Delta_{M_u}^{max} & 0 \end{bmatrix}^T \\ \mathbf{u}_c^{min}(k) &= \begin{bmatrix} M_u^{min} & \delta_f(k) \end{bmatrix}^T & \Delta_{\mathbf{u}}^{min} &= \begin{bmatrix} \Delta_{M_u}^{min} & 0 \end{bmatrix}^T \end{aligned} \tag{3.20}$$

where M_u^{max} and M_u^{min} are the maximum and minimum corrector moment applied on the vehicle's yaw axis, and $\Delta_{M_u}^{max}$ and $\Delta_{M_u}^{min}$ are the maximum and minimum variation of the corrector yaw moment between consecutive sampling instants. And for the low-level control, the constraining vectors are given by:

$$\begin{aligned} \mathbf{u}_c^{max}(k) &= \begin{bmatrix} T_{fl}^{max} & T_{fr}^{max} & T_{rl}^{max} & T_{rr}^{max} & \delta_f(k) \end{bmatrix}^T \\ \Delta_{\mathbf{u}}^{max} &= \begin{bmatrix} \Delta_{T_{fl}}^{max} & \Delta_{T_{fr}}^{max} & \Delta_{T_{rl}}^{max} & \Delta_{T_{rr}}^{max} & 0 \end{bmatrix}^T \\ \mathbf{u}_c^{min}(k) &= \begin{bmatrix} T_{fl}^{min} & T_{fr}^{min} & T_{rl}^{min} & T_{rr}^{min} & \delta_f(k) \end{bmatrix}^T \\ \Delta_{\mathbf{u}}^{min} &= \begin{bmatrix} \Delta_{T_{fl}}^{min} & \Delta_{T_{fr}}^{min} & \Delta_{T_{rl}}^{min} & \Delta_{T_{rr}}^{min} & 0 \end{bmatrix}^T \end{aligned} \tag{3.21}$$

where T_i^{max} and T_i^{min} are the maximum and minimum corrector torque transferred to the i-th wheel, and $\Delta_{T_i}^{max}$ and $\Delta_{T_i}^{min}$ are the maximum and minimum variation of the corrector torque transferred to the i-th wheel between consecutive sampling instants.

In Equations 3.20 and 3.21, the variation of the steering angle between consecutive samples are constrained equal to zero because its value is constrained to a constant value over the prediction horizon.

The proposed MPC design uses the exponential parameterization presented in 2.3.2.3 to increase the computational efficiency by reducing the number of variables of the QP solution. For the exponential parameterization to provide results compatible with the imposed constraint that the frontal steering δ_f must remain constant and equal to its value measured a priori, the η-coefficient associated with the steering command must be equal to zero, and its respective element in the parameter vector $\mathbf{p}$ must be constrained equal to the steer angle measured a priori, such that the only solution is a constant steering angle over the prediction horizon equal to a priori measured value $\delta_f(k)$.

With this parameterization, for high-level controllers, the command vector in the i-th sampling instant of the prediction horizon is given by:

$$\begin{aligned} \mathbf{u}_c(k+i) &= \begin{bmatrix} M_u(k+1) \\ \delta_f(k+1) \end{bmatrix} = M(i)\mathbf{p} \\ M(i) &= \begin{bmatrix} e^{-\lambda\tau_s i} & e^{-\lambda\tau_s i/(1+\alpha)} & \dots & e^{-\lambda\tau_s i/(1+(n_e-1)\alpha)} & 0 \\ 0 & 0 & \dots & 0 & 1 \end{bmatrix} \end{aligned} \tag{3.22}$$

whereas for low-level controllers the command vector in the i-th sampling instant of the prediction horizon is given by:

$$\begin{aligned} \mathbf{u}_c(k+i) &= \begin{bmatrix} T_{fl}(k+1) \\ T_{fr}(k+1) \\ T_{rl}(k+1) \\ T_{rr}(k+1) \\ \delta_f(k+1) \end{bmatrix} = M(i)\mathbf{p} \\ M(i) &= \begin{bmatrix} e^{-\lambda\tau_s i} & e^{-\lambda\tau_s i/(1+\alpha)} & \dots & e^{-\lambda\tau_s i/(1+(n_e-1)\alpha)} & 0 \\ e^{-\lambda\tau_s i} & e^{-\lambda\tau_s i/(1+\alpha)} & \dots & e^{-\lambda\tau_s i/(1+(n_e-1)\alpha)} & 0 \\ e^{-\lambda\tau_s i} & e^{-\lambda\tau_s i/(1+\alpha)} & \dots & e^{-\lambda\tau_s i/(1+(n_e-1)\alpha)} & 0 \\ 0 & 0 & \dots & 0 & 1 \end{bmatrix} \end{aligned} \tag{3.23}$$

in which n_e is the number of exponential used in the parameterization of the controlled commands, λ and α are the coefficients of the exponential parameterization, and τ_s is the sampling time.

The parameterization can be expressed in the compact form as follows:

$$\tilde{\mathbf{u}}(k) = \Pi_e \mathbf{p} \qquad \Pi_e = \begin{bmatrix} M(0) \\ \vdots \\ M(N-1) \end{bmatrix} \tag{3.24}$$

3.4.4 ESC activation criteria

The ESC should not unnecessarily actuate when the driver is able to drive without assistance. To avoid unnecessary actuation in the presence of states error that does not mean a risk of steering instability, the ESC control is kept off while the following activation criteria are not satisfied:

$$|\beta| \geq \beta_{th}^{on} \qquad \text{and} \qquad \left|\dot{\psi}_d - \dot{\psi}\right| \geq \dot{\psi}_{th}^{on} \tag{3.25}$$

in which β_{th}^{on} and $\dot{\psi}_{th}^{on}$ are thresholds of side-slip angle and yaw rate error, respectively, for activating the lateral stability control.

And, once the ESC is off, it remains off while the following deactivation criteria is not satisfied:

$$|\beta| \leq \beta_{th}^{off} \qquad \text{and} \qquad \left|\dot{\psi}_d - \dot{\psi}\right| \leq \dot{\psi}_{th}^{off} \tag{3.26}$$

in which β_{th}^{off} and $\dot{\psi}_{th}^{off}$ are thresholds of side-slip angle and yaw rate error, respectively, for deactivating the lateral stability control.

To avoid excessive on-off switching, the ESC is turned on if the activation criteria are fulfilled for a minimum period denoted by τ_{on}, and it is turned off if the deactivation criteria are fulfilled for a minimum period denoted by τ_{off}.

3.4.5 Tuning procedure

The ESC effectiveness depends on the coefficients of the control design, e.g. the weighting matrices that define the penalty of state errors and control effort. For a properly observation of the benefits and the limitations of the proposed designs, the coefficients of the control algorithm must be well fitted.

In this work, an optimal tuning based on Particle Swarm Optimization (PSO) is performed with MIL simulations to define the configuration of the MPC and the LQR designs. Taking into account the efficiency of the embedded control system, the control sampling time in MIL simulation is configured equally as the computational time profiled in HIL simulation.

3.4.6 Tuning of the LQR-based ESC

The LQR configuration coefficients are the weighting matrices Q and R. The choice of these matrices affects the gain matrix given as result of the discrete-time LQR method, but does not affect the number and complexity of the algorithm's operations, i.e. the configuration of the weighting matrices does not alter the computation effort. However, the calculation time constraint the sampling rate, and the discrete-time LQR' gain matrix depends on the sampling time. Therefore, the configuration of the LQR starts with the measurement of the minimum calculation time in which the embedded control system is able to execute

the algorithm. This calculation time is set as the sampling time of the control signals. And then MIL simulations are performed to find out the optimal matrices that optimize the ESC performance.

The optimization method used to define the optimal weighting matrices Q and R are performed in the MIL simulation environment. The problem is defined as the minimization of a cost function that penalizes the states errors, trajectory error, and control energy, all accumulated from results of MIL simulations for DLC maneuver at 80km/h, 100km/h, and 120km/h. This cost function is defined as follows:

$$\begin{aligned} J_C &= \int_0^{10} \left(|y_e(t)| + \left|\dot{\psi}_e(t)\right| + 10\,|\beta(t)| + 10\,|\phi(t)| + 0.01 u^T(t) u(t) \right) \mathrm{dt} \\ y_e(t) &= y_d(t) - y(t) \\ \dot{\psi}_e &= \dot{\psi}_d - \dot{\psi} \end{aligned} \tag{3.27}$$

where t denotes the simulation time, y_e the lateral position error, y the lateral position, y_d the lateral position in the ideal path, ψ_e the yaw rate error, $\dot{\psi}$ the yaw rate, and $\dot{\psi}_d$ is the desired yaw rate computed by Equation 2.21.

The Matlab's function *particleswarm* with the hybrid method *fmincon* enabled is used to solve the optimization problem. It starts the optimization using the PSO method to perform a stochastic search for Q and R values that minimizes the cost function (Eq. 3.27), then it continues the optimization from PSO results by using the interior point method to found out the optimal values of Q and R.

3.4.6.1 Tuning of the MPC-based ESC

The MPC performance depends on the value of its parameters, such as the weighting matrices, the coefficients of exponential parameterization λ and α and the prediction horizon N.

Theoretically, a long prediction horizon increases the capacity of ESC to act before a dangerous driving condition happens, and also contributes to the stability of MPC [20]. But in practical terms, the increase of the prediction horizon increases the latency of the QP solving to update the control command, i.g the increasing of the prediction horizon decreases the command updating rate, which may decrease the stability performance. Therefore, the sampling time of the control model in MIL simulation is configured equally as the computational time profiled in HIL simulation for the configuration under test.

The weighting matrices Q_u and Q_y (Eq.2.31) and the coefficients η and ξ of the exponential parameterization (Eq. 2.45), and the prediction horizon N are defined by an iterative procedure described by the following steps, starting with the prediction horizon $N = 15$.

1. **Tuning of Q_u, Q_y, η, ξ:**

   The control model of MIL simulation is configured with the chosen horizon. The others parameters are defined by the minimization of the accumulation of states square error, path square error and yaw moment energy, obtained from results of MIL simulation for double lane change maneuver (standard No. ISO 3888:1975 as presented in [37]) at 80km/h, 100km/h, and 120km/h.

2. **Profiling the command update times**

   The controller is configured with the optimum parameters found in the previous step. Than HIL simulations are performed for each horizon $N \in [15, 20, 25, 30, 35, 40, 45, 50, 55, 60, 65]$. The profiling tool of GNU ARM embedded toolchain is used during these simulations to measure the calculation time for each horizon. The HIL simulations are able to test only command update times that are multiples of the HIL platform sampling time, which is 0.8ms. For this reason, the command update time of each N is defined as the smallest multiple of 0.8ms greater than or equal to the calculation time measured for this prediction horizon.

3. **Measure of the stability performances**

   The mean square error (MSE) of the lateral displacement is measured, from results of MIL simulations of the DLC maneuver at 120km/h, for the control model configured for each prediction horizon and its effective update time measured in the previous step. The horizon that gets the smallest MSE measured is the chosen one.

4. **Completion and iteration**

   The procedure repeats while the chosen horizons does not change within consecutive iterations. Since the intention is to test the proposed controllers with the best configuration, the optimal coefficients obtained in the last iteration is used in MPC settings. The matrix C_r are defined such that regulated states include only the states whose error is not zero-weighted in the optimal Q_Y.

This chapter presented the specifications and procedures for implementation and validation of the ESCs proposed in the research. The results obtained for the high and low level controllers, based on MPC and LQR, with and without control of the roll motion are presented in the next chapter.

4 SIMULATIONS AND RESULTS

This research on vehicle stability control resulted in the development of high-level and lower-level DYC systems based on MPC technique. To study the advantages of MPC capabilities, reference designs of the proposed control systems were implemented using LQR instead of MPC, to serve as a basis for comparison with the MPC. The LQR was chosen for this purpose because it is an optimal method, whose optimization problem is similar to that of MPC, its algorithm is more computationally efficient, which means the LQR can achieve higher update rate of the control signals than the MPC running in the same hardware, however, the LQR does not have the MPC's capabilities to handle with constraints. Hence, the comparison between LQR-based and MPC-based ESCs allows to observe the benefits of the MPC and the effects of its low command update rate.

In the design of model-based controllers, such as LQR and MPC, the mathematical model used in control design have a strong influence on control performance. According to the mathematical model of vehicle dynamics (Section 2.1), rolling motion has a strong influence on lateral stability, so the inclusion of roll-degree-of-freedom reduces the model uncertainties and enables some roll control. But using a simpler model without roll-degree-of-freedom can simplify the control algorithm, which contributes to achieving a high update rate of the control signals. To observe the effects of enabling the roll control, the control systems proposed in this research were implemented with and without roll control, and the results obtained with and without roll control were compared with each other.

The proposed control algorithms were implemented as software for an embedded Linux running on ARM Cortex A8 of Beagle Bone Black board to be subject to HIL simulations. The BeagleBone's analog inputs were used to read the feedback signals: vehicle speeds, roll angle, roll rate, yaw rate, and front wheels steer angle, and RJ45 Ethernet connection over UDP was used to send the yaw moment given as control signal.

The performances of the proposed algorithms and their implementations were evaluated using the MIL and HIL simulations as described in Section 3, in which the ESCs are tested on control of the nonlinear of

Table 4.1: Parameters of vehicle dynamics model used in MIL and HIL simulations performed to evaluate the proposed ESCs. Values obtained in [34, 67]

Param.	Value	Param.	Value	Param.	Value	Param.	Value
a	1.1m	b	1.3m	a_0	1.3	a_1	-49
t_f	1.4m	t_r	1.41m	a_2	1216	a_3	1632
h_s	0.55m	h	0.6m	a_4	11	a_5	0.006
m	1070Kg	m_s	900Kg	a_6	-0.04	a_7	-0.4
I_{zz}	$2100Kgm^2$	I_{xx}	$500Kgm^2$	a_8	0.003	a_9	-0.002
I_{xz}	$47.0Kgm^2$	I_s	20	a_{10}	0	a_{11}	-11
$c_{\phi f}$	1050Nms/rad	$c_{\phi r}$	1050Nms/rad	a_{12}	0.045	a_{13}, a_{14}	0
$k_{\phi f}$	32795Nm/rad	$\partial\delta_f/\partial\phi$	0.1	$k_{\phi r}$	32795Nm/rad	$\partial\delta_r/\partial\phi$	-0.1
$C_{\gamma fr}$	-86340N/rad	$C_{\gamma fl}$	-86340N/rad	$C_{\gamma rr}$	-61455N/rad	$C_{\gamma rl}$	-61455N/rad
T_k	0.2	μ	0.75	W	0.2	L_a	20

vehicle dynamics, presented in Section 2.1. Table 4.1 show the parameters of the nonlinear vehicle model used in MIL and HIL simulations.

The platform used for HIL testing can run the real-time simulation of vehicle response with a minimum sampling time of 0.8ms. Since the command update time that can be tested in HIL simulation is limited to multiples of the sampling time of the HIL platform, the minimum command update time that can be tested is equal to 0.8s. The processing limits of the HIL platform do not limit the command update rates that can be configured in MIL tests. But as the purpose of MIL testing is to evaluate in a computational environment the expected behavior for the embedded control system, and the embedded control system will be only evaluated in this research in HIL simulations, then the MIL tests were configured with a command update rates equal to those that can also be configured in HIL tests.

In MIL and HIL simulations, the vehicle's response to control signals is obtained from nonlinear models, whereas the proposed controllers are based on linear models. Thus, all simulations test the controllers in the presence of divergences between the vehicle's response and that predicted by the control algorithm. The linear models used in the design of the controllers were obtained from simplifications for constant longitudinal speed. In the controllers evaluated in this chapter, this constant speed is equal to 100 km/h. So, in simulations of maneuvers at speeds other than constant 100 km/h, in addition to the linearization errors, there are divergences between the linear model response and the simulation model due to the difference in vehicle speed, so these simulations evaluate in some way the robustness of the controller to the mismatch between plant and model. To further inspect the robustness of the controller to model's uncertainties, simulations were also carried out in which the mass, the position of the center of mass and the friction between the tire-road of the simulated vehicle are different from the values used in the configuration of the controllers. Table 4.2 shows the parameter used in these simulations that differ from the nominal value assumed in the ESC algorithms.

Table 4.2: Parameters used in the vehicle simulation to evaluate the proposed ESCs in the presence of model uncertainties. This table shows the parameters that are different from the nominal values assumed in control design, which are the vehicle mass m ,longitudinal distance a between center of mass and front wheels, longitudinal distance b, and tire-road friction coefficient μ.

Parameter	Value	Divergence	Parameter	Value	Divergence
a	1.04 m	-5.4%	m	1177 Kg	+10%
b	1.36 m	4.6%	μ	0.675	+10%

Following in this chapter, the results from the MIL and HIL simulations performed to evaluate the proposed ESCs are shown.

4.1 RESULTS FOR THE HIGH-LEVEL DYCS

The high-level DYCs developed and studied in this research are systems that compute the corrective yaw moment applied to the vehicle body without considering the change to be made in the torque transferred to the wheels to achieve this corrective yaw moment. The inputs of the model used to simulate the vehicle movement are the steering angle and the corrective yaw moment. In the absence of inputs that

control the rotation of the wheels, this model considers that the vehicle longitudinal speed is equal to the initial speed through the simulation time.

4.1.1 LQR-based high-level DYC

The LQR-based high-level DYC were the first ESCs developed as a proof of concept of the control architecture and simulation environment. This task contributed to the definition of the test environment used in the validation of all the controllers proposed in this research, since it was during the MIL tests of the LQR-based high-level DYCs that was detected the need for a simulation model to generate the steering command in response to the trajectory error. That is why the intelligent driver model was added to the simulation environment. This task also contributes to definition of the common control architecture of the ESCs proposed in this research, because the activation criteria were included when the results of simulations for low speed maneuvers show that the high-level DYCs based on LQR exhibit unnecessary non-null commands whenever the state errors are different from zero, even though there is no significant risk of handling destabilization or loss of maneuverability.

Table 4.3 shows the parameters of linear model used in control design, other parameters used in control design and not shown in this table are equal to the values configured for vehicle simulation, presented in Table 4.1. And Table 4.4 shows the value of the LQR weight matrices, which were defined following the tuning procedure defined in Section 3.4.5.

Table 4.3: Parameters used in design of the LQR-based high-level DYC, the parameters of the linear model of vehicle dynamics not shown in this table are equal to the nominal values shown on Table 4.1

Param.	Value	Param.	Value	Param.	Value	Param.	Value
$C_{\alpha fl}$	45292 N/rad	$C_{\alpha fr}$	45292 N/rad	$C_{\alpha rl}$	39018 N/rad	$C_{\alpha rr}$	39018 N/rad
M_{th}	200 Nm	μ	0.75	β_{th}	0.1 rad	T_{on}	0.08 s
ψ_{eth}	0.1 rad/s	T_{off}	0.8s				

Table 4.4: Tuned weight matrices of LQR-based low-level DYC

Controller	Q	R
LQR 4DOF	$\begin{bmatrix} 66.0 & 0 & 0 & 0 \\ 0 & 248.9 & 0 & 0 \\ 0 & 0 & 9.6 & 0 \\ 0 & 0 & 0 & 374.2 \end{bmatrix}$	1e-5
LQR 2DOF	$\begin{bmatrix} 55.4 & 0 \\ 0 & 44.5 \end{bmatrix}$	1e-5

According to Section 3.2, two LQR-based high-level DYCs were implemented: the HL_LQR_2DOF and the HL_LQR_4DOF. In LQR 2DOF, the LQR is defined for the linear model for high-level ESC with roll control off (Section 3.4.1), which is a 2DOF model whose states are the side-slip angle of the vehicle body and the yaw rate. In LQR 4DOF, the LQR is defined for the linear model for high-level ESC with roll control on (Section 3.4.1), which is a 4DOF model whose states are the side-slip angle of the vehicle body, yaw rate, roll rate, and roll angle. The LQR 2DOF has a shorter calculation time because it calculates the control signal from the weighted sum of two state erros, whereas the LQR 4DOF calculates the control

signal from the weighted sum of four state erros. However, the calculation time of both algorithms is shorter than the sampling time of the HIL platform, which is 0.8ms. Therefore, both systems were tested in HIL and MIL simulations with the command update time equal to one sampling time of the HIL platform. The following sections show the results of test scenarios simulated to evaluate these systems. Further description of the test scenarios can be found in Section 3.3.1.

4.1.1.1 MIL simulation of DLC at 80km/h

The results from this test scenario are presented in Figures 4.1 e 4.2. One can confirm from the trajectory obtained for a vehicle without ESC that the driver can perform successfully this maneuver without assistance, such that the vehicle does not cross the DLC boundaries, and after the last lane changing the vehicle follows an error-free straight path. By comparing the results for vehicle without ESC and with ESCs, one can observe that both ESCs does not interfere significantly on steering, however the control signals during the maneuver does not remain equal to zero, which means that these DYCs are not efficient in saving energy and avoiding unnecessary stress on the actuators when no assistance is necessary to keep the steering stable.

Regarding the model uncertainties, it is possible to observe that the side-slip and roll angles remain below 5 degrees, therefore the vehicle's response remains in the trust region of the linear approximations for small angles applied to obtain the model used in the definition of the LQR gain factors.

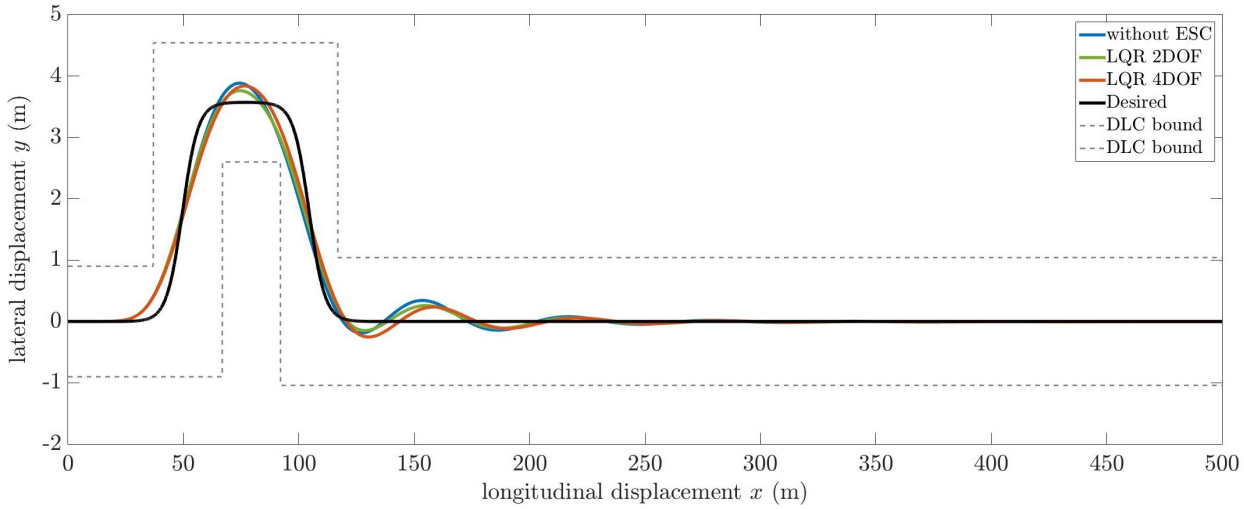

Figure 4.1: Vehicle trajectory from simulation of DLC at 80km/h for vehicle without ESC, with LQR-based high-level DYC based on 4DOF linear model and ESC based on 2DOF linear model

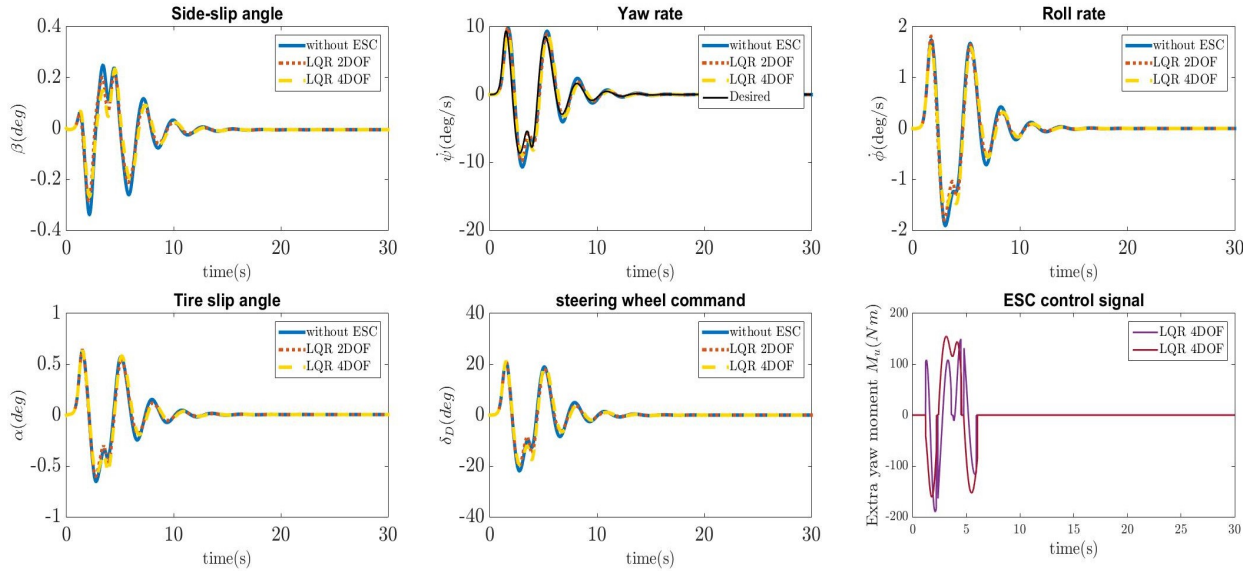

Figure 4.2: Results from simulation of DLC at 80km/h for a vehicle without ESC, with LQR-based high-level DYC based on 4DOF linear model and ESC based on 2DOF linear model

4.1.1.2 MIL simulation of DLC at 100km/h

Figures 4.3 and 4.4 show the results obtained from this simulation. One can confirm from the trajectory obtained from MIL simulation for a vehicle without ESC, which is shown in Figure 4.3, that the driver is not able to perform the maneuver without crossing the boundaries of lateral displacement. On the other hand, with any of both LQR-based high-level DYCs, the DLC maneuver is performed successfully. The results obtained with LQR 2DOF and LQR 4DOF is almost the same, no advantage of including the roll control is perceived for this maneuver. Besides, to avoid the steering instability, The ESCs are efficient to keep the sides-lip angle of the vehicle's body and the tire-slip angle smaller than 5 degrees, such that the vehicle response remains in the trust region of the linear model obtained from simplifications for small angles.

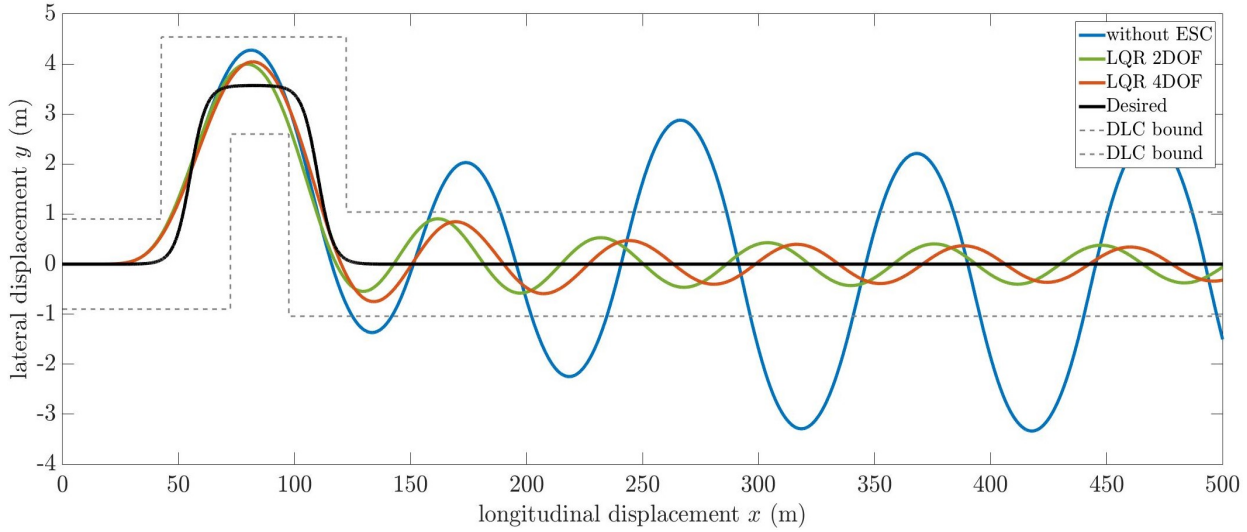

Figure 4.3: Vehicle trajectory from simulation of DLC at 100km/h for vehicle without ESC, with LQR-based high-level DYC based on 4DOF linear model and ESC based on 2DOF linear model

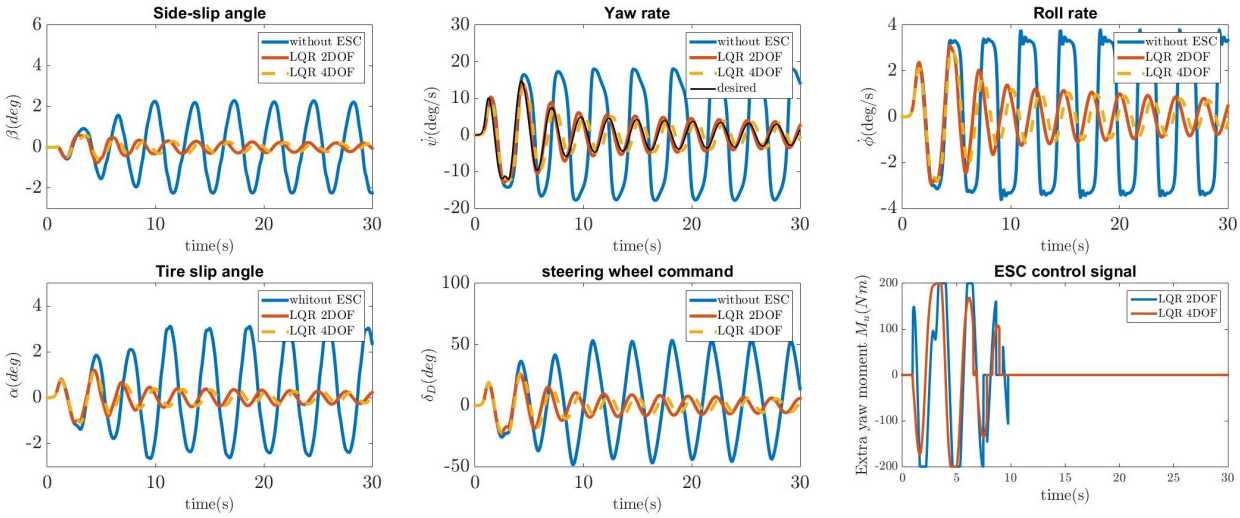

Figure 4.4: Results from simulation of DLC at 100km/h for vehicle without ESC, with LQR-based high-level DYC based on 4DOF linear model and ESC based on 2DOF linear model

4.1.1.3 MIL simulation of DLC at 120km/h

Figures 4.5 and 4.6 show the results obtained from this simulation. From the results for a vehicle without ESC, one can confirm that the driver loses the vehicle control. None of the ESCs is capable of allowing the maneuver to be performed successfully, since the trajectories obtained with both ESCs cross the lateral displacement boundaries of DLC testing and they do not return to a straight movement after the last lane change. Even so, an improvement in stability is achieved with both ESCs, since they prevent the driver from losing vehicle control and reduce the side-slip angle and the yaw-rate error, which improves maneuverability by keeping the vehicle's dynamics closer to the linear region.

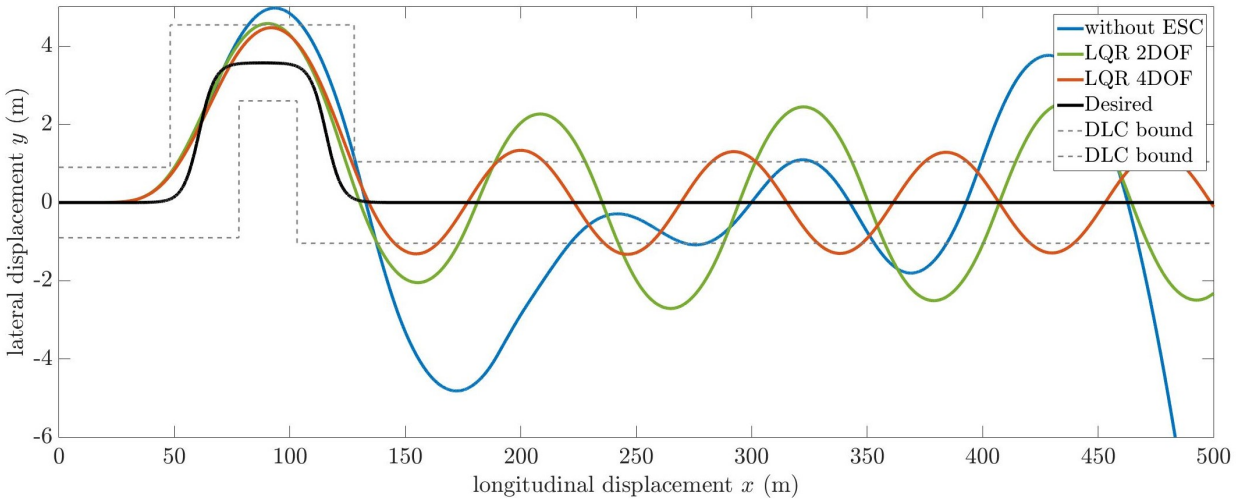

Figure 4.5: Vehicle trajectory from simulation of DLC at 120km/h for vehicle without ESC, with LQR-based high-level DYC based on 4DOF linear model and ESC based on 2DOF linear model

The benefits of enabling roll control can be observed in this scenario by comparing the states shown in Fig. 4.6, from where one can see that the side-slip angle of the vehicle body, the tire-slip angle, and

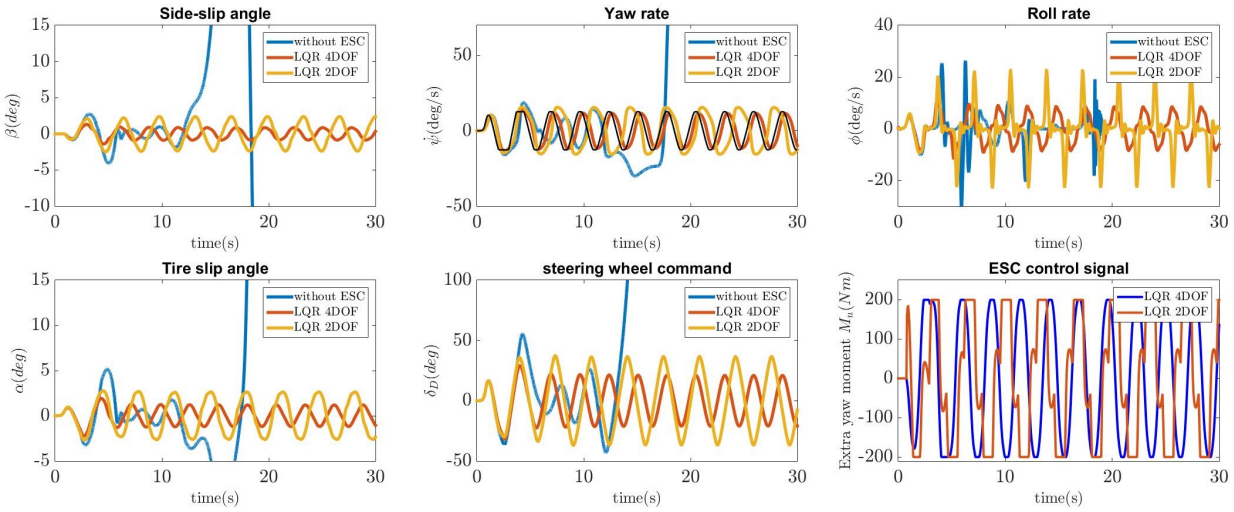

Figure 4.6: Results from simulation of DLC at 120km/h for a vehicle without ESC, with LQR-based high-level DYC based on 4DOF linear model and ESC based on 2DOF linear model

the roll rate obtained with the LQR 4DOF are smaller than those obtained with LQR 2DOF. The reduction of slip contributes to an increase in lateral stability, as it reduces the slip of the vehicle out of the desired trajectory. The reduction of tire slip leads to improving the lateral stability as it prevents the tire dynamics from reaching the saturation region, in which the lateral force generated becomes less responsive to steering wheel command and tire slip angle. And the reduction in the rollover rate means an improvement in passenger comfort.

Another evidence of the benefits of enabling the roll control can be observed by comparing the trajectory shown in Fig. 4.5. One can observe that the lateral displacement from the desired path obtained from simulation for a vehicle with 4DOF ESC is smaller than the obtained from simulation for a vehicle with 2DOF.

4.1.1.4 DLC at 120 km/h with model uncertainties

Figures 4.7 and 4.8 show the results for the LQR 4DOF on control of a vehicle model whose parameters equals the nominal values in control design shown on Tabel 4.1, and on control of a vehicle whose parameters are different from the nominal values used in the design of the controller (Table 4.2). By comparing these results, one can observe that the amplitude of states error, corrective yaw moment, steer wheel angle, and lateral displacement from the desired path are similar. This means that the stability performance is almost the same, which shows that the ESC robustness to model's uncertainties.

4.1.1.5 HIL simulation of the DLC maneuver at 100km/h

Figures 4.9 and 4.10 show results obtained from HIL compared with those obtained from MIL. From the results and the results of MIL simulation of DLC at 100km/h, one can note that the controller is efficient in real-time application to avoid instability. Comparing the results from MIL and HIL, one can see that the stability performance obtained in HIL simulation is better than the predicted by MIL simulation, since the

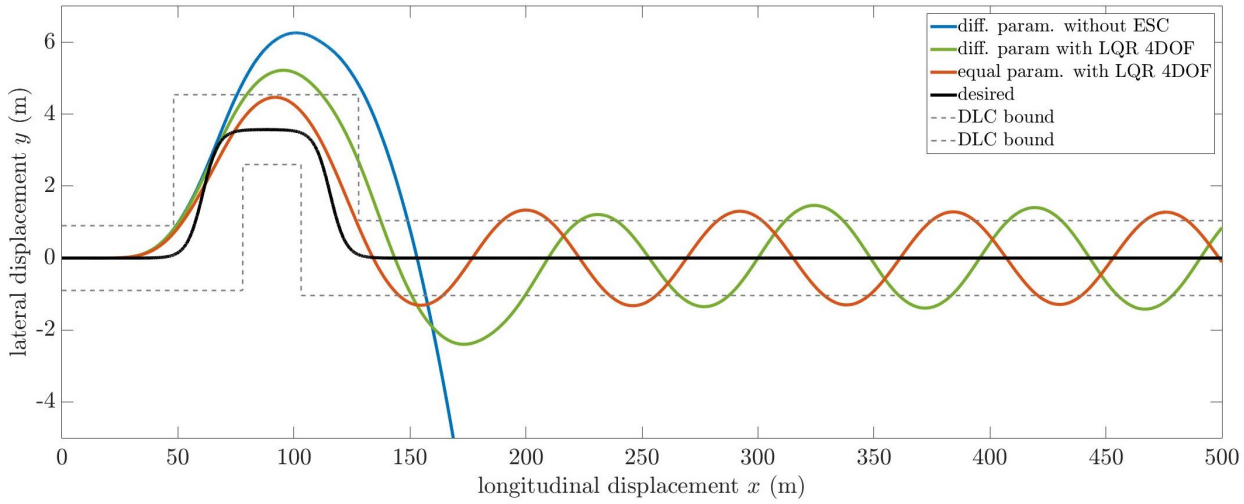

Figure 4.7: Vehicle trajectory from MIL simulation to evaluate the LQR 4DOF on control of a vehicle performing the DLC at 120km/h in presence of model uncertainties

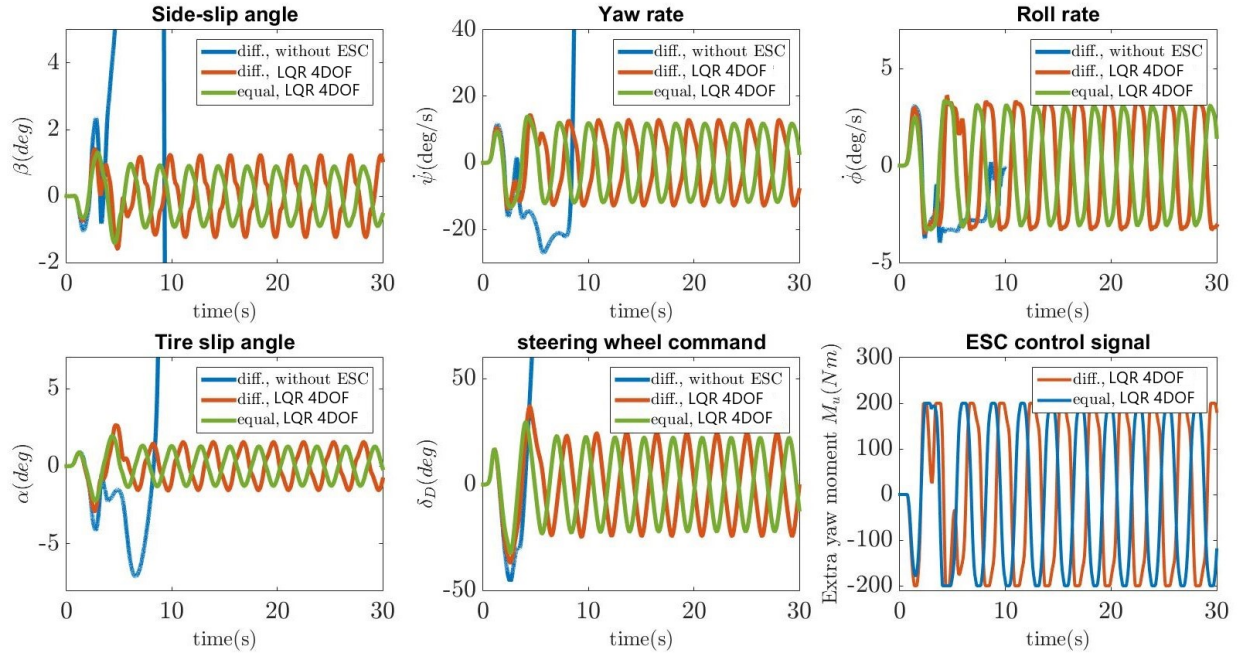

Figure 4.8: Results from MIL simulation to evaluate the LQR 4DOF on control of a vehicle performing the DLC at 120km/h in presence of model uncertainties

amplitudes of lateral displacement from the desired path, side-slip angle and roll rate obtained from HIL testing are quiet small than the predicted by results from MIL simulation. The reason for this is the fact that, at the exit of the last curve, ESC is activated early in HIL due to errors in state measurements. Even so, this result shows that the control algorithm has some undesired sensitivity to nonidealities of acquiring system.

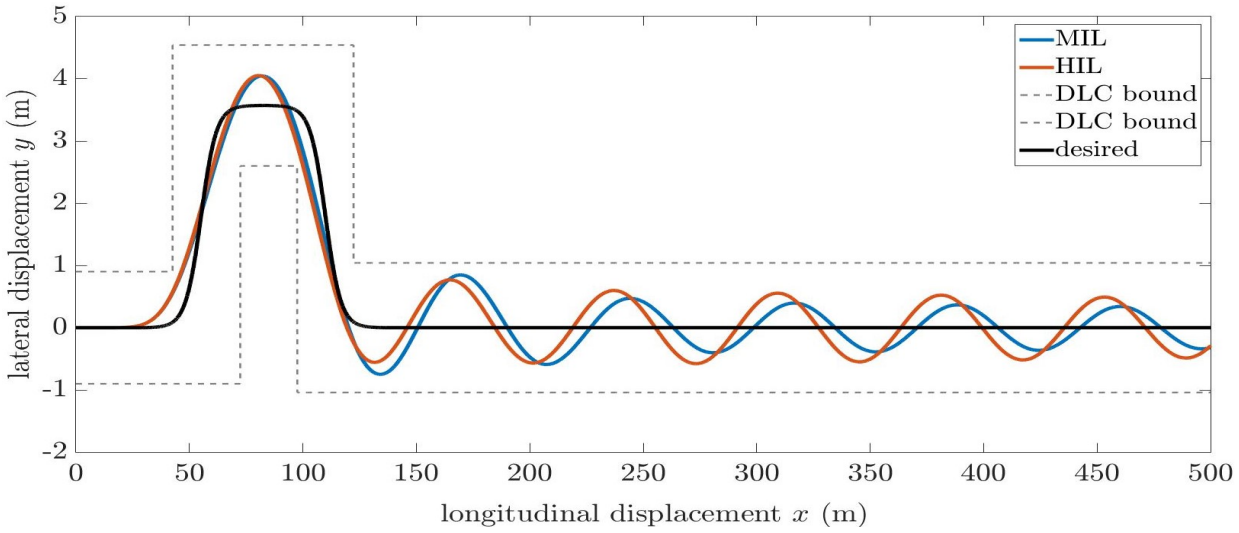

Figure 4.9: Vehicle trajectory from HIL and MIL simulation of DLC at 100km/h for vehicle with LQR-based high-level DYC designed based on a 4DOF linear model

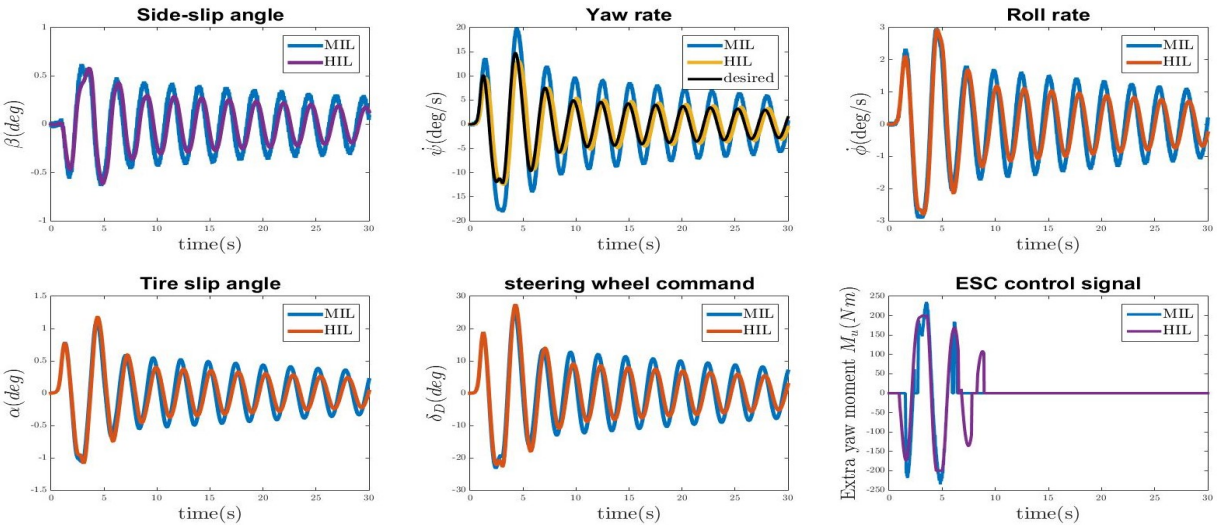

Figure 4.10: Results from MIL and HIL simulation of DLC at 100km/h for vehicle with LQR-based high-level DYC designed based on a 4DOF linear model

4.1.2 MPC-Based high-level DYC

After validating the proof of concept of the control architecture and the simulation environment, the high-level DYC was changed by replacing the LQR controller with an MPC.

This development was useful for definition of the MPC formulation used in this research, which is the formulation for LTI models presented in [25]. However the formulation presented in [25] does not support commands that are not controlled by the MPC. Therefore, it was necessary to make changes to handle commands not controlled by the MPC, such as the steering wheel angle, which is controlled by the driver. Also, the software solutions used to implement the MPC algorithm were defined during this development. The Eagle API is used for operations with matrices and vectors, and the *qpOASES* API is used for solving the QP of MPC formulation.

According to Section 3.2, two versions of this MPC-based high-level DYC were developed: the H_MPC_2DOF, referred to in this topic as ESC with roll control off, and the HL_MPC_4DOF, referred to as ESC with roll control on. Their implementations in Beaglebone Black were submitted to the tuning procedure described in Section 3.4.5 for definition of the optimal configuration of the coefficients Q_u, Q_y, η, ξ, N, and computation time τ. Figure 4.11 shows the minimum computation time and the corresponding mean square error of the lateral displacement obtained in the tuning procedure of ESC with roll control on for different prediction horizons. Its calculation time is monotonically increasing in relation to the prediction horizon because the increase in the horizon makes the QP more computationally complex. Whereas the MSE of the lateral displacement through the maneuver is decreasing in relation to the prediction horizon for horizons up to 50 sampling times and increasing for horizons above it. This result means that, for predictions horizons small than 50 sampling times, the benefits of increasing the predictability is greater than the negative effects of reducing the command update rate and, for horizons grater than 50 sampling times, the negative effects of reducing the command update rate is greater than the benefits of increasing the predictability. Therefore, the configuration N = 50 was chosen for the tests presented in this section.

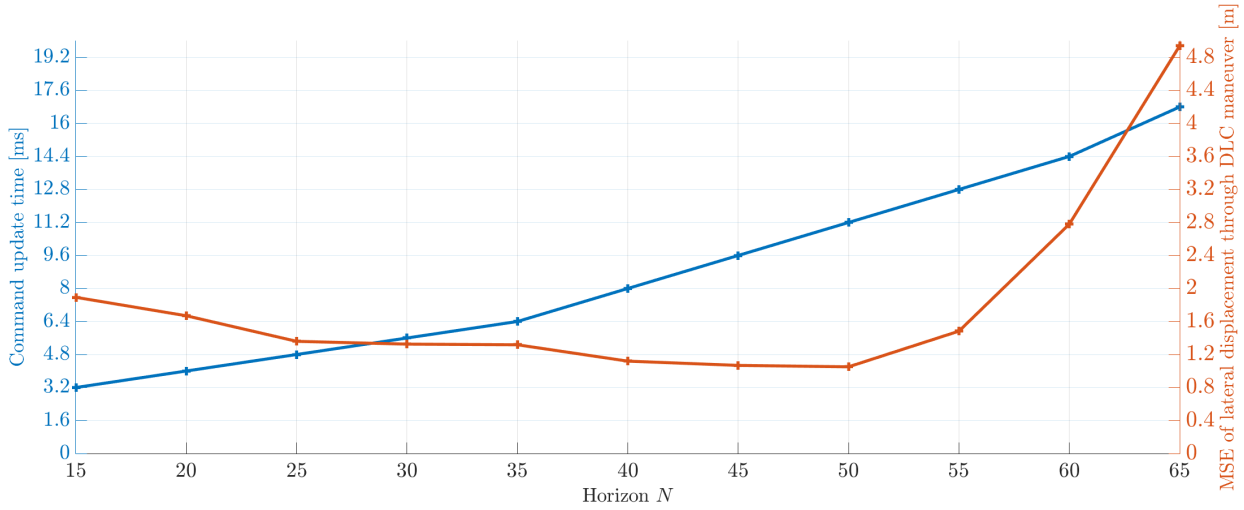

Figure 4.11: Minimum computation-time and mean square error of lateral displacement of trajectory from desired path obtained to different prediction horizons, from the tuning of the MPC-based high-level DYC with roll control enabled

The optimal coefficients obtained from the tuning procedure are shown in Table 4.6, the other parameters used in control design are shown in Table 4.5. An interesting detail of this result is that a better performance is achieved when only the errors in the yaw rate and the roll angle are weighted in the optimization problem to find the optimal control signals, i.e. when the MPC focuses the computational effort to regulate only these states. This shows that the MPC's ability to not necessarily regulate all states of the prediction model is useful for lateral stability control.

The following sections present results from the tests performed to validate the MPC-based high-leve DYCs. Further description of the test cases can be found in Section 3.3.1. In some scenarios, the results obtained with MPC are presented in comparison with the results obtained with LQR (with roll control on). For a fair comparison, the LQR coefficients are configured with the optimal values obtained from a tuning procedure presented in Section 3.4.5, which is similar to that followed to define the MPC's optimal configuration. The computation time of the LQR-based algorithm is considered in MIL and HIL simulations

Table 4.5: Configuration of the parameters used in the control algorithm of the MPC-based high-level DYC

Param.	Value	Param.	Value	Param.	Value	Param.	Value
a	1.1m	b	1.3m	h_s	0.55m	m_s	900Kg
I_{zz}	$2100Kgm^2$	I_{xx}	$500Kgm^2$	I_{xz}	$47.0Kgm^2$	$c_{\phi f}$	1050Nms/rad
$c_{\phi r}$	1050Nms/rad	u	100km/h	$k_{\phi f}$	32795Nm/rad	$\partial\delta_f/\partial\phi$	0.1
$k_{\phi r}$	32795Nm/rad	$\partial\delta_r/\partial\phi$	-0.1	a	1.1 m	b	1.3
$C_{\alpha fl}$	45292μN/rad	$C_{\gamma fl}$	-86340μN/rad	$C_{\alpha fr}$	45292μN/rad	$C_{\gamma fr}$	-86340μN/rad
$C_{\alpha rl}$	39018μN/rad	$C_{\gamma rl}$	-61455μN/rad	$C_{\alpha rr}$	39018μN/rad	$C_{\gamma rr}$	-61455μN/rad
M_{th}	200 Nm	μ	0.75	β_{th}	0.1rad	T_{on}	0.08s
ψ_{eth}	0.1rad/s	T_{off}	0.8s				

Table 4.6: MPC settings obtained from the tuning procedure of MPC-based high-level DYCs

Coefficients of the MPC-based DYC with roll control on							
Param.	**Value**	**Param.**	**Value**	**Param.**	**Value**	**Param.**	**Value**
η	7050.9	N	50	ξ	6499.4	τ	11.2 ms
Q_u	10^{-5}	Q_y	$\begin{bmatrix} 1.10 & 0 \\ 0 & 1.12 \end{bmatrix}$			C_r	$\begin{bmatrix} 0 & 0 & 0 & 0 \\ 0 & 1 & 0 & 0 \\ 0 & 0 & 0 & 0 \\ 0 & 0 & 0 & 1 \end{bmatrix}$
Coefficients of the MPC-based DYC with roll control off							
Param.	**Value**	**Param.**	**Value**	**Param.**	**Value**	**Param.**	**Value**
η	100000	N	50	ξ	8490	τ	10.6 ms
Q_u	10^{-5}	Q_y	20000			C_r	$\begin{bmatrix} 0 & 0 \\ 0 & 1 \end{bmatrix}$

equal to the sampling time of the HIL platform (0.8ms), which is the minimum computation time that can be tested in HIL simulations.

4.1.2.1 MIL simulation of DLC at 80 km/h

The results from MIL simulation of DLC maneuver at 80 km/h are shown on Figures 4.12 and 4.13. It is possible to observe that the extra yaw moment provided by the ESC remains null during the entire maneuver, because the side- slip and the yaw rate errors do not satisfy the conditions for Esc activation. In this way, the same result is obtained with roll control on or off, in which the driver is able to perform the maneuver without ESC assistance. This is a desired performance because it indicates that the ESC does not interfere unnecessarily in driving, even in the presence of an error between the target trajectory and that traveled by the vehicle, since this error does not mean a risk of handling instability.

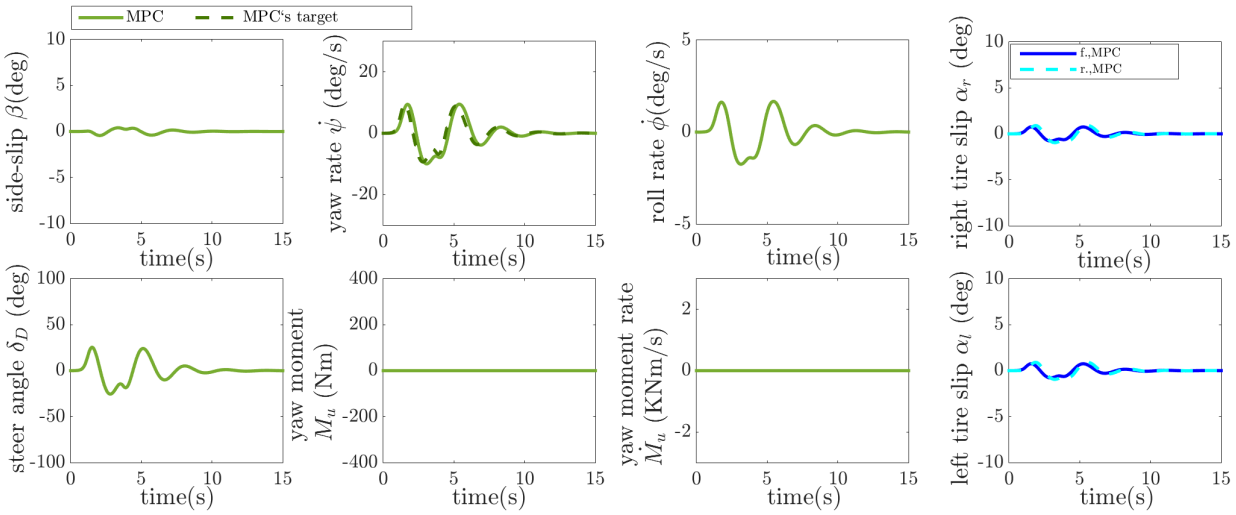

Figure 4.12: Results from MIL simulation of DLC at 80km/h for MPC-based high-level DYC. Since the corrective yaw moment given as control command remains equal to zero through the simulation time, this is the same result obtained from the simulation of DLC at 80 km for a vehicle without ESC. The target yaw rates are computed by Eq. 2.21, which depends on the driver's behavior in steering wheel control during the maneuver.

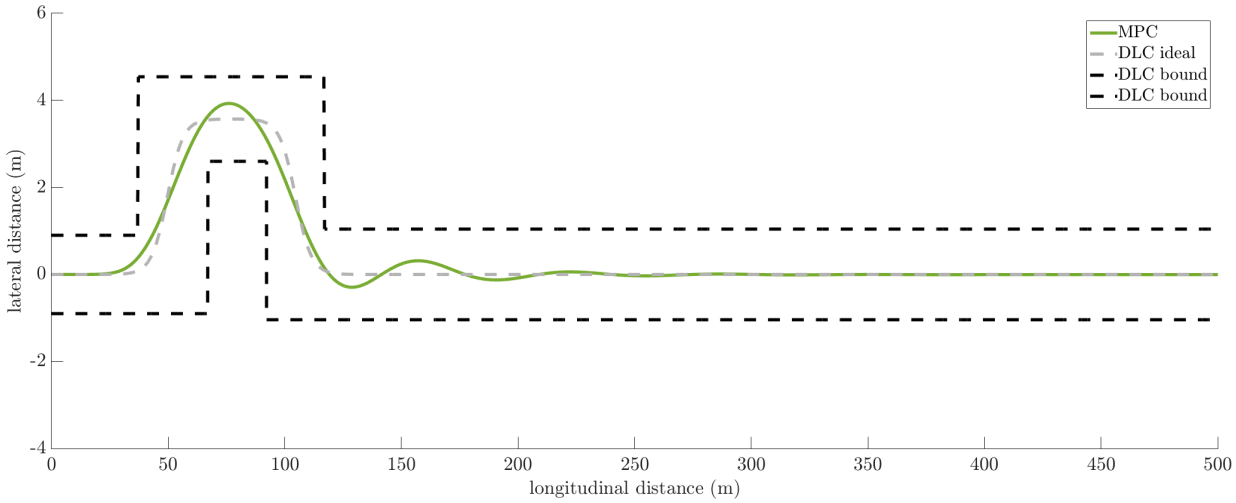

Figure 4.13: Vehicle trajectory from MIL simulation of DLC maneuver at 80 km/h for MPC-based high-level DYC.

4.1.2.2 MIL simulation of DLC at 100 km/h

The Figures 4.14 and 4.15 show the results obtained from the simulation of DLC at 100 km/h for vehicles equiped with the MPC-based and the LQR-based high-level DYCs. From the vehicle's trajectories and the side-slip angles, one can see that the driver loses the control of the vehicle with ESC off. Whereas, both ESCs succeed in preventing the steering instability, such that the driver does not lose the vehicle control with ESC assistance. However, only the MPC-based DYC allows the driver to perform this maneuver without crossing the DLC boundaries of lateral displacement.

The benefits of using MPC for lateral stability can also be seen in the side-slip angles of vehicle body and tires, in which these angles obtained with the MPC are lower than those obtained with the LQR. Comparing the steering signal provided by the driver model, it is possible to observe that smaller oscillation

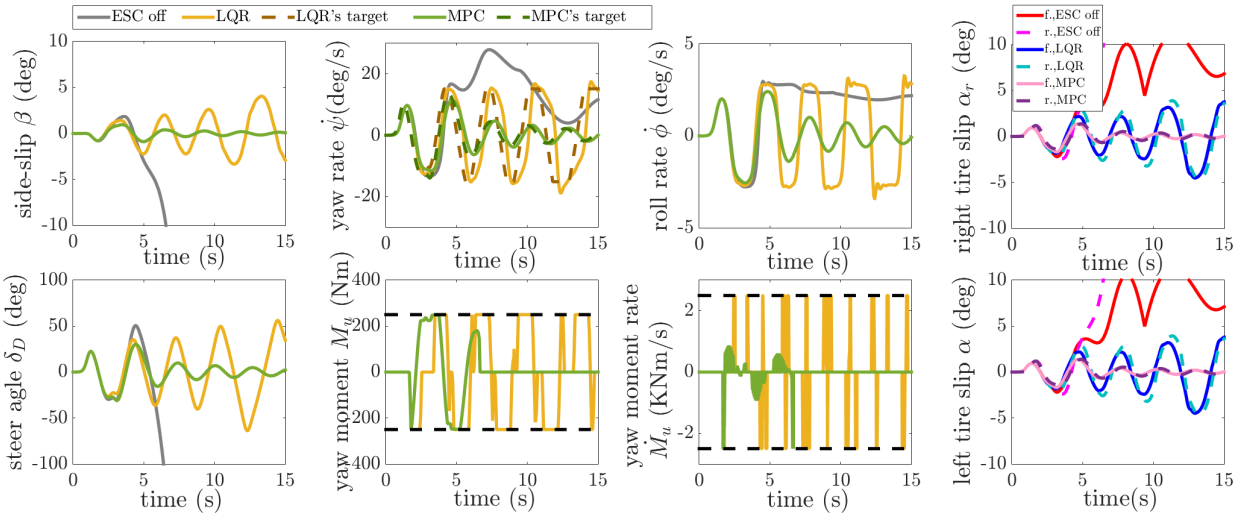

Figure 4.14: Results from MIL simulation of DLC at 100km/h for a vehicle without ESC, with MPC-based high-level DYC and with LQR-based high-level DYC. The target yaw rates are computed by Eq. 2.21, which depends on the driver's behavior in steering wheel control during the maneuver.

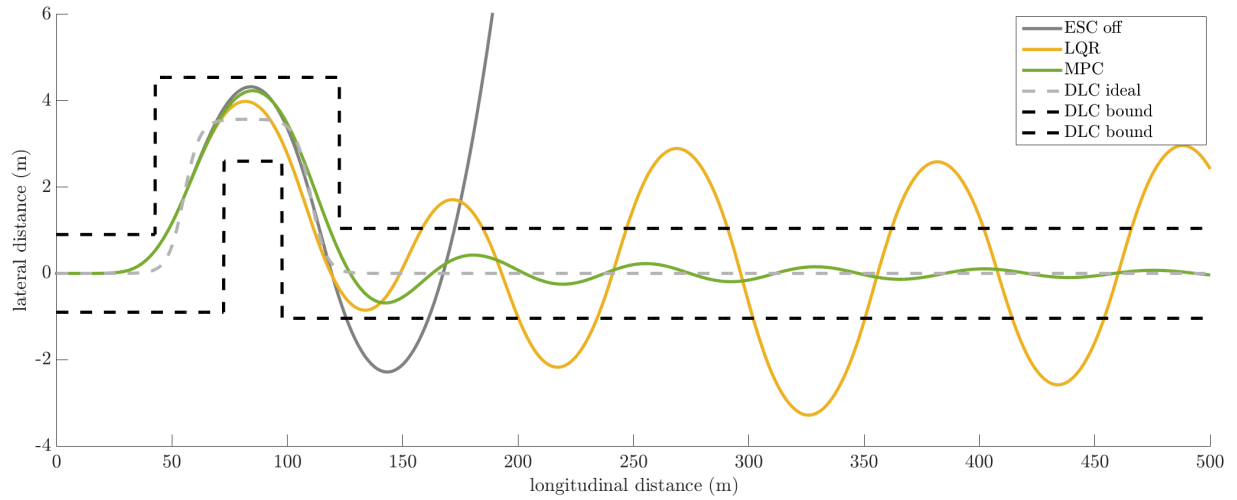

Figure 4.15: Vehicle trajectory from MIL simulation of DLC maneuver at 100 km/h for vehicles without ESC, with MPC-based high-level DYC and with LQR-based high-level DYC.

amplitudes are obtained with the MPC, which indicates that less effort is required from the driver to perform the maneuver with the vehicle equipped with the MPC-based ESC. And comparing the corrective yaw moment, it can be observed that the LQR-based ESC switches on/off more times during the maneuver than MPC-based ESC, which indicates that the MPC is more efficient in actuation, i.e. more stability performance is achieved with less actuation.

The DLC at 100 km/h also was simulated for the MPC-based ESC with roll control disabled. The Fig. 4.16 shows the trajectory obtained from the simulation of DLC at 100km/h performed for vehicles with proposed MPC-based high-level DYC with roll control on and off. Comparing the results, a smaller trajectory error is obtained with the scroll control off This is an interesting result, as it indicates that, in this scenario, the benefits of the higher command update rate obtained when using a simpler prediction model are greater than the benefits of a more accurate prediction obtained when using a more representative

model. However, it is important to note that both controllers are efficient in improving stability so that the maneuver is successfully performed.

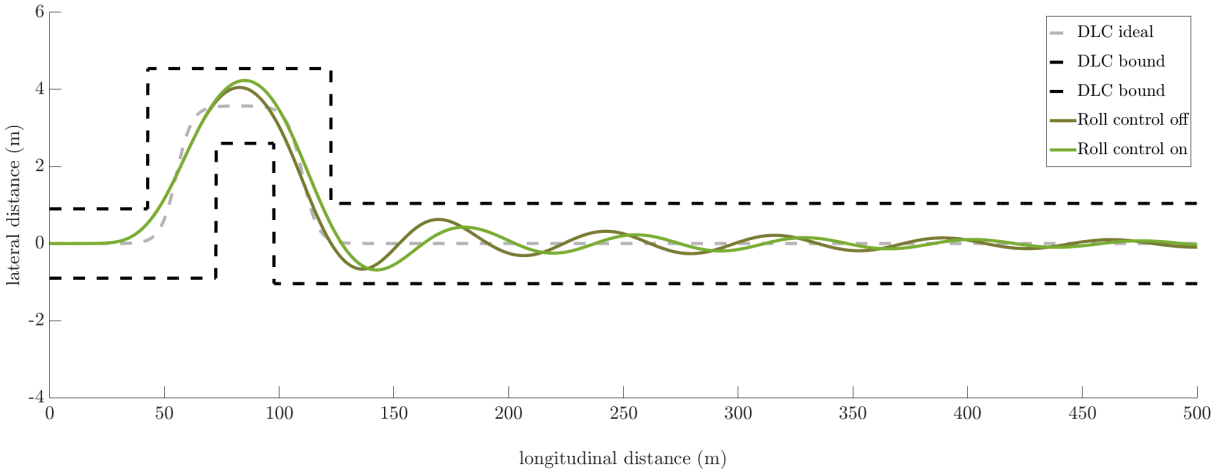

Figure 4.16: Vehicle trajectory from MIL simulation of DLC maneuver at 100 km/h for vehicles with MPC-based high-level DYC with roll control on and off.

4.1.2.3 MIL simulation of DLC at 120 km/h

The DLC at 120km/h was simulated to test the ESC on control of the vehicle at a higher speed than the trim point of the prediction model. The Figures 4.17 and 4.18 show the results obtained for vehicles without ESC assistance, and with LQR and MPC-based ESC. From the trajectory shown in Fig. 4.18, obtained for the vehicle without ESC, one can see that the driver cannot perform the double lane changing at 120 km/h without losing the vehicle control. The trajectories obtained with LQR and MPC-based ESCs have different performances, but with both controllers, the results show that the driver does not lose vehicle control. The vehicle with LQR-based ESC exhibits a higher trajecotory error, whereas the vehicle with MPC-based ESC briefly crosses the bounds of DLC once at the exit of the second lane changing. In the results shown 4.17, the MPC-based ESC exhibits a smoother actuation on yaw moment input, and is still more efficient in reducing of side-slip and roll angles error. With the MPC-base ESC, the side slip and roll angles of the vehicle body and the tire slip angles remain smaller than 5 degrees, which means that the effectiveness of the stability control keeps the vehicle states in the trust region of the vehicle-prediction-linear model.

The DLC at 120 km/h also was simulated for the MPC-based ESC with roll control disabled. Fig. 4.19 shows the trajectory obtained from this simulation, where one can see the benefits of inclusion of roll control, because the trajectory error obtained without roll control on at the exit of the second lane changing is smaller than the obtained with roll control off. And the Fig. 4.20 shows the results of vehicle dynamics obtained from this simulation, in which the vehicle with MPC-based high-level DYC with roll control off exhibits a higher roll rate, which means a higher risk of rollover and lower passenger conform. In addition to the extra roll rate, higher yaw rate, side-slipping, and tire-slipping are obtained for ESC with roll control off, which means a stability performance lower than the obtained with roll control on. And comparing steer angle signal provided by the driver model model, the amplitudes obtained for ESC with roll control off is greater than those obtained with roll control on, which means that without roll control the driver needs to

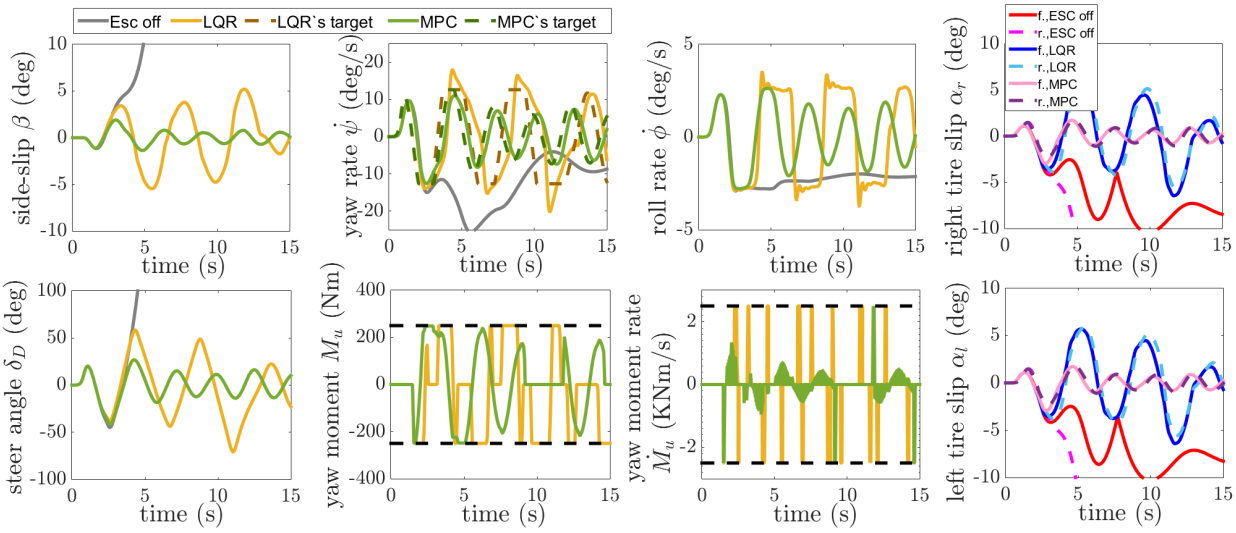

Figure 4.17: Results from MIL simulation of DLC at 120km/h for vehicles without ESC, with MPC-based high-level DYC and with LQR-based high-level DYC. The target yaw rates are computed by Eq. 2.21, which depends on the driver's behavior in steering wheel control during the maneuver.

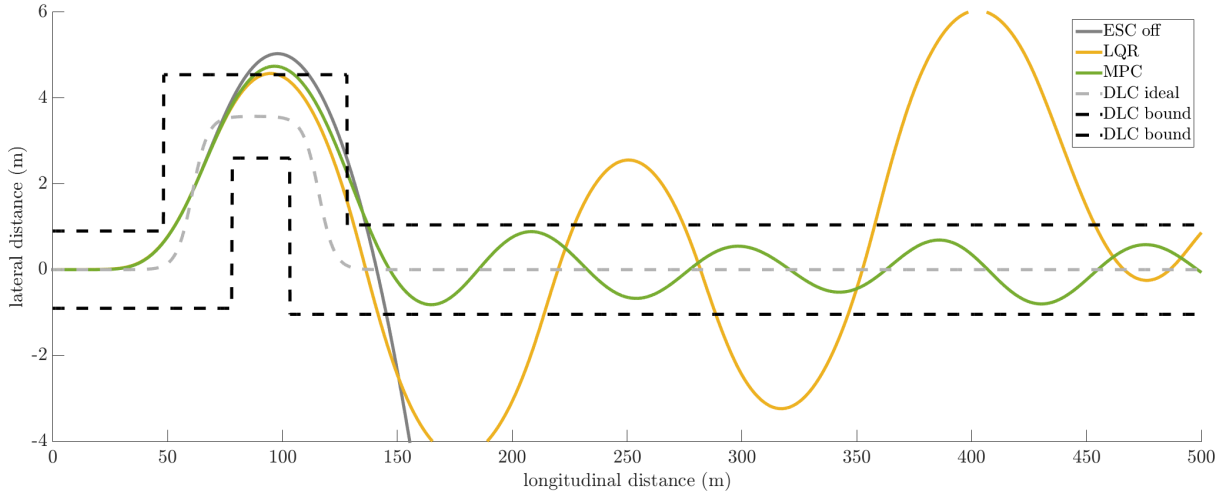

Figure 4.18: Vehicle trajectory from MIL simulation of DLC maneuver at 120 km/h for vehicles without ESC, with MPC-based ESC and with LQR-based ESC.

make an extra effort to maneuver. Based in these results, we can say that, in this scenario, the stability performance is greatly improved by the inclusion of roll control.

The increased influence of roll motion on the vehicle at high speeds is theatrically expected, because, at higher speeds, the roll rate has a stronger influence on yaw rate and tire dynamics. After all, it affects the vertical load transference between tires, which changes the lateral force acting on tires.

4.1.2.4 MIL simulation of DLC at 110 km/h with of model's uncertainties

The effectiveness of the proposed controller on a vehicle whose response is different from that predicted by the linear model also is evaluated. MIL simulation of DLC at 110km/h was performed for the MPC-based high-level DYC with roll control on. In addition to the speed higher than the trim point of the

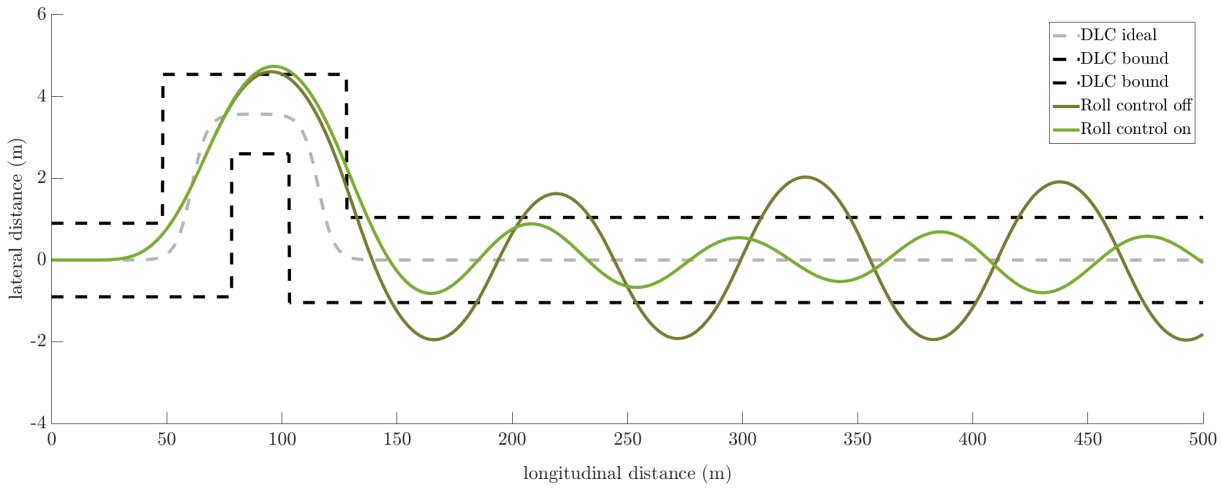

Figure 4.19: Vehicle trajectory from MIL simulation of DLC maneuver at 120 km/h for vehicles with MPC-based high-level DYC with and with roll control on and off.

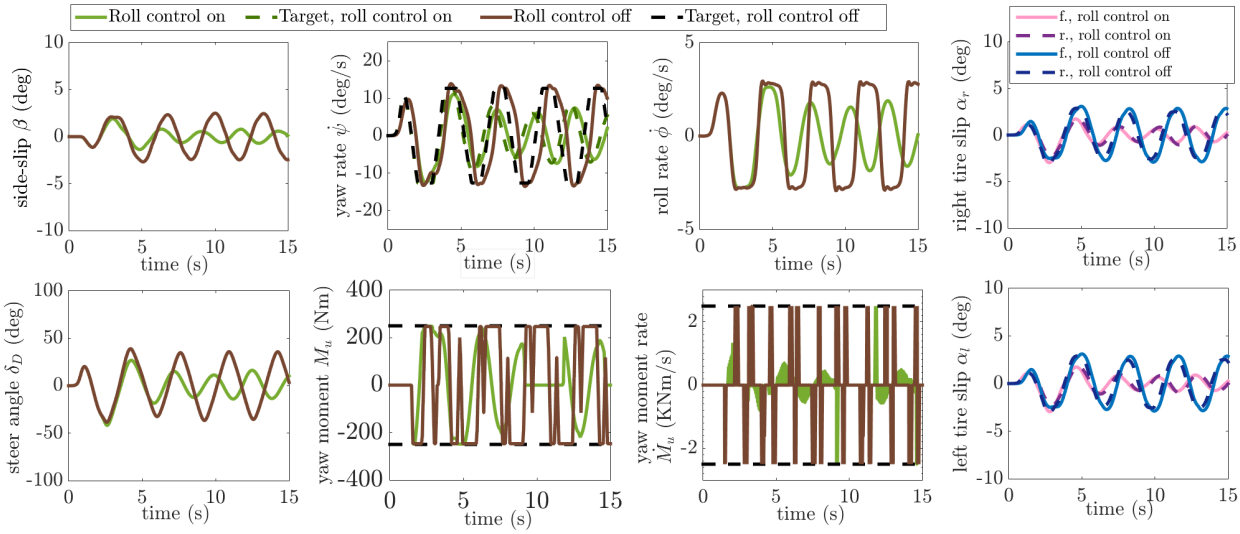

Figure 4.20: Results from MIL simulation of DLC at 120km/h for vehicles with MPC-based high-level DYC with roll control on and off. The target yaw rates are computed by Eq. 2.21, which depends on the driver's behavior in steering wheel control during the maneuver.

linear model, the vehicle simulated in this scenario has mass, center of mass position and tire-road friction different from the values used in configuration of the control algorithms. Parameters used in this simulation are shown in Table 4.2, parameters not shown in this table are equal to parameters shown in Table 4.2. The Fig. 4.21 shows results from this simulation, in which the side-slip angle of vehicle body, the roll rate, and the errors of trajectory and roll rate obtained in presence of model uncertainties is higher than those obtained for a vehicle whose parameters match the values used in the prediction model. This results indicate a performance decreasing in presence of model uncertainties, however the ESC remains effective to prevent the driver from losing vehicle control.

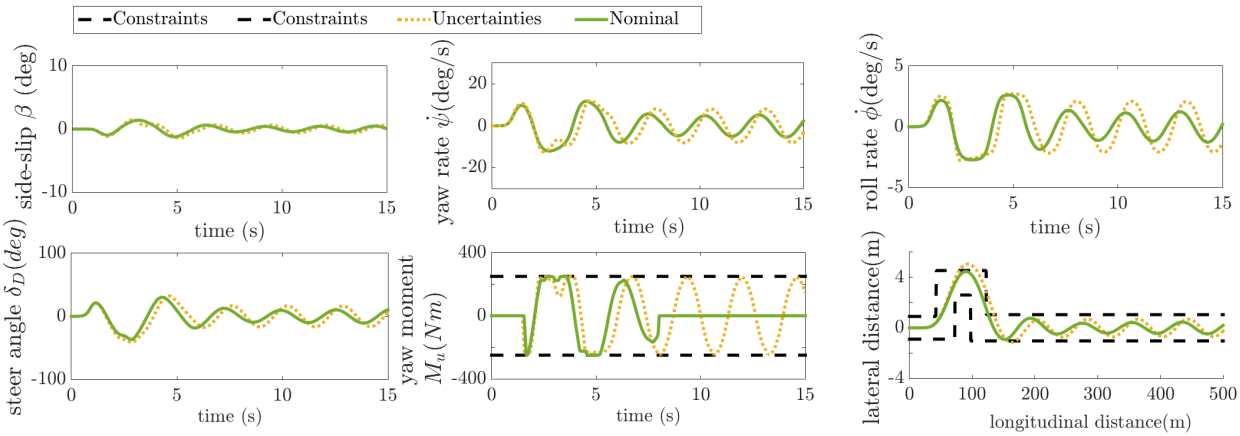

Figure 4.21: Results from MIL simulation of DLC at 110km/h for MPC-based high-level DYC on control of a vehicle model whose parameters are equal to the nominal values, and for MPC-based high-level DYC on control of a vehicle whose CG position, mass and tire-road friction are different from the nominal value used in control design.

4.1.2.5 HIL simulation of DLC at 110 km/h

The Figure 4.22 shows the results obtained from MIL and HIL simulation of DLC at 110 Km/h for the MPC-based high-level DYC with roll control on. In HIL simulation, in addition to the disturbances in the acquisition of feedback signals read by the controller through analog inputs, it also tested the control in presence of disturbances in vehicle response with respect to prediction model, due to the difference between simulated vehicle speed and the constant speed assumed by the prediction model.

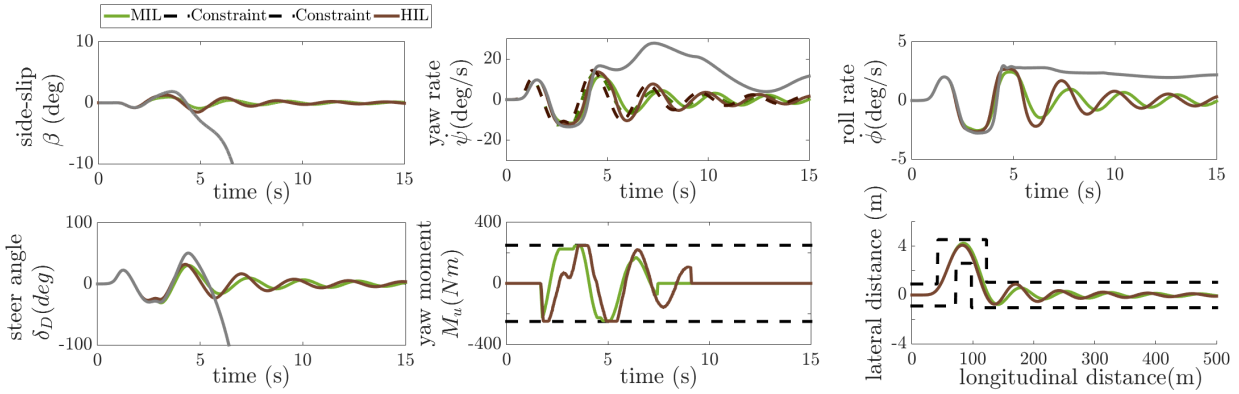

Figure 4.22: Results from HIL and MIL simulation of DLC at 110 km/h for MPC-based high-level DYC designed based on a linear model that considers the roll motion influence on vehicle motion. The target yaw rates are computed by Eq. 2.21, which depends on the driver's behavior in steering wheel control during the maneuver.

Comparing the results in Figure 4.22 from MIL and HIL simulations, there is a difference in the corrective yaw moments (i.e. control signals) that can be understood as consequence of the acquisition disturbances on the control activation, when the state errors are close to the decision threshold, which causes the ESC to activate at briefly different times in the MIL and HIL simulations. This difference in command generates a lag between the oscillations of the states and the trajectory observed in MIL and HIL. However, observing the amplitude of the oscillations of yaw and roll rates, side-slip angle and the trajectory during the maneuver, one can see that performance of implementation tested in HIL is similar to that predicted in MIL.

4.2 RESULTS FOR LOW-LEVEL DYCS

After the development of high-level controllers, which do not consider the effects of the actuation system on vehicle dynamics, the next stage of this research was the development of low-level controllers, which instead of calculating the corrective yaw moment, calculate the corrective torque transferred to each wheels. In this scenario, although the controllers are derived from linearized models for constant longitudinal speed, the non-linear vehicle model used in MIL and HIL simulations includes the longitudinal movement of the vehicle in response to the effects of the ESC's actuation on rotation of the wheels. The inputs of the vehicle model are the steering wheel angle provided by the intelligent driver model and the corrective torque transferred to the wheels. The next sections present the results of the simulations performed to evaluate the low-level DYCs developed in this research.

4.2.1 LQR-based low-level DYC

The first low-level ESC developed in this research is the LQR-based low-level DYC, presented in Section 3.2, which employees the discrete LQR for continuous plant to compute the corrective braking torque transferred to each wheel. In this system, the LQR is defined based on the linear model for ESCs with roll control on, presented in Section 3.4.1. The sampling time and weighting matrices were tuned following the procedure described in Section 3.4.5. The controller configuration used in the tests is shown in Table 4.7 and Table 4.8. Since the measured calculation time is shorter than the minimum sampling time of the HIL platform, the benefits of increasing the command update rate when disabling the roll control could not be observed. Therefore, only the LQR-based low-level DYC with roll control on was evaluated in this research. The results from this evaluation is presented in the following sections (Section 3.3.1 presents further description of the test cases).

Table 4.7: Configuration of the LQR-based low-level design.

Param.	Value	Param.	Value	Param.	Value	Param.	Value
T_{th}	200 Nm	T_{on}	0.08s	Q	$\begin{bmatrix} 0 & 0 & 0 & 0 \\ 0 & 337.9 & 0 & 0 \\ 0 & 0 & 34.2 & 0 \\ 0 & 0 & 0 & 9636.7 \end{bmatrix}$		
ψ_{eth}	0.1 rad/s	T_{off}	0.8s	R	$10^{-5}I^{4\times4}$		

Table 4.8: Parameters of the linear model used in LQR-based low-level design.

Param.	Value	Param.	Value	Param.	Value	Param.	Value
a	1.1m	b	1.3m	h_s	0.55m	m_s	900Kg
I_{zz}	$2100Kgm^2$	I_{xx}	$500Kgm^2$	I_{xz}	$47.0Kgm^2$	$c_{\phi f}$	1050Nms/rad
$c_{\phi r}$	1050Nms/rad	u	100km/h	$k_{\phi f}$	32795Nm/rad	$k_{\phi r}$	32795Nm/rad
$\partial\delta_f/\partial\phi$	0.1	$\partial\delta_r/\partial\phi$	-0.1	$C_{\alpha fl}$	45292μN/rad	$C_{\gamma fl}$	-86340μN/rad
$C_{\alpha fr}$	45292μN/rad	$C_{\gamma fr}$	-86340μN/rad	$C_{\alpha rl}$	39018μN/rad	$C_{\gamma rl}$	-61455μN/rad
$C_{\alpha rr}$	39018μN/rad	$C_{\gamma rr}$	-61455μN/rad	β_{th}	0.1 rad	μ	0.75 s

4.2.1.1 MIL simulations of DLC with initial speed of 80 km/h

The results obtained from simulation of DLC maneuver at 80 km/h are shown in Figures 4.24 e 4.23. From these results, one can see that the driver does not lose vehicle control in this maneuver, even without ESC assistance. The benefits of the ESC can be seen by comparing the trajectories presented in Figure 4.23, in which the vehicle without ESC crosses the DLC boundaries of lateral displacement at the exit of the last lane change, whereas the vehicle with ESC performs this maneuver successfully. The effectiveness of the LQR-based low-level DYC in improving the lateral stability can also be seen in the yaw rate presented in Figure 4.24, in which error amplitudes obtained with LQR-based ESC are smaller than those obtained without it. In addition to improve the lateral performance, the proposed system reduces the roll rate, which means an increase in passenger comfort, and it reduces the amplitude of the steering angle provided by the driver, which means an improvement in maneuverability, since less effort is required from the driver to perform the same maneuver. The efficiency of the ESC activation criterion to avoid unnecessary actuation is noted by checking that the corrective torque transferred to the wheels remains equal to zero most of the simulation time, even when there is an error in controlled states, since this error does not mean an risk of lateral destabilization.

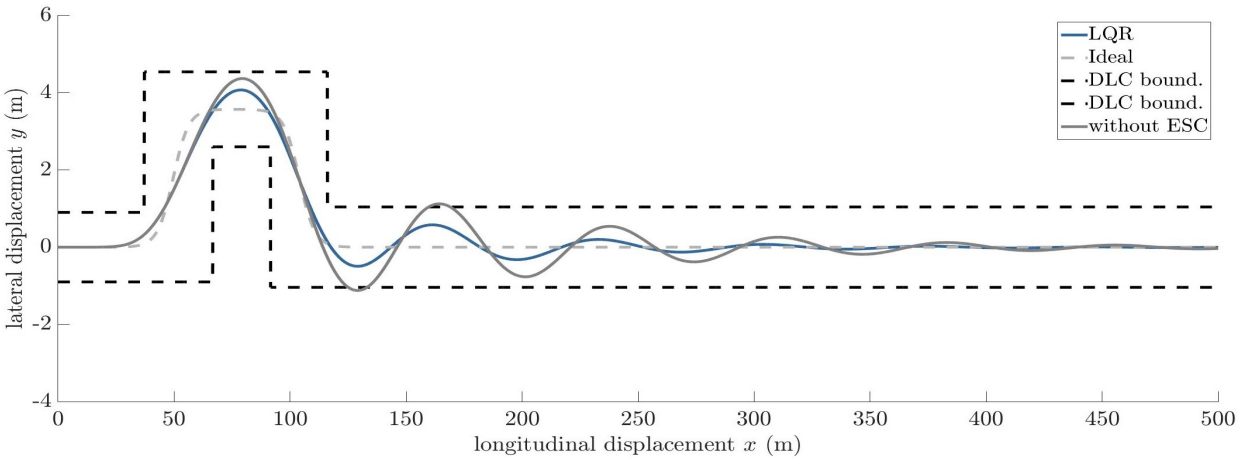

Figure 4.23: Trajectory obtained from simulation of DLC with initial speed of 80 km/h for vehicles with LQR-based low-level ESC and without ESC.

4.2.1.2 MIL simulations of DLC with an initial speed of 100km/h

Figures 4.25 and 4.26 show the result for DLC with initial speed of 100km/h. From the results for vehicle without ESC, one can see that driver loses the vehicle control. This steering destabilization occurs because the lateral slip reaches values greater than 10 degrees, condition in which the forces generated on tires become saturated, hence the yaw rate does not respond to the steering angle. Whereas, from results for vehicle LQR-based DYC, the maneuver is performed almost successfully, such that the vehicle crosses once the limits of lateral displacement. The ESC actuation on braking torque is efficient in keeping the side-slip angle small than 5 degrees, so the forces on tires do not saturate, and therefore the yaw rate responds to the steering wheel so that the driver is able to control the vehicle motion. The braking torque transferred to the wheels remains equal to zero most of the simulation time, even when state errors are not equal to

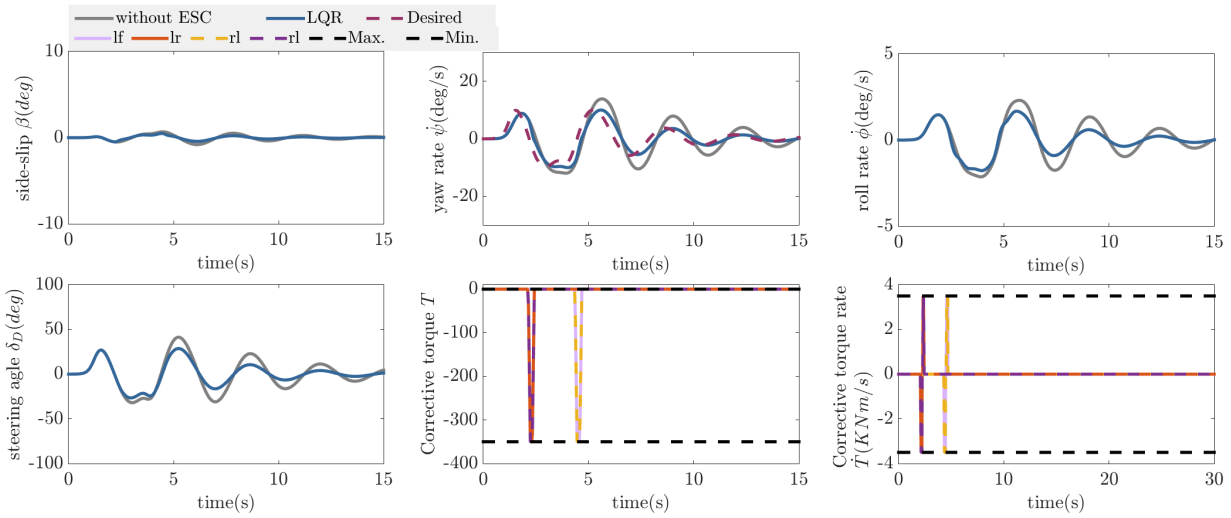

Figure 4.24: Results from simulation of DLC with initial speed of 80 km/h for vehicles with LQR-based low-level ESC and without ESC

zero. This shows the effectiveness of the ESC activation/deactivation criterion to avoid unnecessary action when the states errors do not mean a risk of the handling destabilization.

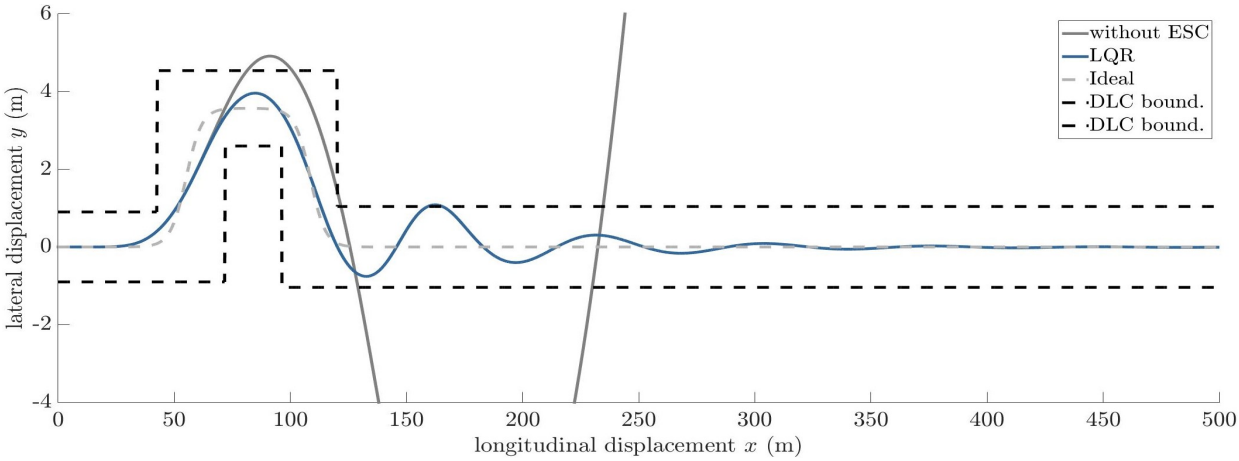

Figure 4.25: Vehicle trajectory from simulation of DLC with initial speed 100km/h for vehicles with LQR-based low-level ESC and without ESC.

Comparing the results obtained for the DLC maneuver with an initial speed of 80 km/h and 100 km/h, the control is activated more times at 100 km/h than at 80 km/h. This is an expected result because the instability risk is higher at higher speeds, i.e. more ESC assistance is required to keep the handling stable at higher speed.

4.2.1.3 MIL simulation of DLC with an initial speed of 120km/h

The Figure 4.27 and the Figure 4.28 show the results from the simulations of the DLC with initial speed of 120 km/h. At this speed, the ESC is not efficient in allowing the maneuver to be performed without the vehicle exceeding the limits of lateral displacement. Even so, the stability performance is still improved, since the ESC prevents the driver from completely losing the vehicle control. In this scenario, the braking

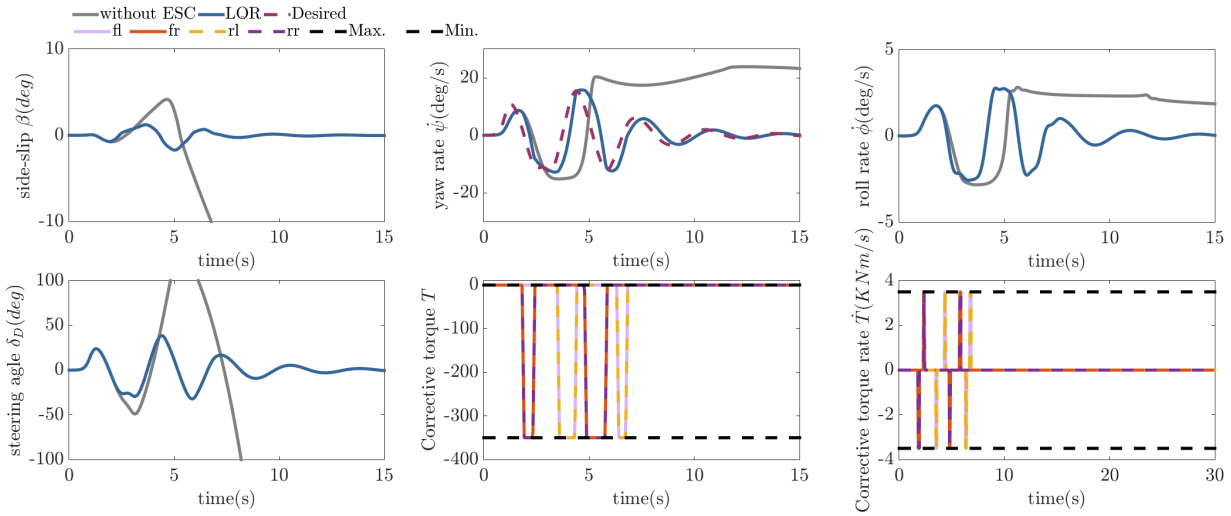

Figure 4.26: Results from simulation of DLC with initial speed of 100km/h for vehicles with LQR-based low-level ESC and without ESC.

of the wheels prevents the side-slip angle from increasing until the forces generated in the tires become saturated, however it does not prevent them from leaving the linear operating regime, so that the movement of the vehicle still responds to the steering wheel commands, but not from usual way that the driver is able to drive.

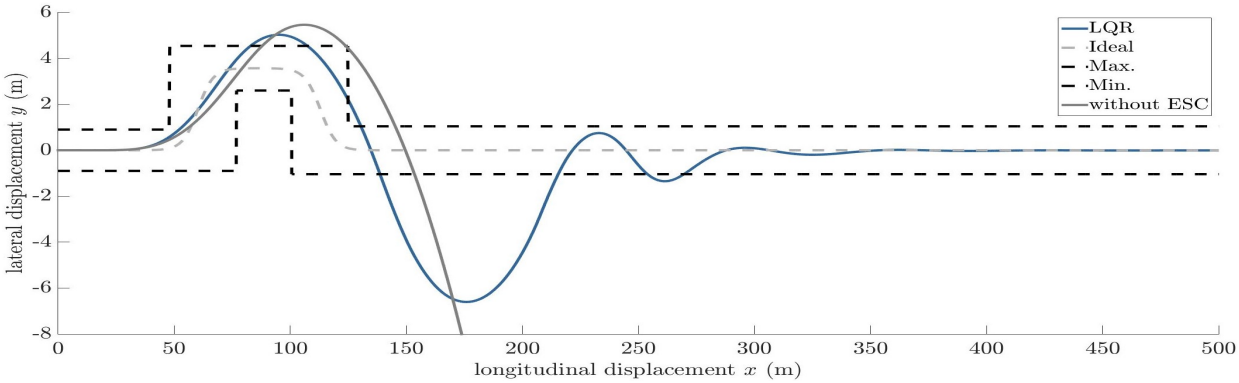

Figure 4.27: Vehicle trajectory from simulation of DLC at 120km/h for vehicles with LQR-based low-level ESC and without ESC.

As in the results obtained for lower speeds, it is possible to observe the effects of the ESC activation criterion on the brake control. Whenever the ESC is activated, the commands reach reach the maximum available braking torque, since the LQR does not consider this limitation, the torque transferred to the wheels is less than that calculated by the LQR. This demonstrates the potential for obtaining better results with controllers capable of handling restrictions imposed on the control signal.

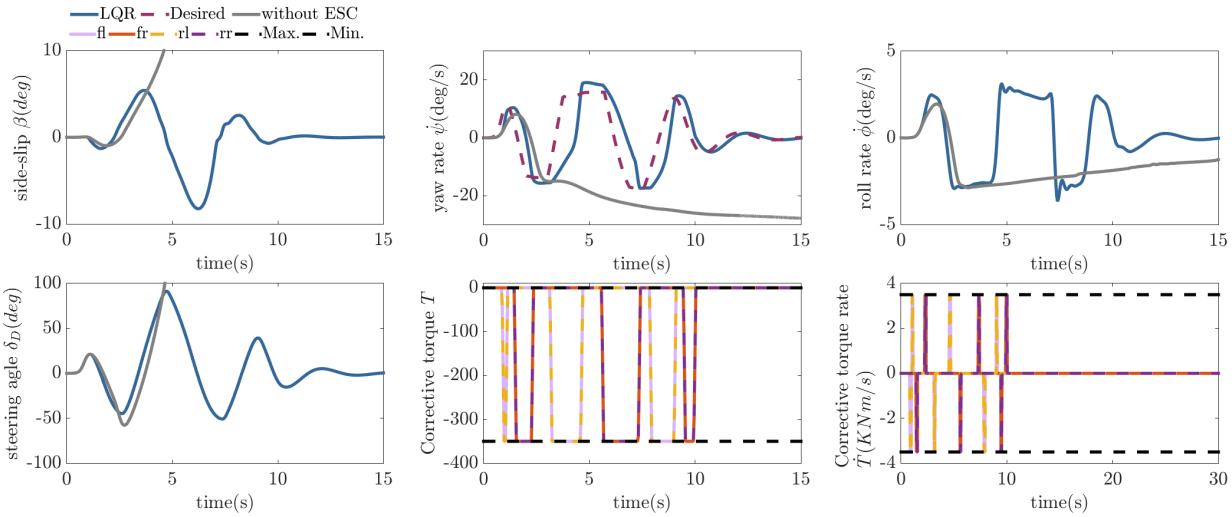

Figure 4.28: Results from simulation of DLC at 120km/h for vehicles with LQR-based low-level ESC and without ESC.

4.2.1.4 MIL simulation DLC with an initial speed of 120km/h and in presence of mode's uncertainties

Figures 4.29 and 4.30 show results of the simulations of DLC with initial speed of 120km/h performed to test the LQR-based low-level DYC on control of a vehicle model whose parameters are different from the values assumed in control design.

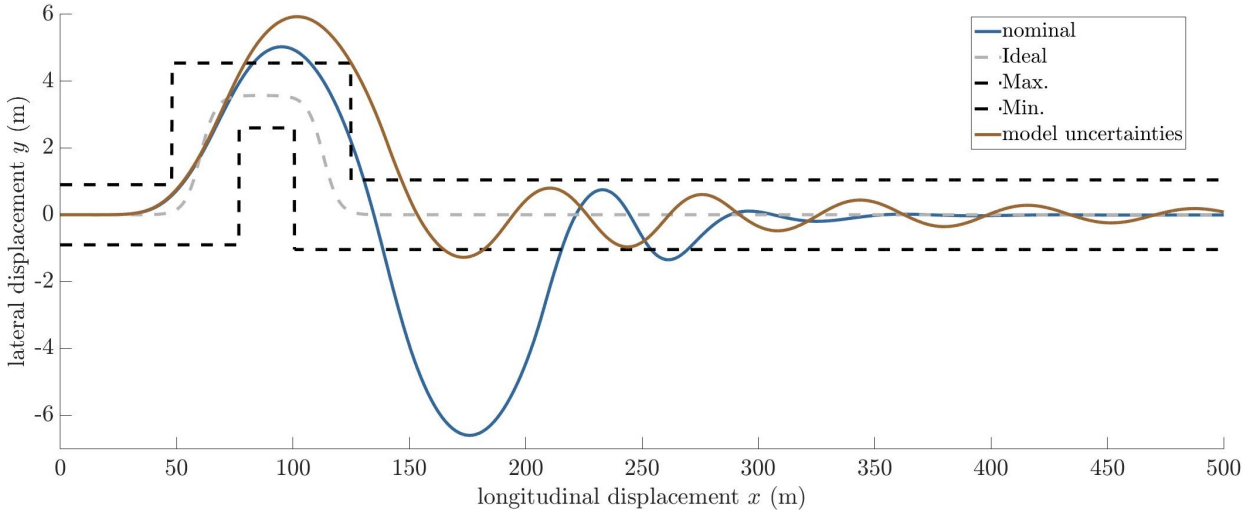

Figure 4.29: Trajectory from simulation of DLC with initial 120km/h performed to test the LQR-based low-level DYC on control of vehicle whose parameters have nominal values used in control design, and on control of a vehicle whose mass, position of the center of mass, and tire-road friction coefficient are different from the nominal parameters.

Comparing trajectories obtained for vehicles with nominal and non-nominal parameters, the trajectory obtained for the vehicle with non-nominal parameters is closer to the ideal. This is occurs because the state errors in the first curve is greater than those obtained for the vehicle with nominal parameters, which leads to earlier ESC activation, which improves performance in the following curves. Although a performance

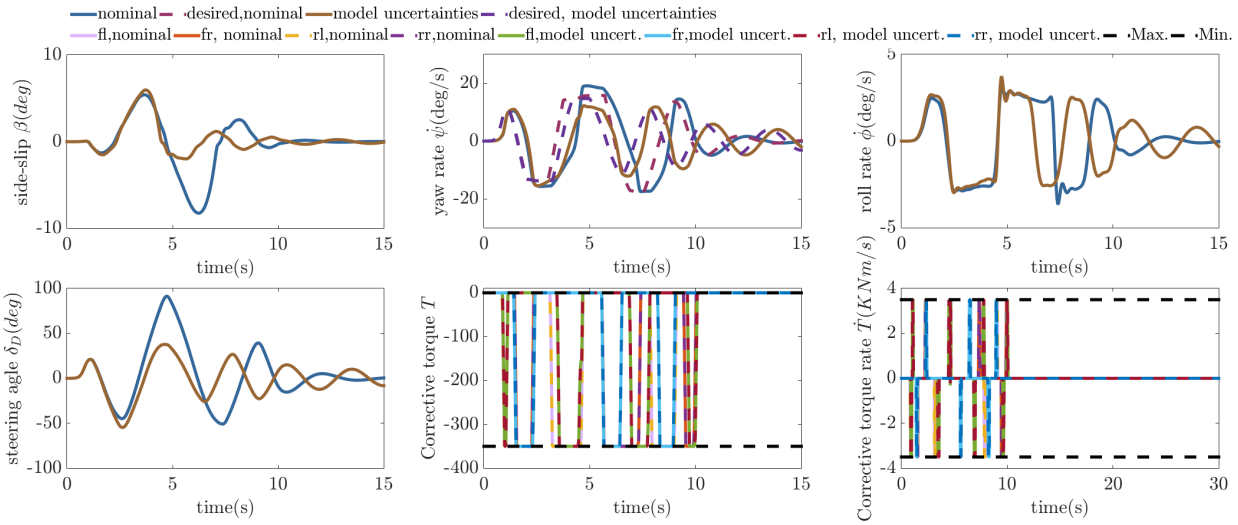

Figure 4.30: Results from simulation of DLC with initial 120km/h performed to test the LQR-based low-level DYC on control of vehicle whose parameters have the nominal values used in control design, and on control of a vehicle whose mass, position of the center of mass, and tire-road friction coefficient are different from the nominal parameters.

was observed in presence of model uncertainties, this sensitivity of the controller to the effects of plant and model mismatch is an undesirable characteristic.

4.2.2 MPC-Based low-level DYC

The ultimate system developed in this research is the MPC-based low-level DYC, which employees the MPC to compute the corrective torque transferred to the wheels. To explore the MPC capability to handle with constraints of the control signal, it is assumed that a differential braking system is used for actuation, such that the torque transferred to each wheel is limited to negative higher than a threshold. And to investigate the benefits of a shorter calculation time versus the benefits of a more accurate prediction, two versions of this system were implemented based in different prediction models: the linear models for low-level with roll on and off. The model with roll control off includes within the states only the side-slip angle and the yaw rate, so it does not take into account the effects of the roll motion on vehicle motion, however it leads to a simpler QP. Whereas, the model with roll control on includes within the states the side-slip angle, the yaw rate, the roll rate and the roll angle, so it gives a more accurate prediction, on the other hand, it takes a longer calculation time, i.e. it leads to lower command update rate. Table 4.1 shows the nominal parameters used in MIL and HIL simulations performed to evaluate these systems.

The tuning of the MPC coefficients Q_u, Q_y, η, ξ, and N was performed as described in Section 3.4.5. Figure 4.31 presents the best calculation time achieved with the ESCs running on ARM Cortex A8 and the mean square error of lateral displacement, for different prediction horizons. As expected, the increase in the prediction horizon leads to higher calculation times, because it makes the QP computationally more complex. However, the error in the lateral displacement is decreasing for horizons up to 50 sampling times, which means that, for this range, the benefits of extending the prediction capacity are greater than the negative effects of decreasing the command update rate. A interesting feature is the fact that, for horizons

up to 50 sampling times, the calculation time increases linearly, whereas the mean square error of lateral displacement does not vary that much, because this result shows the possibility to save the processing time without affecting significantly the ESC performance. For horizons longer than 50 sampling times, the negative effects of reducing the command update rate outweigh the benefits of extending the prediction capacity, such that the mean square error of lateral displacement is increasing in relation to the prediction horizon. To test the controller with its best configuration, the prediction horizon is configured equal to 50 sampling times. Table 4.10 shows the coefficients obtained as a result of this tuning procedure, the other parameters used in control design are shown in Table 4.9. The following sections presents the results obtained from simulations. Further description of the test cases are present in Section 3.3.1.

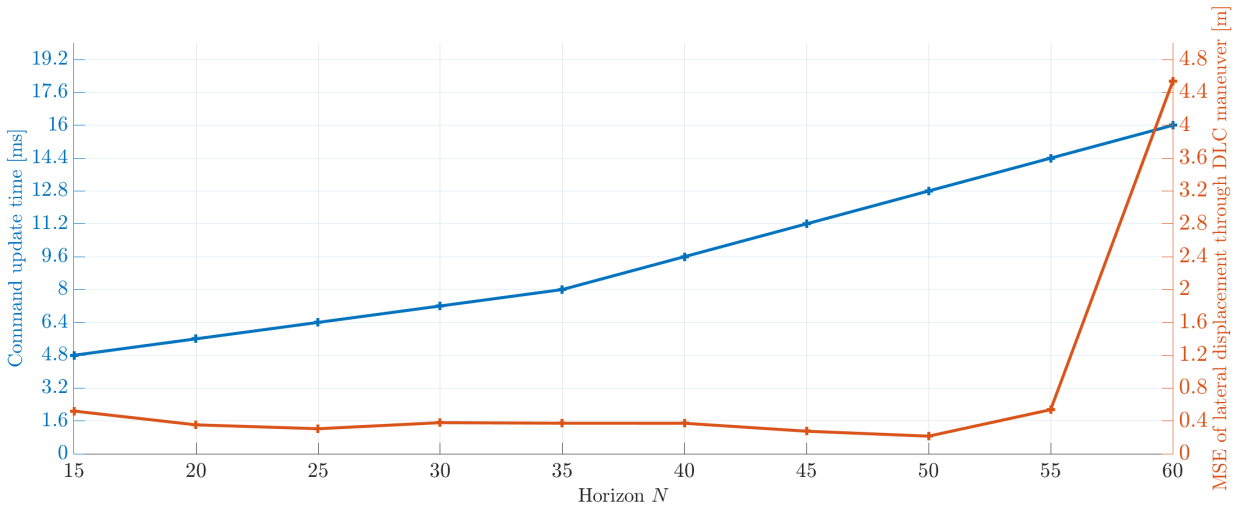

Figure 4.31: Minimum computation-time and mean square error of lateral displacement of trajectory from desired path obtained to different prediction horizons, from the tuning of the MPC-based high-level DYC with roll control enabled

Table 4.9: Configuration of the parameters used in the control algorithm of the MPC-based low-level DYC

Param.	Value	Param.	Value	Param.	Value	Param.	Value
a	1.1m	b	1.3m	h_s	0.55m	m_s	900Kg
I_{zz}	$2100 Kgm^2$	I_{xx}	$500 Kgm^2$	I_{xz}	$47.0 Kgm^2$	$c_{\phi f}$	1050Nms/rad
$c_{\phi r}$	1050Nms/rad	u	100km/h	$k_{\phi f}$	32795Nm/rad	$\partial\delta_f/\partial\phi$	0.1
$k_{\phi r}$	32795Nm/rad	$\partial\delta_r/\partial\phi$	-0.1	a	1.1 m	b	1.3
$C_{\alpha fl}$	45292μN/rad	$C_{\gamma fl}$	-86340μN/rad	$C_{\alpha fr}$	45292μN/rad	$C_{\gamma fr}$	-86340μN/rad
$C_{\alpha rl}$	39018μN/rad	$C_{\gamma rl}$	-61455μN/rad	$C_{\alpha rr}$	39018μN/rad	$C_{\gamma rr}$	-61455μN/rad
M_{th}	200 Nm	μ	0.75	β_{th}	0.1rad	T_{on}	0.08s
ψ_{eth}	0.1rad/s	T_{off}	0.8s				

4.2.2.1 MIL simulation of DLC with an initial speed of 80 km/h

The results obtained from the simulation of DLC maneuver with initial speed of 80km/h are shown in Figure 4.32 and Figure 4.33. The results for the vehicle without ESC confirm that the driver without ESC assistance can not perform this maneuver successfully without exceeding the limits of lateral displacement error. Even so, the steering remains stable, such that the vehicle returns to a straight movement after the

Table 4.10: MPC settings obtained from the tuning procedure of MPC-based low-level DYCs

Coefficients of the MPC-based DYC with roll control on							
Param.	**Value**	**Param.**	**Value**	**Param.**	**Value**	**Param.**	**Value**
η	6717.2	N	50	ξ	680.1	τ	14.4 ms
Q_u	$10^{-5}\mathbb{I}^4$	Q_y	$\begin{bmatrix} 325.2 & 0 \\ 0 & 1742.2 \end{bmatrix}$			C_r	$\begin{bmatrix} 0 & 0 & 0 & 0 \\ 0 & 1 & 0 & 0 \\ 0 & 0 & 0 & 0 \\ 0 & 0 & 0 & 1 \end{bmatrix}$
Coefficients of the MPC-based DYC with roll control off							
Param.	**Value**	**Param.**	**Value**	**Param.**	**Value**	**Param.**	**Value**
η	6632.0	N	50	ξ	583.7	τ	13.6 ms
Q_u	10^{-5}	Q_y	1999.6			C_r	$\begin{bmatrix} 0 & 0 \\ 0 & 1 \end{bmatrix}$

lane changes. Comparing the results with and without ESC, one can see that the proposed controller with roll control on or off is efficient to enable the maneuver to be successfully performed. In this scenario, the lateral performance is obtained by correcting mainly the yaw rate, which can be seen by checking that the amplitude of the side-slip angle through obtained without ESC is similar to that obtained with both ESCs, whereas the yaw rate error is reduced by ESC actuation. In addition to improve maneuverability, the ESC enhances the passenger comfort by reducing the roll rate.

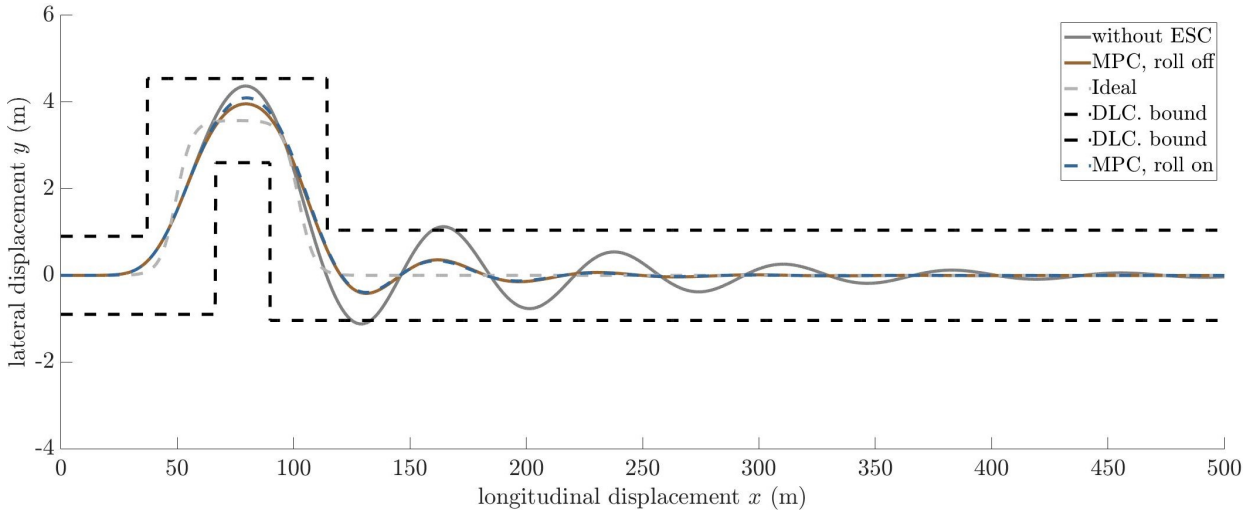

Figure 4.32: Vehicle trajectories from simulation of DLC with an initial speed of 80km/h performed by vehicle without ESC; with MPC-based low-level DYC with roll control on; and with MPC-based low-level DYC with roll control off.

Regarding energy savings and avoiding unnecessary action, it is possible to observe the benefits of the ESC actuation criteria in the Figure 4.33, in which the corrective braking torque transferred to the wheels remains equal to zero most of the simulation time, even at intervals where the state errors are not zero.

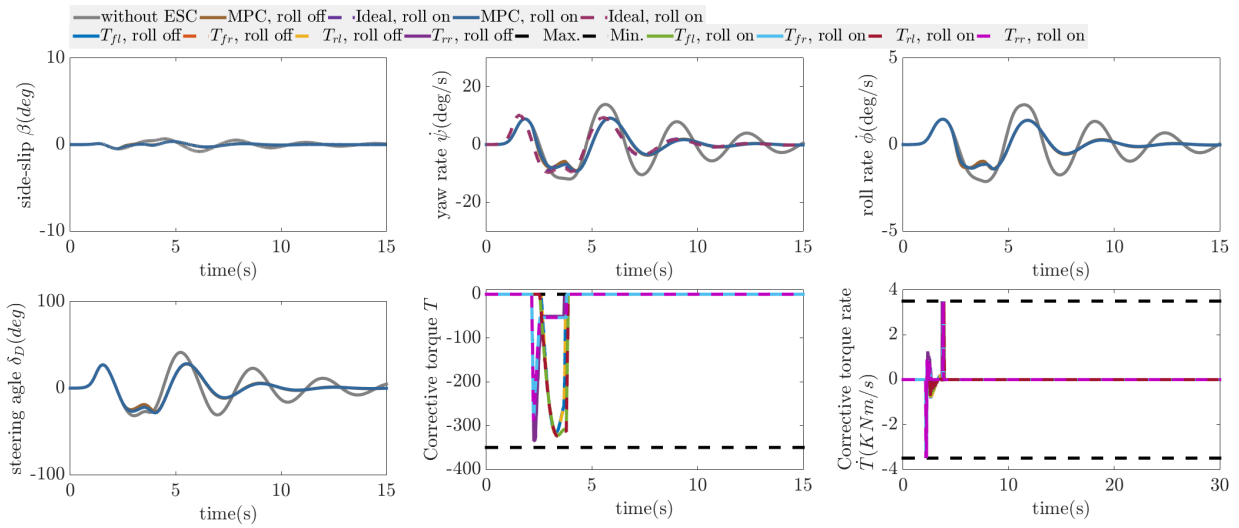

Figure 4.33: Results from simulation of DLC with an initial speed of 80km/h performed by vehicles without ESC; vehicle with MPC-based low-level DYC with roll control on; and vehicle with MPC-based low-level DYC with roll control off.

4.2.2.2 MIL simulation of DLC with an initial speed of 100 km/h

The results obtained from the simulation of DLC maneuver with initial speed of 100 km/h are shown in Figure 4.34 and Figure 4.35. In results obtained for vehicle without ESC assistance, it is possible to see that the driver loses the vehicle control. This destabilization happens because the forces generate on tires saturate at high side-slip angles (greater than 10 degrees) and thus the vehicle movement becomes non responsive to the steering wheel command. Besides the lateral displacement due to the side-slipping, the vehicle goes off the desired path due to the yaw error that causes the vehicle to not be properly oriented to follow the desired direction of motion.

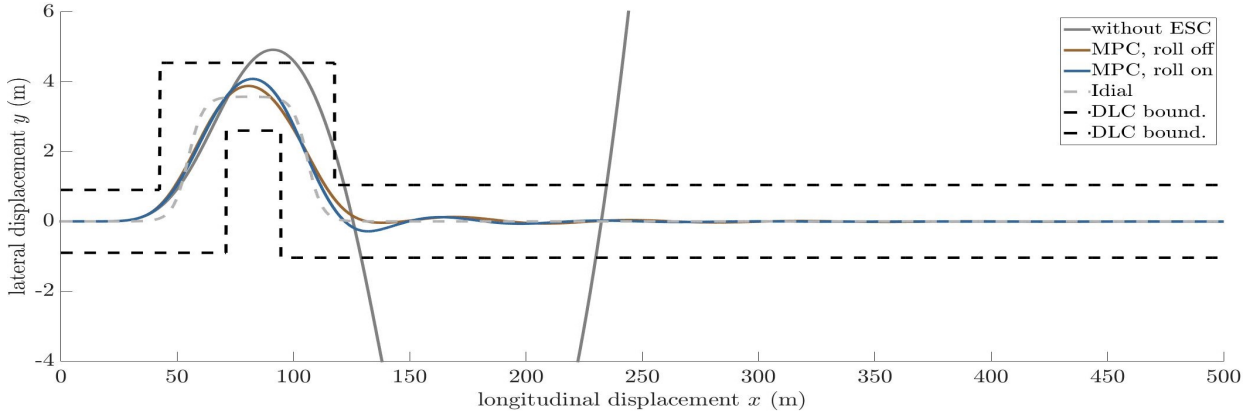

Figure 4.34: Vehicle trajectories from simulation of DLC with an initial speed of 100km/h performed by vehicle without ESC; with MPC-based low-level DYC with roll control on; and with MPC-based low-level DYC with roll control off.

From results for vehicle with ESCs, one can see that the ESCs with roll control on and off are efficient to avoid the destabilization with similar performance, in which the maneuver is performed successfully without exceeding the limits of lateral displacement error. This improvement in stability performance is obtained by controlling the side-slip and yaw rate. In addition to avoid steering instability, the ESCs reduce

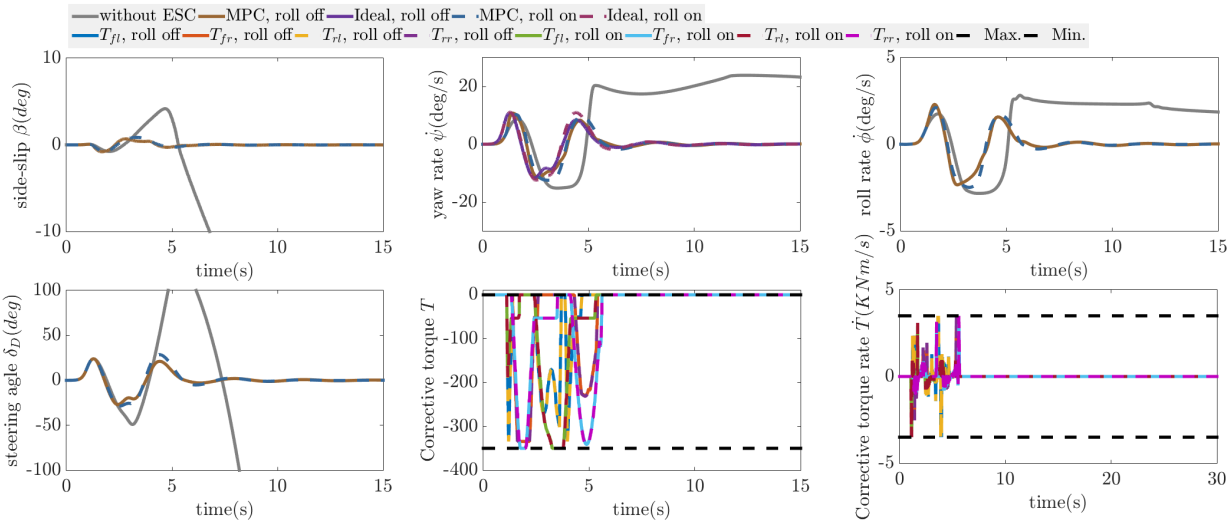

Figure 4.35: Results from simulation of DLC with an initial speed of 100km/h performed by vehicles without ESC; vehicle with MPC-based low-level DYC with roll control on; and vehicle with MPC-based low-level DYC with roll control off.

the roll rate, which contributes to increasing the passenger comfort. The lateral displacement from the ideal path obtained with the roll control off is smaller than that obtained with roll control on. The reason for that is the fact that the corrective braking torques reduces the rolling movement and its effects on the vehicle response. Therefore, in this scenario, it is more advantageous to reduce the calculation time, by using a prediction model that does not include the roll motion, than to take into account the roll mition in the predtion model.

Comparing the corrective braking torques obtained from simulations with initial speeds of 80 km/h (Figure 4.33) and 100 km/h (Figure 4.35), the time in which the control signals are different from zero is longer in the maneuver with initial speed of 100 km/h. This is a expected result because the instability risk increases with the speed, so the state errors met the ESC activation condition more times at 100km/h than at 80 km/h. Even so, there is in Figure 4.35 intervals in which the corrective braking torques remains equal to zero while the state error are not equal to zero, which shows that the ESC activation criterion is efficient to avoid unnecessary actuation when states errors do not mean a instability risk.

4.2.2.3 MIL simulation of DLC with an initial speed of 120 km/h

The results obtained from simulations of DLC maneuver with initial speed of 120 km/h are shown in Figure 4.36 and Figure 4.37. In results for the vehicle without ESC, the driver loses the vehicle control, which was expected since at 100 km/h the driver already loses control of the steering. In the results obtained for vehicle with ESCs, both controllers (with roll control on and off) are efficient to avoid the steering destabilization, which can be checked in Figure 4.36, in which the vehicle with any of the ESCs returns to a straight movement after the lane changes. However, none of the ESCs enable the maneuver to be performed without exceeding the limits of lateral displacement error.

Comparing the paths shown in Figure 4.36, the lateral displacement from the ideal path obtained with the roll control enabled is better than that obtained with the roll control enabled. This means that, in

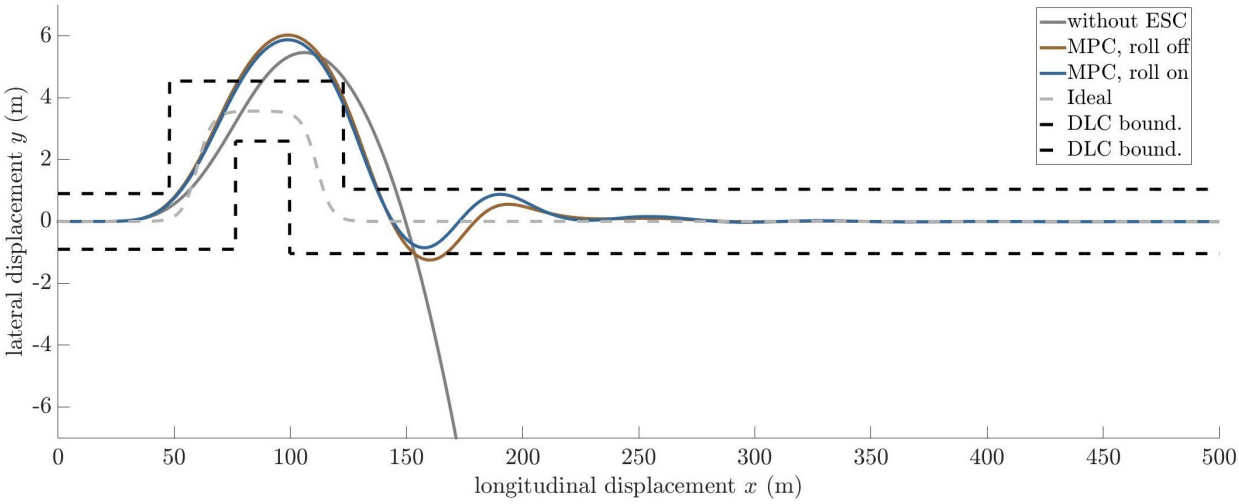

Figure 4.36: Vehicle trajectories from simulation of DLC with an initial speed of 120km/h performed by vehicle without ESC; with MPC-based low-level DYC with roll control on; and with MPC-based low-level DYC with roll control off.

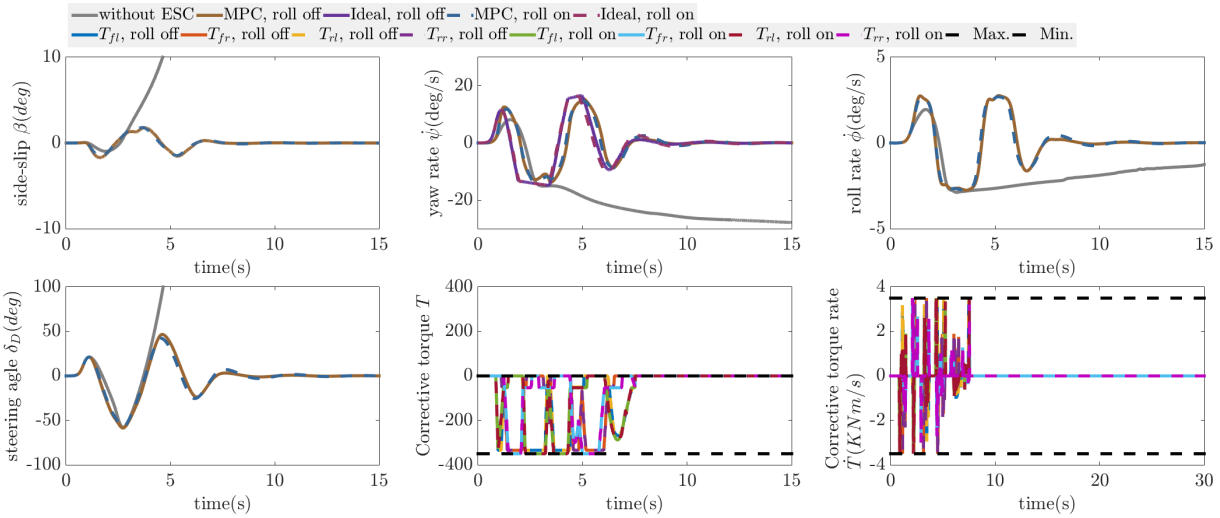

Figure 4.37: Results from simulation of DLC with an initial speed of 120km/h performed by vehicles without ESC; vehicle with MPC-based low-level DYC with roll control on; and vehicle with MPC-based low-level DYC with roll control off.

this maneuver, it is more advantageous to obtain a more accurate prediction from a model that takes into account the effects of rolling motion, than to achieve a higher update rate by removing the effects of rolling motion from the prediction model. This is different from what is observed in the maneuver with initial speed of 100 km/h (Figure 4.34, in which a better performance is obtained without roll control. This is justified because at higher speeds the roll motion has more influence on the vehicle's response.

4.2.2.4 MIL simulation of DLC with an initial speed of 120 km/h in presence of model uncertainties

The Figures 4.38 and 4.39 show the results from simulations of DLC, with initial speed of 120 km/h, for a vehicle with parameters equal to the nominal values assumed in controller configuration, versus the

results obtained for a vehicle whose mass, center of mass, tire-road friction coefficient are different from the nominal values. In these scenario, the trajectory error is greater in the presence of model uncertainties, although the amplitudes of the states errors are similar. This loss of performance is an issue in the the calculation of the desired yaw rate, which depends on the distance from wheels to the center of mass, such that the uncertainty generates an error in the reference yaw rate. Even so, these results attest to some robustness to model uncertainties, since the proposed ESC maintains its effectiveness in preventing the driver from losing control of the vehicle.

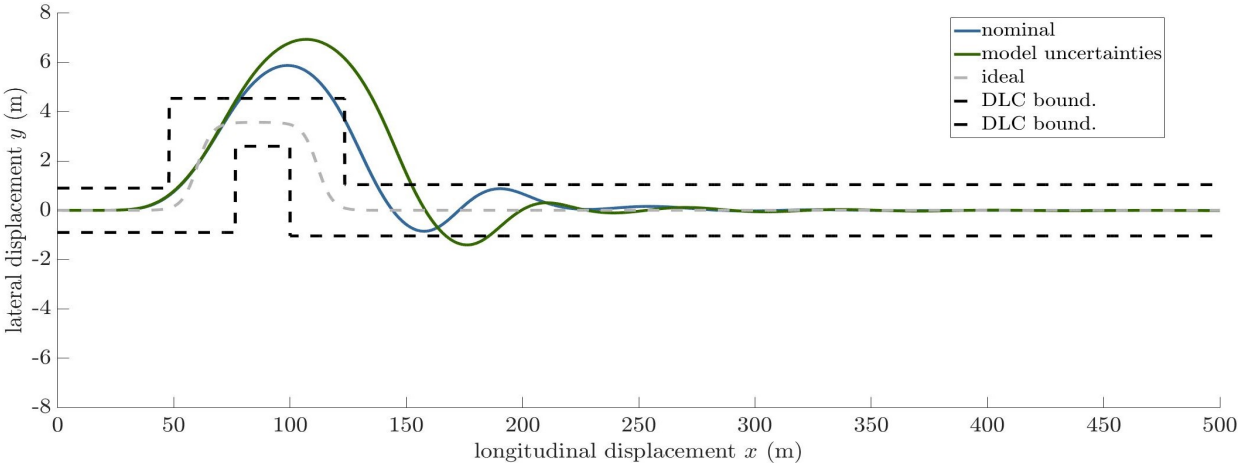

Figure 4.38: Trajectories obtained from MIL simulations of DLC maneuver with initial speed of 120 km/h for ESC (MPC-based low-level DYC with roll control on) on control of a vehicle whose parameter are equal to the nominal values assumed in configuration of the control algorithm, versus the results obtained for a vehicle whose mass, longitudinal position of the center of mass, tire-road friction coefficient are different from the nominal values.

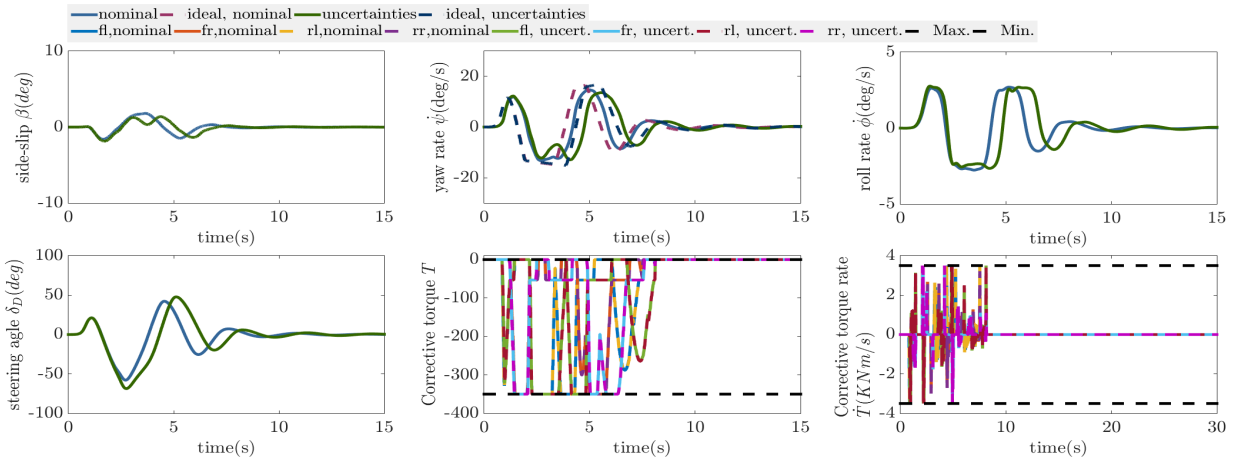

Figure 4.39: Results obtained from MIL simulations of DLC maneuver with initial speed of 120 km/h for ESC (MPC-based low-level DYC with roll control on) on control of a vehicle whose parameter are equal to the nominal values assumed in configuration of the control algorithm, versus the results obtained for a vehicle whose mass, longitudinal position of the center of mass, tire-road friction coefficient are different from the nominal values

4.2.2.5 HIL simulation of DLC with an initial speed of 120 km/h in presence of model uncertainties

HIL simulations of DLC with initial speed of 120 km/h were performed to test the implementation of MPC-based low-level DYC with roll control on, running in the ARM CORTEX A8, on control of a vehicle with mass, center of mass, and road-tire friction coefficients different from the nominal values assumed in configuration of the controller. So, this scenario tests the ESC robustness to disturbances in vehicle response with respect to the prediction, in addition to errors in acquisition of the input signals (i.e. longitudinal and lateral speeds, yaw rate, roll rate, roll angle and steering angle).

The results obtained from HIL versus those obtained from MIL simulation of the same scenario are shown in Figure 4.40 and Figure 4.41, in which the lateral displacement error, side-slip angle, roll rate and steering angle obtained from HIL and MIL are similar.

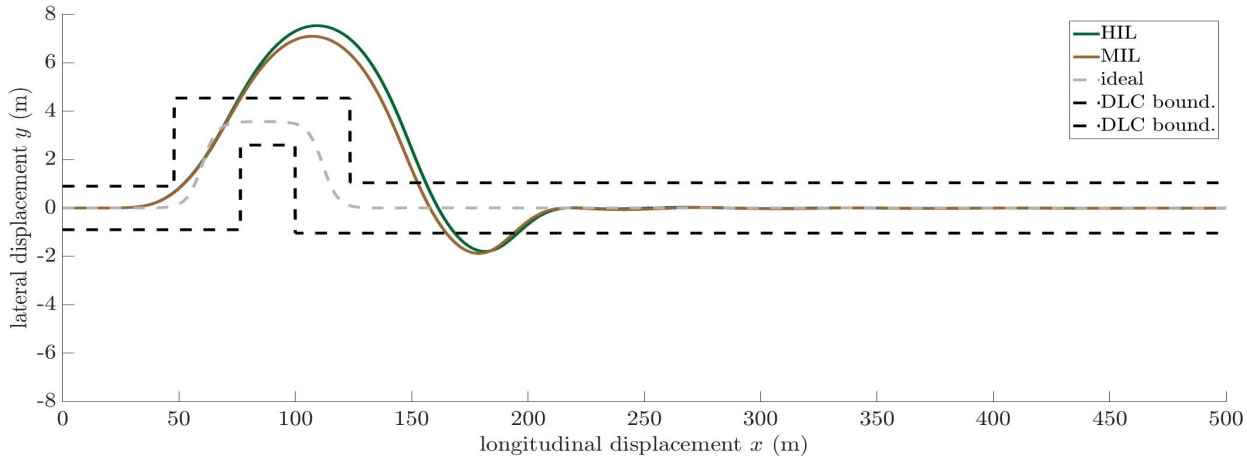

Figure 4.40: Trajectories obtained from MIL and HIL simulations of the DLC with initial speed of 120 km/h, performed to evaluate the MPC-based low-level DYC (with roll control enabled) on control of a vehicle whose mass, position of the center of mass, and the tire-road friction coefficient are different from the nominal values used in the prediction model.

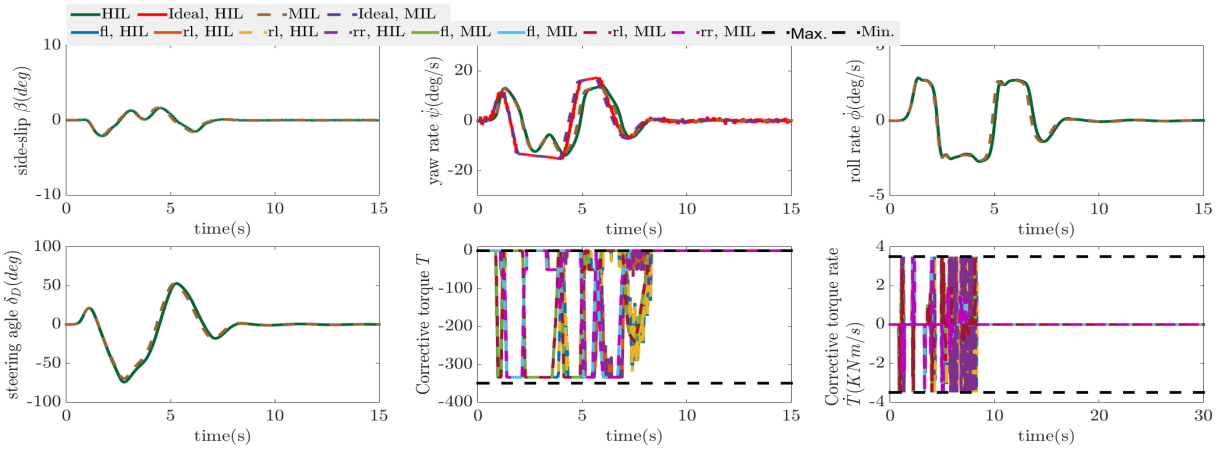

Figure 4.41: Results obtained from MIL and HIL simulations of the DLC with initial speed of 120 km/h, performed to evaluate the MPC-based low-level DYC (with roll control enabled) on control of a vehicle whose mass, position of the center of mass, and the tire-road friction coefficient are different from the nominal values used in the prediction model.

The effects of errors in acquisition of the input signals can be seen in the yaw rate and the corrective braking torques. In the yaw rate, one can see that the desired values for MIL and HIL simulation are not the same, however the yaw rate error is similar. The reason for that is the sensitivity of the calculation of the desired yaw rate (Equation 2.21) to errors in acquisition of the longitudinal speed and the steering angle. And the the differences in the corrective braking torque occurs because the errors in acquisition of lateral speed, longitudinal speed and yaw rate affects the time in which the activation/deactivation criteria is met. Even so, these results attest some robustness of proposed ESC, since the lateral stability improvement obtained in MIL and HIL are similar and sufficient to prevent the driver from losing the steering control.

4.2.2.6 MPC effectiveness compared to LRQ

The figures 4.42 and 4.43 show the vehicle trajectories obtained from simulation of DLC maneuvers with initial speeds of 100 km/h and 120 km/h performed to evaluate the LQR and MPC-based low-level DYCs. As previously shown in the figures 4.25 and 4.35, these are maneuvers in which the driver loses the control of vehicle without ESC assistance, and both ESCs are effective in avoiding this instability. The commands update rate achieved with LQR is eighteen times greater than the achieved with MPC. Even so, the MPC performance is better in both scenarios, in which the lateral displacement errors obtained with MPC are smaller than those obtained with LQR. This result means that it is advantageous to spend more processing time running the MPC algorithm, because the benefits of the MPC's capabilities overcome the negative effects of reducing the commands update rate.

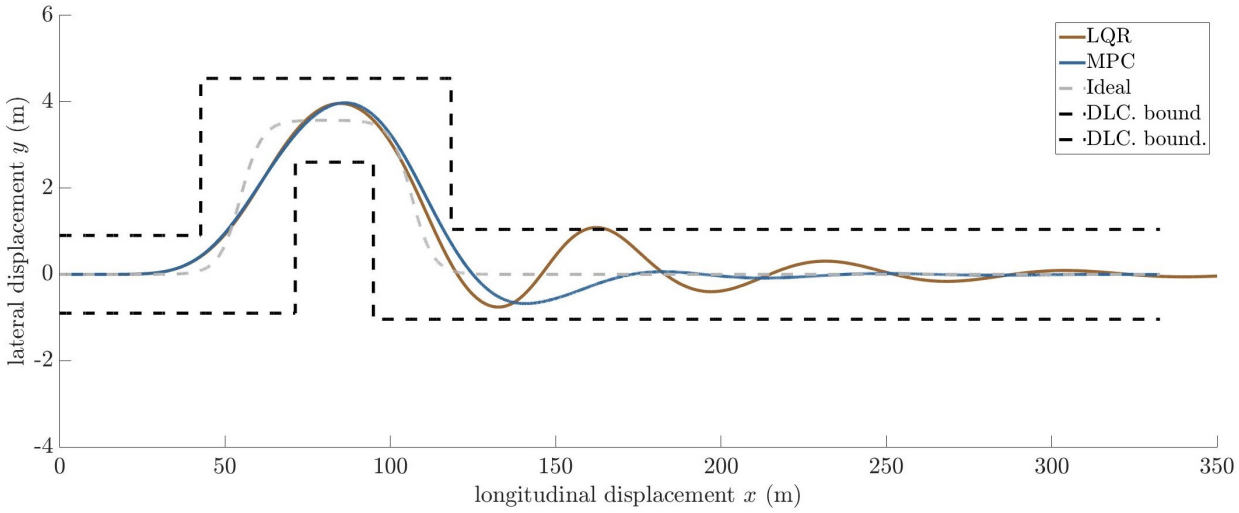

Figure 4.42: Trajectories obtained from MIL simulations of the DLC with an initial speed of 100 km/h, performed to evaluate the LQR and the MPC-based low-level DYC, with roll control enabled.

The performance advantage of the MPC over the LQR is more notable in the results obtained for DLC with initial speed of 120 km/h. This is a more challenging maneuver for lateral stability control, in which the side-slip angle, the yaw rate error and the roll rate are greater. As in LQR, the control signals are obtained from a weighted sum of the states errors, without taking into account any restrictions, the braking limits act as sources of disturbances between the vehicle's response and that expected by the controller. So that at higher speeds, due to greater errors in the states, the LQR commands tend to exceed the saturation limits more times, making the ESC to face more model uncertainties. Whereas, the MPC-based ESC faces

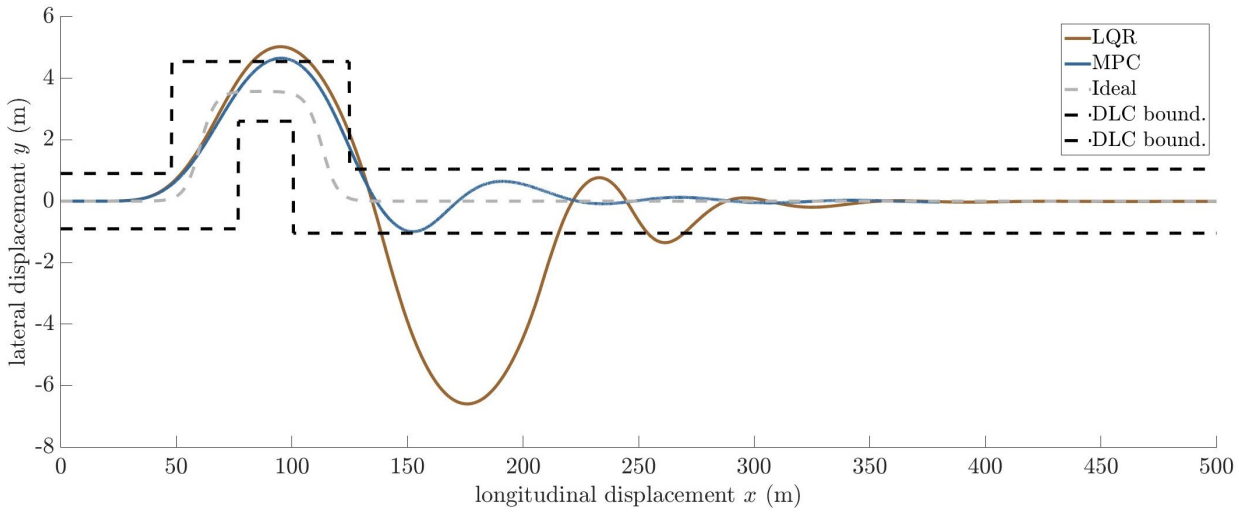

Figure 4.43: Trajectories obtained from MIL simulations of the DLC with an initial speed of 120 km/h, performed to evaluate the LQR and the MPC-based low-level DYC, with roll control enabled.

less disturbances in vehicle response because it only provides feasible commands and, in addition to that, it is more robust to these uncertainties than LQR, as can be seen by comparing the results presented in Sections 4.2.1.4 and 4.2.2.4.

4.2.2.7 MIL simulations with side-slip angle constrained

The optimal configuration obtained from the tuning procedure (Table 4.10) do not include the side-slip angle within the regulated states. As the increase of the side-slip angle lead to destabilization, efforts have been made to propose a version of the low-level controller that uses the MPC's ability to limit states to restrict the absolute value of the side-slip angle below 5 degrees. Simulations with different maneuvers, at different speeds, and different tire-road friction coefficient was performed to search for a scenario where the MPC-based ESCs is effective to avoid the steering instability and the side-slip angle reaches the 5 degrees. The results from these simulations show that whenever the ESC succeeds to avoid the steering destabilization, the side-slip angle remains below this limit. This threshold is only exceeded in very aggressive conditions, 200 km/h with 0.1 of friction coefficient, in which the ESC is not able to maintain stability. Then, to observe the controller's effectiveness in restricting the side-slip angle, the constraint was reduced to a value lower than the maximum side-slip angle obtained for scenarios in which the ESC is effective to keep the steering stable. The result from this test is that when enabling the side-slip restriction, the controller fails because there is no solution for the QP that satisfies the braking and sliding limits over the prediction horizon.

5 CONCLUSIONS

After all the presented results, it is possible to conclude that the objectives were achieved: MPC based high-level and low-level DYCs were developed; results from MIL simulations show that these systems are effective to avoid steering instability; the control algorithms was tested in HIL simulations and the results show that these implementations are effective in improving the lateral stability in real-time application. The robustness of the proposed ESCs to model uncertainties were evaluated in MIL simulations; LQR-based ESCs were developed, and the results obtained with MPC were compared with those obtained with LQR; the control algorithms were designed using linear models with and without roll-degree-of-freedom; simulations were performed to compare their performances and to understand the effects of including the roll-degree-of-freedom.

In MIL simulation, all proposed ESCs have proven their effectiveness in preventing steering destabilization in DLC maneuver at different speeds. And the results from HIL simulations shows that the control algorithms are computationally efficient, such that their implementation in low cost hardware achieve update rates of the control signals high enough to keep the steering stable.

Higher stability performances were obtained with ESCs based on MPC than with those based on LQR, which means that it is advantageous to spend more processing time running the MPC algorithm to explore the benefits of its ability to predict the destabilization and handle constraints of control signals, even if it means longer intervals between periodic command updates. Besides that, MPC-based controllers showed more robustness to disturbances in the vehicle's response in relation to the model used in control design, due to linearization errors, variation between plant coefficients and nominal values assumed by the controller, and errors in the acquisition of feedback signals.

The development of MPC-based ESCs using different linear models was performed to compare the benefits of a more accurate prediction, obtained when using a model that considers the roll motion, with the advantages of achieving a shorter calculation time, when using a simpler model that includes only the yaw rate and the side-slip angle within the states.

For high-level DYC, the advantages of more accurate prediction outweigh the effects of increased calculation time, so that the higher the speed, the greater the performance improvement obtained when taking into account the roll motion on prediction. Which makes sense, since the roll influence on vehicle movement increases with speed.

From results for MPC-based low-level DYC, it was observed that as the actuation through braking system slows down the vehicle, the ESC reduces the roll influence on vehicle's movement. In the DLC with an initial speed of 100 km/h, a better performance was achieved using the prediction model that includes only the yaw rate and the slip angle. This means that, in this scenario, it is better to use the processing power to update the control signals more quickly than to calculate the roll effects on movement. In other hand, in the DLC with initial speed of 120 km/h, a better performance was obtained using the linear model with roll-degree-of-freedom. This indicates that, at higher speeds, the error of neglecting the roll motion is greater, such that it is advantageous to use the processing time to consider the roll motion

in prediction, even at the cost of reducing the update rate of the control signals. Since the risk of steering destabilization is greater at higher speeds, the linear model that includes the roll movement is a better choice for the MPC-based DYCs.

Regarding the relationship between the calculation time and the prediction horizon, an interesting result observed in the tuning of the MPC-based low-level DYC is that, for prediction horizons less than 50 samples, the reduction of the prediction horizon improves the calculation time without greatly affecting the stability performance. This characteristic can be useful in ECUs that implement other features besides the lateral stability control

5.1 RESEARCH LIMITATIONS

The simulation environment developed in this research includes an intelligent driver model to calculate the steering wheel angles over the maneuver. Unlike what is expected from a human driver, the driver simulated by this model does not braking or accelerating during the maneuver. So, the observed results allow analysis of the lateral stability performance, but they may be very representative of what would be observed in a real vehicle. Another limitation of this driver model is that it supports only desired trajectories in which the lateral position is a function of the longitudinal position, i.e. for each longitudinal position there is only one desired lateral position. Because of this, some maneuvers useful for lateral stability analysis were not tested in this research. Such that the proposed systems were tuned and tested only for the DLC maneuver.

Another difference between the simulation environment and the real vehicle is in the interface between the controller and the acquisition and actuation systems. In real vehicles, the ECUs access the input signals and supplies the control signals through vehicle communication buses, in which there is a latency and a limit for the update rate of these signals. In the HIL platform used in this research, the controller access input signals through analog inputs and provides the control signals trough ethernet connection. Therefore, the characteristics of the vehicle communication bus is not being considered.

The processing power of the computer used on the HIL platform imposes a limitation on the sampling rate of the real-time simulation of the vehicle movement. The sampling achieved by the HIL platform was equal to 0.8 ms. That is why the controllers based on LQR, even reaching smaller calculation times, were tested with a sampling time of 0.8 ms. So, the performance comparisons between LQR and MPC based ESCs are not entirely fair, because only MPC-based controllers could be tested with the highest command update rate achieved by implementing hardware ESC.

5.2 FURTHER RESEARCH

This research shows the potential of the proposed ESC algorithms to be applied in real time application, the benefits of using the MPC methods taking into account the calculation time, and the effects of using different prediction models (with and without roll motion). The next steps should be towards validating the

algorithms in a real vehicle. For that, the algorithms must be implemented in a hardware that follows the standards of automotive ECUs, in which the interface with the acquisition and actuation systems is made by vehicular communication networks.

Before testing the controllers in a real vehicle, further testing should be done in simulation environments that best represent the real scenario. A possibility of improvement for the simulation environment developed in this research is the inclusion of a driver model that provides other commands besides steering steering, and supports maneuvers in which the lateral position does not need to be a function of the longitudinal position. Another improvement opportunity for the simulation environment is the inclusion of the communication model between the controller and the acquisition and actuation systems, which emulates the vehicular communication network.

Another issue to consider is that in a real vehicle there is competition for access to the braking system, for example, in a critical maneuver, the conditions that activate ABS or ESC can be satisfied simultaneously. So a suggested work is the development of a strategy to integrate these automotive control systems.

Bibliography

1 CHAKRABORTY, S.; LUKASIEWYCZ, M.; BUCKL, C.; FAHMY, S.; CHANG, N.; PARK, S.; KIM, Y.; LETEINTURIER, P.; ADLKOFER, H. Embedded systems and software challenges in electric vehicles. *Proceedings -Design, Automation and Test in Europe, DATE*, p. 424–429, 2012. ISSN 15301591.

2 BLAKE, D. *Systems and Vehicle Innovation*. [S.l.], 2005. 86–87 p.

3 ZANTEN, A. T. V.; ERHARDT, R.; PFAFF, G. Vdc, the vehicle dynamics control system of bosch. *SAE Technical Papers*, n. 41 2, 1995. ISSN 0178-2312.

4 GLOBAL status report on road safety 2018. [S.l.], 2018.

5 HOYE, A. The effects of electronic stability control (esc) on crashes - an update. *Accident Analysis and Prevention*, Elsevier Ltd, v. 43, n. 3, p. 1148–1159, 2011. ISSN 00014575.

6 LIE, A.; TINGVALL, C.; KRAFFT, M.; KULLGREN, A. The effectiveness of electronic stability control (esc) in reducing real life crashes and injuries. *Traffic Injury Prevention*, v. 7, n. 1, p. 38–43, 2006. ISSN 10286586.

7 EFFECTIVENESS of Electronic Stability Control on Single-Vehicle Accidents. *Traffic Injury Prevention*, v. 16, n. 4, p. 380–386, 2015. ISSN 1538957X.

8 CHOUINARD, A.; LÉCUYER, J. F. A study of the effectiveness of electronic stability control in canada. *Accident Analysis and Prevention*, v. 43, n. 1, p. 451–460, 2011. ISSN 00014575.

9 VAA, T.; PENTTINEN, M.; SPYROPOULOU, I. Intelligent transport systems and effects on road traffic accidents : state of the art. *Intelligent Transport Systems*, p. 81–88, 2007.

10 ERKE, A. Effects of electronic stability control (esc) on accidents : A review of empirical evidence. v. 40, p. 167–173, 2008.

11 RESEARCH Note: Estimating Lives Saved by Electronic Stability Control, 2011–2015. n. March, 2015.

12 NATIONS, U. *Global plan for the Decade of Action for Road Safety 2011–2020*. [S.l.], 2011. 25 p.

13 SHI, L.; WANG, H.; HUANG, Y.; JIN, X.; YANG, S. A novel integral terminal sliding mode control of yaw stability for steer-by-wire vehicles. *Chinese Control Conference, CCC*, Technical Committee on Control Theory, Chinese Association of Automation, v. 2018-July, p. 7787–7792, 2018. ISSN 21612927.

14 LIU, M.; HUANG, J.; CHAO, M. Multi-states combination nonlinear control of in-wheel-motor-drive vehicle dynamics stability. In: *Energy Procedia*. [S.l.: s.n.], 2017. ISSN 18766102.

15 LE, A.-T.; CHEN, C.-K. Adaptive sliding mode control for a vehicle stability system. In: *2015 International Conference on Connected Vehicles and Expo (ICCVE)*. [S.l.: s.n.], 2015. ISBN 978-1-5090-0264-1.

16 RAJAMANI, R.; PIYABONGKARN, D. N. New paradigms for the integration of yaw stability and rollover prevention functions in vehicle stability control. *IEEE Transactions on Intelligent Transportation Systems*, 2013. ISSN 15249050.

17 ZHOU, H.; LIU, Z. Vehicle yaw stability-control system design based on sliding mode and backstepping control approach. *IEEE Transactions on Vehicular Technology*, v. 59, p. 3674–3678, 2010. ISSN 00189545.

18 JIN, X. J.; YIN, G.; CHEN, N. Gain-scheduled robust control for lateral stability of four-wheel-independent-drive electric vehicles via linear parameter-varying technique. *Mechatronics*, 2015. ISSN 09574158.

19 JIN, X. J.; YIN, G.; ZENG, X.; CHEN, J. Robust gain-scheduled output feedback yaw stability control for in-wheel-motor-driven electric vehicles with external yaw-moment. *Journal of the Franklin Institute*, 2017. ISSN 00160032.

20 MAYNE, D. Q.; RAWLINGS, J. B.; RAO, C. V.; SCOKAERT, P. O. Constrained model predictive control: Stability and optimality. *Automatica*, v. 36, n. 6, p. 789–814, 2000. ISSN 00051098.

21 LEE, J. Model predictive control: Review of the three decades of development. *International Journal of Control, Automation and Systems*, v. 9, 06 2011.

22 INTERFACE checks of the automotive embedded software components. *2017 IEEE 7th International Conference on Consumer Electronics - Berlin (ICCE-Berlin)*, p. 163–16, 2017. ISSN 21666822.

23 PLUMMER, A. R. Model-in-the-loop testing. *Proceedings of the Institution of Mechanical Engineers. Part I: Journal of Systems and Control Engineering*, v. 220, n. 3, p. 183–199, 2006. ISSN 09596518.

24 CICEO, S.; MOLLET, Y.; SARRAZIN, M.; GYSELINCK, J.; AUWERAER, H. V. D. Model-based design and testing for electric vehicle energy consumption analysis. *Electrotehnică Electronică Automatică*, v. 63, n. 4, p. 2–5, 2015. ISSN 1582-5175.

25 ALAMIR, M. *A Pragmatic Story of Model Predictive Control: Self-Contained Algorithms and Case-Studies*. [S.l.]: CreateSpace Independent Publishing Platform, 2013.

26 CHENG, S.; LI, L.; MEMBER, S.; GUO, H.-q.; CHEN, Z.-g.; SONG, P. Stability adaptive control system based on mpc of autonomous vehicles. *IEEE Transactions on Intelligent Transportation Systems*, IEEE, PP, p. 1–10, 2019.

27 ZHENG, Y.; SHYROKAU, B. A real-time nonlinear mpc for extreme lateral stabilization of passenger vehicles. *Proceedings - 2019 IEEE International Conference on Mechatronics, ICM 2019*, IEEE, v. 1, p. 519–524, 2019.

28 LI, L.; LU, Y.; WANG, R.; CHEN, J. A three-dimensional dynamics control framework of vehicle lateral stability and rollover prevention via active braking with mpc. *IEEE Transactions on Industrial Electronics*, 2017. ISSN 02780046.

29 Guo, Y.; Guo, H.; Yin, Z.; Cui, M.; Chen, H. Vehicle lateral stability controller design for critical running conditions using nmpc based on vehicle dynamics safety envelope. In: *2019 IEEE International Symposium on Circuits and Systems (ISCAS)*. [S.l.: s.n.], 2019. p. 1–8.

30 WONG, J. *Theory of Ground Vehicles*. [S.l.]: Wiley, 2001. ISBN 9780471354611.

31 PACEJKA, H. B. *Tyre and Vehicle Dynamics (Second Edition)*. Second edition. Oxford: Butterworth-Heinemann, 2006. ISBN 978-0-7506-6918-4.

32 DAHMANI, H.; PAGÈS, O.; HAJJAJI, A. E. Observer-based state feedback control for vehicle chassis stability in critical situations h. *IEEE TRANSACTIONS ON CONTROL SYSTEMS TECHNOLOGY*, v. 24, n. 2, 2016.

33 MASHADI, B.; MAJIDI, M.; DIZAJI, H. P. Optimal vehicle dynamics controller design using a four-degrees-of-freedom model. *Proceedings of the Institution of Mechanical Engineers, Part D: Journal of Automobile Engineering*, 2010. ISSN 09544070.

34 ZHENG, S.; TANG, H.; HAN, Z.; ZHANG, Y. Controller design for vehicle stability enhancement. *Control Engineering Practice*, v. 14, p. 1413–1421, 2006. ISSN 09670661.

35 GILLESPIE, T. D. Fundamentals of vehicle dynamics. 01 2000.

36 ULSOY, A. G.; PENG, H.; ÇAKMAKCI, M. *Automotive Control Systems*. [S.l.]: Cambridge University Press, 2012.

37 REŃSKI, A. Identification of driver model parameters. *International Journal of Occupational Safety and Ergonomics*, v. 7, n. 1, p. 79–92, 2001. ISSN 10803548.

38 MOUSAVINEJAD, I.; ZHU, Y.; VLACIC, L. Control strategies for improving ground vehicle stability state-of-the-art review. In: *2015 10th Asian Control Conference (ASCC)*. [S.l.: s.n.], 2015.

39 BENINE-NETO, A.; MOREAU, X.; LANUSSE, P. Robust control for an electro-mechanical anti-lock braking system: the crone approach. *IFAC-PapersOnLine*, v. 50, n. 1, p. 12575 – 12581, 2017. ISSN 2405-8963. 20th IFAC World Congress. Disponível em: <http://www.sciencedirect.com/science/article/pii/S2405896317328689>.

40 Dias de Carvalho Dantas Maia, I. Modeling and control of anti-lock braking systems considering different representations for tire-road interaction. In: *2019 23rd International Conference on System Theory, Control and Computing (ICSTCC)*. [S.l.: s.n.], 2019. p. 344–349. ISSN 2372-1618.

41 CUALAIN, D. O.; HUGHES, C.; GLAVIN, M.; JONES, E. Automotive standards-grade lane departure warning system. *IET Intelligent Transport Systems*, v. 6, n. 1, p. 44–57, 2012. ISSN 1751956X.

42 WANG, C.; ZHANG, Y.; GU, M. Target Tracking and Classification Algorithm for Adaptive Cruise Control System via Internet Technology. *Wireless Personal Communications*, Springer US, v. 102, n. 2, p. 1307–1326, 2018. ISSN 1572834X.

43 AN innovative decision rule approach to tyre pressure monitoring. *Expert Systems with Applications*, Elsevier Ltd, v. 124, p. 252–270, 2019. ISSN 09574174.

44 JIN, C.; SHAO, L.; LEX, C.; EICHBERGER, A. Vehicle side slip angle observation with road friction adaptation. *IFAC-PapersOnLine*, Elsevier B.V., v. 50, n. 1, p. 3406–3411, 2017. ISSN 24058963.

45 ENGINEER, Y. C.; SHIMADA, K.; TOMARI, T. Improvement of vehicle maneuverability by direct yaw moment control. *Vehicle System Dynamics*, Taylor & Francis, v. 22, n. 5-6, p. 465–481, 1993.

46 ARIPIN, M. K.; Md Sam, Y.; DANAPALASINGAM, K. A.; PENG, K.; HAMZAH, N.; ISMAIL, M. F. A review of active yaw control system for vehicle handling and stability enhancement. *International Journal of Vehicular Technology*, v. 2014, 2014. ISSN 16875710.

47 GUO, H.; LIU, F.; XU, F.; CHEN, H.; CAO, D.; JI, Y. Nonlinear model predictive lateral stability control of active chassis for intelligent vehicles and its fpga implementation. *IEEE Transactions on Systems, Man, and Cybernetics: Systems*, 2017. ISSN 21682232.

48 LIAN, Y. F.; WANG, X. Y.; ZHAO, Y.; TIAN, Y. T. Direct yaw-moment robust control for electric vehicles based on simplified lateral tire dynamic models and vehicle model. *IFAC-PapersOnLine*, 2015. ISSN 24058963.

49 CAIRANO, S. D.; TSENG, H. E.; BERNARDINI, D.; BEMPORAD, A. Vehicle yaw stability control by coordinated active front steering and differential braking in the tire sideslip angles domain. *IEEE Transactions on Control Systems Technology*, v. 21, n. 4, p. 1236–1248, 2013. ISSN 10636536.

50 JALALI, M.; KHOSRAVANI, S.; KHAJEPOUR, A.; CHEN, S.-k.; LITKOUHI, B. Model predictive control of vehicle stability using coordinated active steering and di ff erential brakes. *Mechatronics*, Elsevier, v. 48, n. October, p. 30–41, 2017. ISSN 0957-4158.

51 La Torre, D.; KUNZE, H.; RUIZ-GALAN, M.; MALIK, T.; MARSIGLIO, S. Optimal control: Theory and application to science, engineering, and social sciences. *Abstract and Applied Analysis*, v. 2015, p. 2–4, 2015. ISSN 16870409.

52 LAURITZEN, N. *Convex optimization*. [S.l.: s.n.], 2013. 223–251 p. ISBN 9780521833783.

53 FERREAU, H. J.; KIRCHES, C.; POTSCHKA, A.; BOCK, H. G.; DIEHL, M. qpOASES: a parametric active-set algorithm for quadratic programming. *Mathematical Programming Computation*, v. 6, n. 4, p. 327–363, 2014. ISSN 18672957.

54 MURILO, A. *Contributions à la Commande Prédictive Non Linéaire pour les Systèmes à Dynamiques Rapides*. Tese (Doutorado) — Institut polytechnique de Grenoble, 2009.

55 DRGOňA, J. *Model Predictive Control with Applications in Building Thermal Comfort Control*. Tese (Doutorado), 06 2017.

56 BEMPORAD, A.; MORARI, M.; DUA, V.; PISTIKOPOULOS, E. The explicit linear quadratic regulator for constrained systems. *Automatica*, v. 38, p. 823–828, 2002. ISSN 00189286.

57 CHEN, C. *On the Robustness of the Linear Quadratic Regulator via Perturbation Analysis of the Riccati Equation*. Tese (Doutorado) — Dublin City University, 2014.

58 LEVINE, W. *The Control Handbook*. [S.l.]: Taylor & Francis, 1996. (Electrical Engineering Handbook). ISBN 9780849385704.

59 OGATA, K. *Modern Control Engineering*. [S.l.]: Prentice Hall, 2010. (Instrumentation and controls series). ISBN 9780136156734.

60 WEB of Science. <https://www.webofknowledge.com>. Accessed: 2019-11-05.

61 CHOI, M.; CHOI, S. B. Model predictive control for vehicle yaw stability with practical concerns. *IEEE Transactions on Vehicular Technology*, IEEE, v. 63, n. 8, p. 3539–3548, 2014. ISSN 00189545.

62 ATAEI, M.; KHAJEPOUR, A.; JEON, S. Reconfigurable integrated stability control for four- and three-wheeled urban vehicles with flexible combinations of actuation systems. *IEEE/ASME Transactions on Mechatronics*, IEEE, v. 23, n. 5, p. 2031–2041, 2018. ISSN 10834435.

63 ATAEI, M.; KHAJEPOUR, A.; JEON, S. Model predictive control for integrated lateral stability , traction / braking control , and rollover prevention of electric vehicles. *Vehicle System Dynamics*, Taylor & Francis, v. 0, n. 0, p. 1–25, 2019. ISSN 0042-3114.

64 MASHADI, B.; MOSTAANI, S.; MAJIDI, M. Vehicle stability enhancement by using an active differential. In: *Proceedings of the Institution of Mechanical Engineers. Part I: Journal of Systems and Control Engineering*. [S.l.: s.n.], 2011. ISSN 09596518.

65 YOGURTCU, I.; SOLMAZ, S.; BASLAMISH, S. C. Lateral stability control based on active motor torque control for electric and hybrid vehicles. In: *2015 IEEE European Modelling Symposium (EMS)*. [S.l.: s.n.], 2015. p. 213–218. ISBN 978-1-5090-0206-1.

66 FARIAS, A. B. C. D.; RODRIGUES, R. S.; MURILO, A.; LOPES, R. V.; AVILA, S. Low-cost hardware-in-the-loop platform for embedded control strategies simulation. *IEEE Access*, v. 7, p. 111499–111512, 2019.

67 VO-DUY, T.; C. Ta, M. A signal hardware-in-the-loop model for electric vehicles. *ROBOMECH Journal*, 2016. ISSN 21974225.